University of Ulm

Institute for Anatomy and Cell Biology

Prof. Dr. med. Tobias M. Böckers

Modeling C9ORF72 Pathomechanisms in Patient-derived Cells

Dissertation

for obtaining the doctoral degree (Dr.med.)

of the Medical Faculty of the University Ulm

submitted by

Lena Luisa Semelink-Sedlacek

from Lauingen, Bayern

2016

Incumbent Dean	**:**	**Prof. Dr. T. Wirth**
1st Correspondent	**:**	**Prof. Dr. T. Böckers**
2nd Correspondent	**:**	**Prof. Dr. M. Otto**
Day of Dissertation	**:**	**25.06.2020**

Declaration with reference to the Creative Commons Attribution License

Higelin, J., Catanese, A., Semelink-Sedlacek, L.L., Oeztuerk, S., Lutz, A.-K., Bausinger, J., Barbi, G., Speit, G., Andersen, P.M., Ludolph, A.C., Demestre, M., and Boeckers, T.M. 2018. NEK1 loss-of-function mutation induces DNA damage accumulation in ALS patient-derived motoneurons. Stem Cell Research, 30:150-162. Online available under: https://doi.org/10.1016/j.scr.2018.06.005

Table of contents

List of abbreviations

ACh	acetylcholine
AD	alzheimer´s disease
ALS	amyotrophic lateral sclerosis
Amp	ampicillin
AP	alanine-proline
APS	ammonium persulfate
AS	amino acids
ATM	ataxia telangiectasia mutated
α	anti
BDNF	brain derived neurotrophic factor
BMP	bone morphogenetic protein
BRCA1	breast cancer 1
BSN	bassoon
C9ORF72	chromosome nine open reading frame 72
cAMP	cyclic adenosine monophosphate
ChAT	choline acetyltransferase
c-MYC	v-myc myelocytomatosis viral oncogene homolog
CNS	central nervous system
CT	cycle treshold
Ctrl	control
DAPI	4´,6-diamidin-2-phenylindol
DENN	differentially expressed in normal and neoplastic cells
DMEM	dulbecco´s modified eagle medium
DPR	dipeptide repeat
DSB	double strand break
DTT	dithiothreitol
EB	embryoid body

ECL	enhanced chemiluminescent
E. coli	escherichia coli
EDTA	ethylenediaminetetraacetic acid
EGF	epidermal growth factor
ERK	extracellular signal-regulated kinase
ESC	embryonic stem cell
FACS	fluorescence-activated cell sorting
FALS	familiar ALS
FBS	fetal bovine serum
FGF	fibroblast growth factor
FISH	fluorescence in situ hybridisation
FUS	fused in sarcoma
FXTAS	fragile X-associated tremor/ataxia syndrome
GA	glycine-alanine
GDNF	glia-derived neurotrophic factor
GEF	guanosine exchange factor
GFAP	glial fibrillary acidic protein
GP	glycine-proline
GR	glycine-arginine
GST	gluthatione-S-transferase
HB9	homebox protein 9
HD	huntington´s disease
HDAC1	histone deacetylase1
HESC	human embryonic stem cell
HIPSC	human induced pluripotent stem cell
HKGS	human keratinocyte growth supplement
HM	hormone mix
HMBS	hydroxymethybilane synathase
hnRNP	heterogeneous nuclear ribonucleoprotein
hnRNPK	heterogeneous nuclear ribonucleoprotein K

hnRNPA1	heterogeneous nuclear ribonucleoprotein A1
HOMER	homer scaffolding protein
HRP	horseradish peroxidase
ICM	inner cell mass
IF	immunofluorescence
IGF1	insulin growth factor 1
IGF2	insulin growth factor 2
IgG	immune globulin G
IP	immunoprecipitation
IPTG	isopropyl-b-D-thiogalactopyranosid
IRES	internal ribosomal entry sites
JAK	janus kinase
KLF4	krueppel-like factor 4
LB	lysogeny broth
MAPK	mitogen-activated protein kinase
MAP2	microtubule-associated protein 2
MN	motoneuron
MND	motoneuron disease
mRNA	messenger ribonucleic acid
miRNA	microRNA
MYC	v-myc myelocytomatosis viral oncogene homolog
NANOG	nanog homebox
NE	neuro epithelial rosette
NEAA	non essential amino acids
NEFH	neurofilament, heavy polypeptide
NHEJ	non-homologous end-joining
NMDA	N-methyl-D-aspartate

NMJ	neuromuscular junction
NP	neural precursor
Ns	non-significant
OCT4	POU class 5 homebox 1
OLIG2	oligodendrocyte lineage transcription factor 2
PAX6	paired box 6
PBS	phosphate buffered Saline
PCR	polymerase chain reaction
PD	parkinson's disease
PFA	paraformaldehyde
PG	proline-glycine
PI3-K	phosphoinositide-3-kinase
PLO	poly-L-ornithine
PLL	poly-L-lysine
PM	purmorphamine
PR	proline-arginine
ProSAP	proline-rich synapse-associated proteins
PSD	postsynaptic density
qRT-PCR	real time quantitative polymerase chain reaction
RA	retinoid acid
RAN	repeat associated non-ATG-initiated
Rb	rabbit
REF	rat embryonic fibroblasts
Rpm	rounds per minute
ROCK	Rho-associated, coiled-coil containing protein kinase
RT	reverse transcriptase; room temperature
SALS	sporadic ALS

SC	santa cruz
SD	standard deviation
SDS-PAGE	sodium dodecyl sulfate polyacrylamide electrophoresis
SG	stress granule
Shank/ S1,2,3	SH3 and multiple ankyrin repeat domains protein 1,2,3
SHH	sonic hedgehog
SMAD	SMAD family member
SMI-32 / NEFH	sternberger monoclonal-incorporated antibody 32/ neurofilament heavy polypeptide
SNAP	synaptosome-associated protein
SNARE	soluble N-ethylmaleimide-sensitive factor attachment protein receptors
SOB	super optimal broth
SOD1	superoxide dismutase 1
SOX1/2	sex determining region Y-box 1/2
SSEA4	stage specific embryonic antigen 4
STAT3	signal transducer and activator of transcription 3
SYP	synaptophysin
TAE	tris-acetate EDTA
TARDBP/TDP-43	TAR DNA binding protein/-43
TBK1	TANK-binding kinase 1
TBS	tris buffered saline
TBST	tris buffered saline with tween
TEMED	N,N,N',N-tetramethylethylenediamine
TGF-β	transforming growth factor, beta
TIA1	TIA1 cytotoxic granule associated RNA binding protein
Tm	melting temperature
TUB-β3	neuron specific class III β-tubulin
WB	western blot

1. Introduction

1.1 Amyotrophic lateral sclerosis and its genetic background

Amyotrophic lateral sclerosis (ALS) is a progressive disease that leads to degeneration of motoneurons. As the most common motoneuron disease (MND), ALS has an incidence of 1-3 per 100.000 people per year and a prevalence of 5 per 100.000 people in western countries (Wijesekera and Leigh 2009). ALS affects upper and lower motoneurons, including pyramidal neurons in the primary motor cortex, which give rise to the corticospinal tracts, as well as motoneurons located in the brainstem and spinal cord (Tandan and Bradley 1985, Shaw 2005). Symptoms of muscle weakness and wasting usually begin in the limbs or in bulbar muscles at a mean age of 60 years. Besides paralysis, spasticity in the atrophic limbs is a sign of pyramidal cell lesion. Due to muscle atrophy of the diaphragm and chest wall muscles, most patients die from respiratory failure within 1 to 5 years from the onset of the symptoms. Cognitive decline is also reported in a number of studies (Lomen-Hoerth 2004, Wijesekera and Leigh 2009). However, the disease mechanisms have not been clarified yet, such that therapy remains supportive and palliative.

The molecular mechanism causing motoneuron degeneration in ALS is unknown, but an interplay between various pathogenic cellular mechanisms is likely (Shaw 2005). Dysfunction of mitochondria resulting in oxidative stress and altered energy metabolism was early on implicated in mechanisms causing motoneuron degeneration, in consideration of the high energy requirements of motoneurons. Motoneurons have an extremely high ATP consumption in order to maintain their characteristic resting membrane potential, synaptic function and transport of metabolites along the neuronal processes (Lin and Beal 2006, Le Masson et al. 2014). Later, glutamate mediated excitotoxicity and dysfunction of RNA metabolism, as well as protein aggregation with neuroinflammation came to be considered as disease-causing processes (Cleveland and Rothstein 2001, Cluskey and Ramsden 2001, Manfredi et al. 2015). Most ALS cases (90 %) occur sporadically; however, up to 10 % of cases have autosomal dominant inheritance, meaning they are familial (Connolly 2012, Majounie et al. 2012). Intense studies of

these familial ALS cases brought up several candidate genes directly linked with ALS pathology. Among the important ALS genes are those encoding superoxide dismutase 1 (SOD1) (Rosen et al. 1993), TAR DNA binding protein (TDP-43) (Mackenzie et al. 2013), fused in sarcoma (FUS) (Vance et al. 2009), ataxin-2 (Elden et al. 2011), angiogenin (Wu et al. 2007), dynactin (Schymick et al. 2007), histone deacetylase 1 (HDAC1) (Lazo-Gómez et al. 2013), optineurin (Maruyama et al. 2010) and TANK-binding kinase 1 (TBK1) (Freischmidt et al. 2015).

The chopper-zinc SOD1 gene was the first candidate known to be involved in the disease process of ALS, and is now recognized as being responsible for 20 % of autosomal dominant familial ALS (FALS) and 2 % of sporadic ALS (SALS) cases (Gurney et al. 1994). The SOD1 enzyme catalyses the conversion of highly reactive superoxide anions (O^{2-}) into the less reactive hydrogen peroxide (H_2O_2) molecule and molecular oxygen. However, the assertion that oxidative stress due to dysfunctional SOD1 receded in importance when it was shown that the ALS-associated mutations do not influence enzymatic activity, and that mice with a gain of function mutation in the SOD1 gene develop ALS-like pathology (Ghadge et al. 1997, Bruijn et al. 2004, Lemmens et al. 2007, Saccon et al. 2013). Thus, the disease mechanisms in motoneurons caused by SOD1 mutations remain to be identified. The initial proposal, that a loss of function is induced by the SOD1 mutation, has not been investigated further. Instead, a gain of function mutation with potentially dominant negative effect on wild-type SOD1 is increasingly considered as the disease-causing mechanism of mutated SOD1 (Rosen et al. 1993, Saccon et al. 2013).

Recently, RNA binding protein dysfunction with protein aggregation emerged as a new focus of ALS research. In 2006, mutations in the *TARDBP* gene that encodes the TAR-DNA binding protein (also named DNA/RNA binding protein TDP-43) was identified as the particular intraneuronal protein accumulating in the majority of ALS cases. TDP-43, which is an RNA and DNA binding protein, is involved in several steps of the RNA metabolism, including transcription, splicing and processing of micro RNA (miRNA) (Mackenzie et al. 2010). Protein aggregation is a rather common feature of neurodegenerative diseases; inclusions of TDP-43 have been identified in several other neurodegenerative diseases, such as

Parkinson´s disease (PD), Alzheimer's disease (AD) and Huntington´s disease (HD) (Kunihiro et al. 2007, Tada et al. 2013).

Additionally, mutations in FUS, another RNA-binding protein, have been linked to 5 % of FALS and 1 % of all SALS cases (Dejesus-hernandez et al. 2012). The mutations mostly concern the nuclear localisation signal and lead to a redistribution of FUS into the cytoplasm (Dormann et al. 2010, Aoki et al. 2012).

In 2011, two groups identified an abnormal expansion of a $(GGGGCC)_n$ hexanucleotide repeat in the non-coding first intron of the chromosome 9 open reading frame 72 gene (C9ORF72) as an ALS causing mutation (Connolly 2012, Dejesus-hernandez et al. 2012). C9ORF72 is an evolutionarily conserved protein with as yet incompletely clarified function. Healthy people have fewer than 30 of these hexanucleotide repeats, while patients have up to several hundred copies. This mutation is now known to be the most common genetic abnormality in familial and sporadic ALS cases (Mackenzie et al. 2013). Indeed, 30 % of FALS and 25 % of SALS cases are caused by this repeat expansion (Connolly 2012). Different disease mechanisms have been discussed since the discovery of the hexanucleotide repeat expansion in C9ORF72, but the protein´s function remains poor-understood, such that the underlying mechanisms of how the intronic repeat expansion mutation contributes to neurodegeneration is unclear.

The latest identified mutation to be associated with ALS is a loss-of-function mutation in the TBK1 gene encoding TANK-binding kinase. TBK1 is known to participate in autophagosome-mediated degradation processes. Dysregulation of optineurin as a consequence of mutated TBK1 is now known to be a cause of ALS. Optineurin regulates, for example, autophagy of cytosolic protein aggregation or damaged mitochondria, this highlighting its importance for ALS pathogenesis (Freischmidt et al. 2015, Reuveni et al. 2015).

1.2 Structure and function of C9ORF72

The C9ORF72 gene locus is situated in the short arm of chromosome nine and consists of 12 exons, including 2 alternate noncoding first exons (exons 1a and 1b) as indicated in figure 1. Three C9ORF72 transcripts exist, but transcript 2 and

3 lead to the same 481 amino acids (AS) long isoform encoded by exons 2 to 11. Only transcript 1 uses an alternate splice site, leading to a short isoform that only consists only of 222 AS, extending from exon 2 to 5 (Xiao et al. 2015). Both isoforms are highly expressed in brain and testis, but not in liver or lymphoblast cells. Expression analysis revealed isoform-specific expression alterations during development and adulthood (Atkinson et al. 2015). The function of C9ORF72 remains unknown. Recent biostatistics analysis have found wide homology to the DENN (differentially expressed in normal and neoplastic cells)-like protein family of guanosine exchanging factors (GEFs), which regulate intracellular cell trafficking (Xiao et al. 2015). Possible functions of C9ORF72 include mediation of endocytic trafficking to facilitate autophagy and proteasome function, as well as mediation in RNA metabolism via its interaction with different heterogeneous nuclear ribonucleoproteins (hnRNPs) (Farg et al. 2014). The mutated form of C9ORF72 contains up to hundreds or even thousands of GGGGCC repeats, compared to normal individuals, which have only up to 23 repeats in intron 1. This defect may influence C9ORF72 pathogenesis through a large variety of cellular pathways.

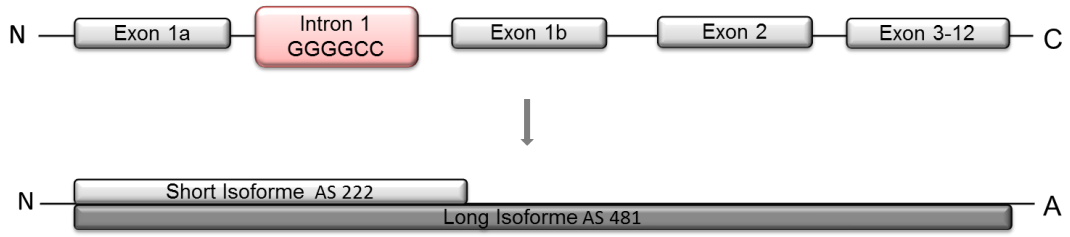

Figure 1 Structure of C9ORF72 gene locus
The gene locus of C9ORF72 consists of 12 exons including 2 alternate noncoding first exons (exons 1a and 1b). A different splice site in the hnRNA of C9ORF72 leads to a long (281AS) and a short (222AS) isoform. The disease-causing mutation in C9ORF72 is a $(GGGGCC)_n$ hexanucleotide repeat expansion in the intron 1. Normal individuals only have up to 23 repeats. Figure is based upon data described in Xiao et al. 2015.

1.3 Disease-causing mechanisms of repeat expansions in neurodegenerative diseases and neuropathology in C9ORF72-ALS

Repeat expansions can produce neurodegeneration through a variety of mechanisms in different diseases. For example, in Friedreich's ataxia, repeat

expansions in noncoding regions of the *frataxin* gene lead to transcriptional down-regulation and loss of function of associated genes (Delatycki et al. 2000). In Huntington's disease, however, tri-nucleotide expansions in the htt gene, which codes for huntingtin protein, cause abnormal poly-Glu expansions and thereby lead to a gain of function with protein toxicity (Dyer and McMurray 2001). Tri-nucleotide repeats smaller than 26 are normal, whereas repeats larger than 40 are considered to be disease-causing (Myers 2004).

However, several repeat expansion disorders cannot be classified similarly as the two above-mentioned diseases; in recent years, several diseases with an RNA-based disease mechanism have been identified. In myotonic dystrophy, for example, toxic RNA aggregates can emerge from expansions in noncoding transcribed gene regions. These nuclear RNA foci can sequester RNA binding proteins, and their resulting functional lack propagates to mis-regulation of gene splicing or transcription of numerous other non-repeat containing RNAs, ultimately leading to RNA dysregulation. Some repeat expansions, i.e. those occuring in fragile X tremor ataxia syndrome, have been shown to produce non-ATG–initiated peptides. These peptides build intracellular aggregates, which could also contribute to neurodegeneration (Todd 2011).

C9-ALS is termed a hexanucleotide repeat expansion disease, because normal individuals have 30 or fewer GGGGCC repeats, while abnormal repeat numbers in ALS patients can number in the 100s. A strict cut-off of 30 repeats must be used with caution, because healthy individuals can have 30 or few more hexanucleotide repeats (Manuscript 2014). Previous research on the diseases described above and other repeat expansion diseases has led to three major hypotheses about the mechanisms evoking neurodegeneration in C9-ALS, as illustrated in figure 2 A (Taylor 2013).

The first hypothesis asserts that the repeats construct a specific tertiary structure, called G-quadruplexes (compare figure 2 B), that hinder expression of the C9ORF72 gene, leading to a loss of function as in the case of Friedreich´s ataxia (haploinsufficiency). However, Friedreich´s ataxia follows a recessive inheritance pattern indicating involvement of both alleles, whereas C9ORF72 has a dominant inheritance pattern (Taylor 2013). This fact, along with the understanding that other genes that are involved in ALS pathogenicity make it unlikely that a loss of

function of C9ORF72 protein can be the only cause of the disease. A second hypothesis of disease mechanism holds that the RNA-mediated toxicity of noncoding repeat G-quadruplexes associate with RNA-binding proteins, leading to abnormal RNA splicing (gain of function). Heterogeneous nuclear ribonucleoprotein A1 (hnRNPA1) and nucleolin, both of which are RNA binding proteins, have already been shown to bind to GGGGCC repeats, in support of the notion of RNA mediated toxicity (Taylor 2013, Sareen et al. 2013). A third potential mechanism evokes the cytotoxicity of RAN protein aggregation. These proteins are generated by repeat-associated non-ATG (RAN) translation, where translation starts without an initiating AUG codon, but rather in secondary structures built by the repeats. This scenario is analogous to the secondary structures of internal ribosomal entry sites (IRES), as observed for spinocerebellar ataxia type 8 or fragile X tremor/ataxia syndrome (FXTAS) (Taylor 2013). This unconventional translation occurs in all reading frames of the sense and antisense transcripts, leading to six different long homopolymeric peptides (Tao et al. 2015). The aggregates can consist of poly Gly-Ala, Gly-Pro or Gly-Arg and poly Pro-Arg, Pro-Gly,or Ala-Pro, as shown in Figure 2 C. All dipeptide repeat proteins have been detected in insoluble, high molecular weight materials within cerebellar extracts from postmortem brain of C9ORF72 patients. Additionally, the dipeptide aggregates have been found in hippocampus, and throughout the neocortex (Todd 2011, Gendron et al. 2013, Taylor 2013, Mackenzie et al. 2013). It remains unclear if the RAN translation products are toxic or how they might influence pathology. Recent studies show that dipeptide repeats (DPRs) cause nucleolar stress, followed by impairment of stress granule formation and rRNA synthesis, thereby leading to cell death (Tao et al. 2015). In addition, patients with C9ORF72 repeat expansion show pathological accumulations of TDP-43 within neuronal and oligodendroglial inclusions in the frontal and temporal cortex, hippocampus and pyramidal motor system. There are also p61 and ubiquitine positive, but TDP-43 negative cytoplasmic and intranuclear inclusions in such cases. Furthermore, there are nuclear RNA foci in hippocampus, frontal cortex and cerebellum (Mackenzie et al. 2013).

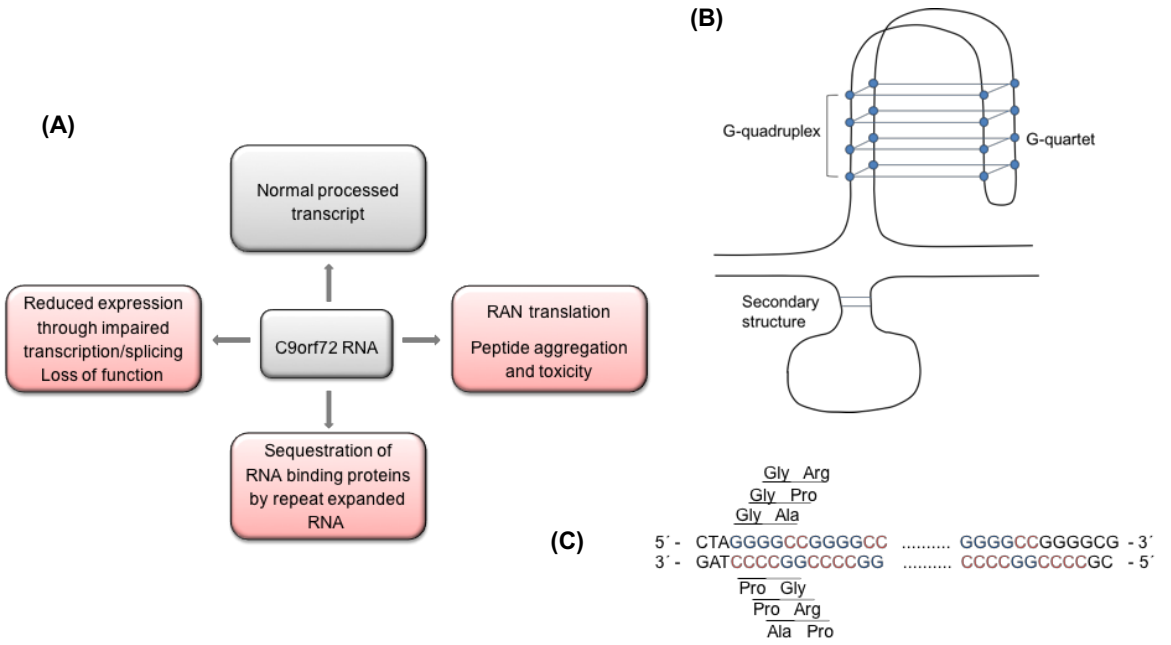

Figure 2 Scheme of disease-causing mechanisms in C9-ALS
(A) Possible disease-causing alterations include loss of function mutations, peptide aggregation of RAN translation products and RNA dysregulation due to RNA foci. (B) G-quadruplex formation of guanine-rich repeats, G bases bind to form square planar structures called G-quartets. These G-quartets then build a G-quadruplex and impair DNA transcription or build RNA aggregates; (C) Sense and antisense homopolymeric dipeptides in all reading frames are generated by RAN translation of GGGGCC or CCCCGG repeats. Figure is based upon data shown in Gendron et al. 2013, Taylor 2013 and Todd 2011.

1.4 DNA damage in ALS

An accumulation of DNA damage has been associated with many neurodegenerative disorders such as Alzheimer´s disease and Parkinson´s disease. Accumulation of DNA damage also occurs in fALS cases associated with FUS mutations. FUS is known to be important for efficient DNA repair through its interaction with HDAC1, a histone deacetylase responsible for cell cycle gene expression and DNA repair (Wang et al. 2013). Through the interaction between C9ORF72 and FUS or through its independent function in nuclear trafficking processes, C9ORF72 expansions may also contribute to defective DNA repair meachanisms, thereby exacerbating the accumulation of DNA damage. Additionally, by the formation of hairpins or G-quadruplexes, hexanucleotide repeat expansions of C9ORF72 could increase the exposure of cellular nucleic acids to DNA damage, such as arises from ionizing irradiation. Furthermore, the varied structure of the repeat expansions may impair polymerase function or may

even sequester proteins important for DNA repair, thus increasing transcriptional and genomic instability (Haeusler et al. 2016). Accumulation of DNA damage and impairment of DNA repair may increase the vulnerability of motoneurons to various types of cell stress, leading to elevated levels of apoptosis.

1.5 Laboratory model systems in ALS research and different types of stem cells

The investigation of postmortem ALS tissue has enabled the identification of culpable ALS genes. As it is not yet possible to isolate and culture viable motoneurons from patients, different laboratory model systems have been established to study ALS pathogenesis. These laboratory model systems include various cell systems and animal models, including the roundworm *Caenorhabditis elegans*, the zebrafish, the fruit fly *Drosophila*, and rodents (Lemmens et al. 2007, Chen et al. 2011). The first of these transgenic rodent animal models to be developed was a mouse overexpressing the fALS mutated form of SOD1 gene (Gurney et al. 1994). These mice develop a motoneuron disease comparable to that observed in ALS patients, including a progressive paralysis. Surprisingly, knock-out of SOD1 does not cause ALS pathology in mice (Sentman et al. 2006). Other rodent models based on the TDP-43 or FUS gene have been also developed and rodent models incorporating the C9ORF72 gene have been generated now (Hukema et al. 2014, O'Rourke et al. 2015, Hayes and Rothstein 2016, Liu et al. 2016). Many of these models clinically resemble aspects of ALS, but do not fully emulate the disease. For example, O´Rourke et al. developed transgenic mice using a construct containing the whole C9ORF72 gene. They found in these mice sense and antisense RNA foci, as well as DPR proteins, but no evidence for motoneuron degeneration (O'Rourke et al. 2015). In 2016, Jiang et al. developed transgenic mouse lines using constructs containing C9ORF72 exons 1–5. As in previous studies, these mice did not show motoneuron degeneration, but did manifest a cognitive phenotype (Hayes and Rothstein 2016). Recently, Liu et al. (2016) reported the generation of a mouse line by introduction of mutant C9ORF72-BAC constructs, displaying motoneuron degeneration as well

as cortical and hippocampal neurodegeneration. Additionally, they observed RNA foci and RAN translation products in these transgenic mice with full size C9ORF72 (Liu et al. 2016). These discrepancies are difficult to interpret, and there is so far no consensus that these findings are applicable to the human disease.

With respect to cell systems in ALS research, it is possible to isolate from animal models hippocampal or motoneurons, which can than be studied in vitro regarding morphology and deviations from normal cell behaviour (Grabrucker et al. 2009, Schlachetzki et al. 2013). Another common in vitro technique entails the transfection of rodent neurons or cell lines with plasmids containg ALS-causing mutations. These studies revealed, for example in the case of mutant SOD1, pathological mechanisms such as protein aggregation, and increased signs of apoptosis in transfected cells in culture (Bruijn et al. 2004, Boillée et al. 2006).

Despite these successes, it has been hitherto impossible to transfect the large DNA repeats or RNA foci of the expanded C9ORF72 hexanucleotide repeat expansion into a cell line or primary cell system, so as to afford a study of the effects of the repeats or RNA pathology of C9-ALS. Additionally, the absence of a specific, non-cross-reactive antibody against the C9ORF72-encoded protein renders studies of intrinsic C9ORF72 a difficult challenge. The establishment of human embryonic stem cells (hESCs) and particularly human-induced pluripotent stem cells (hIPSCs) and their differentiation into motoneurons seem to be a promising model system to study ALS aetiology in a human setting, with intrinsic full spectrum pathologies (Zhang et al. 2001, Hu and Zhang 2009).

1.6 Stem cells and stem cell potency

A defining characteristic of stem cells is their ability for asymmetric division, self-renewal and differentiation into different cell types (Zukor and He 2011). The potential to differentiate into various cell types is termed as the potency. For example, the zygote up to the 16-cell state of the morula can form a complete organism, including embryonic and extra-embryonic tissues. Therefore, it is defined as being totipotent. When the first differentiation occurs in the blastocyst stage, an inner cell mass (ICM)/embryoblast can be distinguished from the outer cell mass/trophoblast, surrounding the ICM. As the embryoblast cannot longer give

rise to extra-embryonic tissues, but is the progenitor of all embryonic tissues, the ICM is defined as pluripotent (Thomson et al. 1998, Amit et al. 2000). Classically, the ICM is divided into the three germ layers ectoderm, mesoderm and endoderm, which together compromise the organism. The ectoderm includes skin or nervous system, mesoderm builds bone or muscle cells, and endoderm compromises other tissues such as the lung epithelia and gastrointestinal tract.

Multipotent stem cells are able to form a finite number of cell lineages. Throughout the life of an organism, these types of stem cells reside in stem cell niches, which support the survival of stem cells in an undifferentiated state by secreting factors such as transforming growth factor β (TGF-β) (Fuchs et al. 2004, Jaenisch and Young 2008). Multipotent stem cells are responsible for the regeneration of the epidermis and the renewal of the hematopoietic system. In contrast to multipotent stem cells, lymphoid or myeloid progenitor cells that can differentiate into only a few specific cell types are defined as oligopotent. Finally, monopotent cells are committed to form one specialised cell type, i.e. spermatogonial stem cells (Fuchs et al. 2004).

The maintenance of stem cells at different potency levels depends on a specific gene expression pattern. For example, human embryonic stem cells (hESCs) typically express the nuclear factors NANOG, OCT4 (POU class 5 homebox) and SOX2 (Sex determining region Y-box 2) (Jaenisch and Young 2008). Additionally, hESCs express telomerase and alkaline phosphatase. Furthermore, specific glycoproteins TRA-1-60 and TRA-1-81 and glycolipid antigen SSEA4 (stage specific embryonic antigen) are expressed in pluripotent stem cells (Thomson et al. 1998). The potential of pluripotent hESCs is manifest when they form three-dimensional embryoid bodies (EBs), and differentiate into all three germ layers. Exposure to extrinsic factors can be used to preserve pluripotency and proliferation capacity of stem cells. Specifically, fibroblast growth factor 2 (FGF2), insulin-like growth factor 2 (IGF2), TGF-β, activin, nodal and bone morphogenic proteins (BMPs) are among the factors known to promote self-renewal capacity and inhibit differentiation of stem cells (Ding et al. 2010, Pera and Tam 2010).

1.7 Human embryonic stem cells and human induced pluripotent stem cells

In 1998, hESCs were first isolated from embryos and cultured for research purposes. There arose some considerable controversy about hESCs in relation to religious dictates, and fears about human cloning and deliberate modification of human characteristics (Hyun 2010). Indeed, publically-funded hESC research remains illegal in the United States.

In the face of prohibitions, the IPS cell technique presented by Takahashi and Yamanaka in 2006 opened a new avenue for research, while circumventing ethical controversies. IPSCs can be generated by reprogramming of mitotically active somatic cells, using retroviruses to insert into the somatic cells four particular stem cell–associated genes: *OCT4*, *SOX2*, *v-myc myelocytomatosis viral oncogene homolog (c-MYC)*, and *Krueppel like factor (KLF4)* (Hyun 2010). These differentiated somatic cells can be fibroblasts or keratinocytes, thus obviating any need for embryonic tissues (Linta et al. 2012). Keratinocytes present a distinct advantage over fibroblasts in that they can be harvested simply by plucking a hair, whereas fibroblasts must be cultured from a more invasive skin biopsie. For the reprogramming procedure, the factors OCT4, SOX2, c-MYC and KLF4 are needed to induce chromatin changes and epigenetic modifications of DNA methylation, thereby leading to selective gene expression pattern and reattribution of pluripotency (Minal Patel & Shuying Yang 2011). These factors can be introduced into the nucleus via lenti- or retroviruses, and by non-viral methods. Lentiviruses are able to infect proliferating and non-proliferating cells compared to retroviruses, but since these originate from immunodeficiency viruses, safety concerns are pronounced.Through the process of viral transduction, the reprogramming factors become integrated into the host genome, and can later be excised via cre-lox-P system to generate IPSCs lacking the exogenous transgenes (Zhou and Zeng 2013). After the reprogramming process, hIPSCs have a characteristic undifferentiated morphology including a round shape, a large nucleus to cytoplasmic ratio, and ostentatious nucleoli, as illustrated in Figure 3 (Aasen et al. 2008). Furthermore, they express genes characteristic of stem cells, including the nuclear factors NANOG, OCT4 and SOX2, as well as the surface markers SSEA4, TRA-1-60 and TRA-1-80 (Aasen et al. 2008, Linta et al. 2012, Illing et al. 2013). However, direct reprogramming of keratinocytes into IPSCs is technically

demanding due to the inherently low reprogramming rate, and the prolonged interval required for reprogramming.

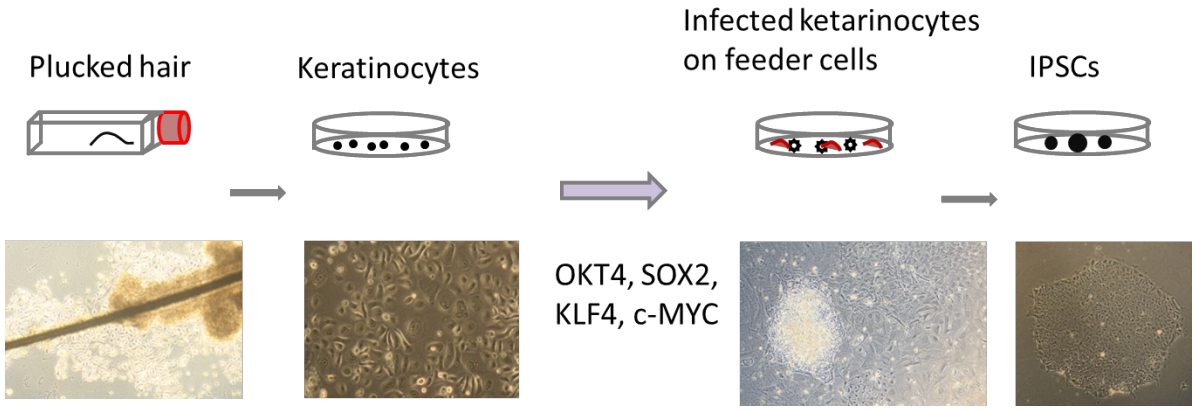

Figure 3 Reprogramming of human keratinocytes
Bright-field microscopy and schematic images of the reprogramming process. Keratinocytes are seen emerging from the outer root sheath of a plucked human hair. Keratinocytes are infected with a lentivirus transducing a multicistronic cassette harbouring *OCT4*, *SOX2*, *KLF4* and *c-MYC* on two subsequent days. After one day, infected cells can be split onto irradiated feeder cells. About one week later, small hiPSC colonies can be picked manually and cultured under feeder-free conditions. Figure is based upon data shown in Linta et al. 2012.

1.8 Embryonic and neuronal differentiation of human stem cells

After the fertilisation of a tertiary folliculus by a sperm, the zygote divides exponentially until it reaches the 64 cell stage, which is known as the blastocyst. It is at the blastocyst stage that the first differentiation into trophoblast and embryoblast occurs. The trophoblast gives rise to extra-embryonic tissues like the chorion, which is the embryonal part of the placenta. The embryoblast gives rise to all intra-embryonic tissues. In this process, the embryoblast first divides into the epi- and the hypoblast. The primitive ectodermal cells of the epiblast engender all three germ layers, from which develop the various intraembryonic structures. At the onset of hIPSCs differentiation, there arise three-dimensional embryoid bodies (EBs) that correspond to the gastrula stage in general embryonic development. The subsequent neurulation steps and motoneuron formation can be imitated through the use of specific growth media and conditions. The first step of embryonic neurogenesis is the formation of the neuronal plate, which gives rise to the the neural tube, when the edges of the plate elevate and fuse above the neural plate thickening. The neural tube is divided into the ventral floor plate and the

dorsal roof plate, which together give rise to the entire central nervous system. The ventral neurons develop as efferent cells and the dorsal neurons as afferent cells, in response to the local concentration of signalling factors. The formation of the neural tube is marked by neuronal precursor (NP) cells expressing proteins such as paired box 6 (PAX6) or SOX1, and thus represents also the first essential step in the neuronal differentiation of hIPSCs (Hu and Zhang 2009). We developed NP cells after plating the embryoid bodies and supplying media with the necessary neural growth factors. HIPSCs can be differentiated into specific types of neurons such as motoneurons or dopaminergic neurons, when the in vivo neurulation process is adequately mimicked in vitro. Among the most important factors for motoneuron development are sonic hedgehog (SHH) and retinoic acid (RA). SHH is considered to be a ventralizing morphogen leading to the floor plate development and motoneuron differentiation (Okada et al. 2004). RA is considered to be a caudalizing morphogen which promotes formation of motoneurons and other cell types in the brainstem and the spinal cord (Mobassarah et al. 2014). With the addition of RA and SHH, motoneuron differentiation is further induced, leading to the formation of OLIG2 expressing motoneuron progenitors (pMNs), as reviewed by Jessell in 2000. When the pMN- spheres are replated after 1 week in suspension, the expression level of oligodendrocyte lineage transcription factor 2 (OLIG2) decreases, while that of homebox protein 9 (HB9) increases (Jessell 2000). This divergence marks the final differentiation into postmitotic motoneurons, which occurs after 28 days of differentiation in culture. Mature motoneurons express the motoneuron specific marker sternberger monoclonal-incorporated antibody 32 (SMI-32), and can form synaptic contacts with other neurons and with myocytes (Demestre et al. 2015). As such, the co-cultivation of interacting motoneurons and skeletal muscle cells differentiated from IPSCs from the same patient offers a powerful technique for studying the behaviour of ALS-affected cells.

1.9 Neuronal synapses and the neuromuscular junction

The human nervous system consists of billions of neurons, which communicate amongst themselves via synaptic contacts. The motoneuron axon gives rise to axonal terminals that form junctions with the dendrites, soma, and axonal terminals from other neurons. Chemical signalling between one neuron and another is obtained when depolarization of the presynaptic axon leads to calcium-dependent fusion of synaptic vesicles and release of their stored contents by exocytosis. The neurotransmitter molecules then diffuse across the 30 nm wide synaptic cleft and interact with receptors at the postsynaptic side. Synapses are commonly differentiated as being excitatory or inhibitory, depending on the effect of receptor activation on the polarization of the post-synaptic membrane. Glutamate, for example is the typical excitatory neurotransmitter signalling between the upper and the lower motoneuron.

The synapse consists of a number of structural components, notably those composing the presynaptic density, which is an electron-dense active zone containing SNAP/SNARE proteins. Fusion of the vesicle is mediated by these proteins, and the general architecture and function of the active zone is orchestrated by Bassoon (BSN), a large protein of the presynaptic matrix. These cytoskeletal molecules are produced in the somatic Golgi apparatus and delivered to the synaptic terminal by anterograde transport within dense core vesicles; their delivery to the active zone of the axon terminal axon represents an important step in synaptogenesis and maintenance of existing synapses.

On the opposing membrane of the synaptic cleft there is another electron-dense structure known as the postsynaptic density (PSD). This structure serves as an anchor for neurotransmitter receptors, subserves signal transduction, and mediates many other functions. The PSD is vastly complex, consisting of a large variety of different proteins (Sheng and Hoogenraad 2007, Sheng and Kim 2011). SAP90/PSD-95 is a typical scaffolding molecule of the PSD. It directly interacts with N-methyl-D-aspartate (NMDA) receptors that mediate excitatory glutamate transmission and proline-rich synapse-associated proteins (ProSAP/Shank), which together represent the master scaffolding molecules of the PSD. Within the PSD, the ProSAP/Shank molecules are juxtaposed between the membrane-bound receptors and the actin cyto-

skeleton of the post-synaptic neuron (Boeckers et al. 2005). This molecular scaffold has the ability to induce spinogenesis, maturation of spines and recruitment of glutamate receptors, thereby creating functional synapses (Roussignol et al. 2005). The PSD undergoes continual molecular changes in developing and mature neurons, especially in response to neuronal activity (Sheng and Kim 2011).

The neuromuscular junction (NMJ) is a specialized synapse that connects the axonal terminal of the lower motoneuron to the motor endplate of a muscle fibre, where contractile action potentials can be initiated. In contrast to the glutamatergic synapse between the upper and the lower motoneuron, the typical excitatory neurotransmitter of the NMJ leading to muscle contraction is acetylcholine (ACh). A notable structural feature of the NMJ motor endplate is the extensive infoldings of the sarcolemma, which serve to increase the surface area available for ACh receptor localisation. The initiation and maintenance of NMJs requires reciprocal signalling between the muscle cell and the motoneuron, otherwise the motoneuron denervates the receipient myocyte, leading to atrophy and degeneration.

1.10 Aims of this thesis

An important prerequisite for the study of ALS cellular disease processes is having a wide range of model systems, which emulate pathologies of human disease as accurately as possible. Model systems in ALS research typically include cell lines, primary cell culture, different animal models and postmortem tissue from patients. In the recent years, aspects of ALS pathomechanisms have been studied using patient-derived IPSCs and their respective differentiated MNs in culture (Almeida et al. 2013, Donnelly et al. 2013, Sareen et al. 2013, Devlin et al. 2015). These studies *in vitro* are assuming an increasing role in research because they offer a human model system of viable motoneurons with patient-specific genetic background, which is critical considering the multiple and complex genetic factors. Additionally, the ALS-causing mutation in the IPSCs has not been induced artificially, such that no overexpression of C9ORF72 or other mutated proteins, is needed. ALS research focussing on the C9ORF72 mutation presents a number of different obstacles. There is currently no technique to transfect the huge repeat expansion of C9ORF72 that might enable us to study different pathologies, as shown in other cell models of other ALS-mutated proteins such as FUS or TDP-43 (Dormann and Haass 2011, Mitchell et al. 2013). In addition, the analysis at the protein level is limited, because the hitherto available several C9ORF72 antibodies are considered to be unspecific (Satoh et al. 2012).

Given the considerations, the aims of this doctoral thesis were (1) to detect the precise localisation of wt C9ORF72 in neuronal systems by overexpression experiments, and (2) compare immunofluorescence (IF)-stainings using commercial antibodies and in-house generated antibodies against C9ORF72. An additional aim (3) was to assertain whether some of the pathomechanisms associated with the C9ORF72-ALS mutation could be reproduced in our systems in vitro using different cellular models. Therefore, we analysed synapse numbers and RAN translation products in rat hippocampal neurons overexpressing C9ORF72 or dipeptide constructs. To address our final objective (4), we analysed RNA and protein expression alterations in IPS cell lines created from C9ORF72-ALS patients. We stressed the cells to provoke alterations, given that other ALS associated proteins result in defective response to stress and protein aggregation (Deng et al. 2014, Ishigaki et al. 2014, Lenzi et al. 2015, Japtok et al. 2015).

2. Material and methods

2.1 Materials

Table 1 Tools and machines

Tools and machines	Company
Cell culture plates 6 well	Nunc, Wiesbaden, Germany
Cell culture plates 24 well	Nunc, Wiesbaden, Germany
Cell culture flasks 25 cm²	Nunc, Wiesbaden, Germany
Cell culture low-attachement T75 flasks	Nunc, Wiesbaden, Germany
Cell culture T175 flasks	Nunc, Wiesbaden, Germany
Cell scraper	TPP, Trasadingen, Switzerland
Centrifuge Avanti J-25	Beckmann, Krefeld, Germany
Centrifuge Multifuge	Heraeus Holding, Hanau, Germany
Cover glasses 13 mm	Menzel, Braunschweig, Germany
Cuvettes	Sarstedt, Nürnbrecht, Germany
Electroporation machine	BioRad, Munich, Germany
Eppendorf cups	Eppendorf, Hamburg, Germany
Erlenmeyer flasks	VWR, Darmstadt, Germany
Falcon tubes 15 ml and 50 ml	Nunc, Wiesbaden, Germany
Freezer tubes 1.8 ml	Nunc, Wiesbaden, Germany
gel collector	BioRad, Munich, Germany
Glutathione Magnetic Beads	Thermo Scientific, Waltham, USA
iEMS reader	Thermo Scientific, Waltham, USA
Incubator BBD 6220	Thermo Scientific, Braunschweig
Incubator HERAcell	Thermo Scientific, Braunschweig
Libra S12 UV/Vis Spectrophotometer	Biochrom, Berlin, Germany
Microscope Axiovert 25	Zeiss, Oberkochen, Germany
Microscope Axiokope 2 mot plus	Zeiss, Oberkochen, Germany
Microwave	BSH, Giengen, Germany

µ dishes 35 mm, treated	Ididi, Munich, Germany
Neubauer counting chamber	Brandt, Wertheim, Germany
Nanodrop 2000 spectrophotometer	Thermo Scientific, Waltham, USA
Object slides	Menzel, Braunschweig, Germany
Pasteur pipettes	Brandt, Wertheim, Germany
PCR Mastercycler	Eppendorf, Hamburg, Germany
Pipette tips 10 µl, 200 µl, 1 ml	Eppendorf, Hamburg, Germany
Pipettboy	Hirschmann, Eberstadt, Germany
Pipettes	Eppendorf, Hamburg, Germany
PVDF Membrane Hybond-P	GE Healthcare, Buckinghamshire, GB
Reaction tubes 0.5 ml, 1.5 ml, 2 ml	Eppendorf, Hamburg, Germany
RotorGene Q System	Quiagen, Hilden, Germany
RT-PCR stripes	Quiagen, Hilden, Germany
Shaker IKA KS 260 basic	IKA Werke, Breisgau, Germany
Sterile bench Laminar flow	Nunc, Wiesbaden, Germany
Sterile filters 0.45 µm	Schleicher & Schuell, Dassel, Germany
Thermo mixer	Eppendorf, Hamburg, Germany
Thermo cycler	Eppendorf, Hamburg, Germany
UV transluminator	Leica, Unterendfelden, Switzerland
Vortexes	VWR, Darmstadt, Germany
Water bath 37°C	VWR, Darmstadt, Germany
Whatman gel blotting papers	GE Healthcare, Buckinghamshire, GB

Table 2 Software and e-tools

Software	**Company**
Axio Vision 4.8.3.0	Zeiss, Oberkochen, Germany
GENtle 1.9.4	Magnus Manske, University Cologne, Germany
Image J 1.46	Open source, NIH, USA

Mendeley	Mendeley Ltd., London, UK
PRISM Version 5.1	GraphPad, La Jolla, USA

Table 3 Markers

DNA Ladder	**Size**	**Company**
Gene Ruler 1 kb DNA Ladder	250 bp – 10kbp	Thermo Scientific, Waltham, USA
Protein Ladder	**Size**	**Company**
Page Ruler Prestained Protein Ladder protein	170, 130, 100/92, 70, 55, 40, 35, 25, 15, 10 kDa	Fermentas, Amherst, USA

Table 4 Kits

Kit	**Company**
Genomed Jet Quick Gel Extraction Spin Kit/ 50	Genomed, Leinfelden-Echterdingen, Germany
QIAamp DNA Mini and Blood Mini Handbook	Quiagen, Hilden, Germany
QIAquick Spin Handbook	Quiagen, Hilden, Germany
Quiagen Plasmid Midi Kit	Quiagen, Hilden, Germany
RNAeasy Mini Kit	Quiagen, Hilden, Germany
Rotor-Gene SYBR Green RT-PCR Kit	Quiagen, Hilden, Germany
StemLight Pluripotency Kit	Cell Signalling, Danvers, USA
µMACS Epitope Kit	Miltenyi Biotec, Bergisch Gladbach, Germany
Pierce ECL Western blotting substrate	Thermo Scientific, Waltham, USA

Table 5 Expression constructs

Construct	Plasmid	Restriction sites
C9ORF72 long-myc	pCMV6-XL5(+)NM_018325.1	BamHI, KpnI
C9ORF72 long-GFP	pEGFP-C1(+)NM_018325.1	BamHI, KpnI
C9ORF72 short-myc	pCMV6-XL5(+)NM_145005.3	SgfI, MluI
GA 10	pCDNA3.1(+)HA Tag-GA10	BamHI, XbaI
GA 100	pCDNA3.1(+)HA Tag-GA100	BamHI, XbaI
GP 10	pCDNA3.1(+)HA Tag-GP10	BamHI, XbaI
GP 100	pCDNA3.1(+)HA Tag-GP100	BamHI, XbaI
Control GFP	pEGFP-C1	

Table 6 Antibodies
If a manufacturer is not mentioned, the antibodies were generated in-house

Primary Antibodies	Dilution	Species	Company
ß-Actinin	1:200 (IF)	Mouse	Chemcon
Bassoon	1:1000 (IF)	Rabbit	Synaptic Systems
ß-III-Tubulin	1:1000 (IF)	Rabbit	Chemcon
Caspase-3	1:500 (IF)	Rabbit	R&D Systems
Catenin	1:500 (IF)	Mouse	Abcam
C9ORF72	1:100 (IF)	Rabbit	Santa Cruz
FUS	1:500 (IF)	Rabbit	Bethyl
GFP	1:3000 (WB) 1:2000 (IF)	Mouse	Bd Bioscience
HDAC1	1:1000 (IF)	Rabbit	Bethyl
hnRNPK1	1:200 (IF)	Rabbit	Epitomics

MYC	1:750 (IF) 1:3000 (WB)	Mouse	Roche
MAP2	1:500 (IF)	Mouse	Sigma Aldrich
Nanog	1:200 (IF)	Rabbit	Cell signalling
NEFH	1:1000 (IF)	Chicken	Covance
OCT4	1:200 (IF)	Rabbit	Cell signalling
Poly(GA)	1:1500 (IF)	Rabbit	Cosmobio
SOX2	1:200 (IF)	Rabbit	Cell signalling
SSEA4	1:200 (IF)	Mouse	Cell signalling
SYP	1:500 (IF)	Guinea pig	Synaptic Systems
TDP-43	1:500 (IF)	Rabbit	Cosmobio
TIA1	1:1000 (IF)	Goat	Santa Cruz
TRA-1-60	1:200 (IF)	Mouse	Cell signalling
TRA-1-81	1:200 (IF)	Mouse	Cell signalling
γH2AX	1:2000 (IF)	Rabbit	Abcam

Secondary Antibodies	**Dilution**	**Modification**	**Company**
Anti-mouse IgG	1:1000	Alexa Fluor 488	Invitrogen
Anti-mouse IgG	1:1000	Alexa Fluor 568	Invitrogen
Anti-mouse IgG	1:1000	Alexa Fluor 647	Invitrogen
Anti-rabbit IgG	1:1000	Alexa Fluor 488	Invitrogen
Anti-rabbit IgG	1:1000	Alexa Fluor 568	Invitrogen
Anti-rabbit IgG	1:1000	Alexa Fluor 647	Invitrogen
Anti-guinea pig IgG	1:1000	Alexa Fluor 647	Invitrogen
Anti-goat IgG	1:1000	Alexa Fluor 568	Invitrogen

Table 7 Chemicals used for cell culture

Substance	Company
LE Agarose	Lonza, Basel, Suitzerland
Ampicillin	Roth, Karlsruhe, Germany
Antibiotic Antimycotic	Invitrogen, Carlsbad, USA
Colchicine	Eurobio, Les Ulis, France
DMEM	Invitrogen, Carlsbad, USA
DMEM/F12	Invitrogen, Carlsbad, USA
Donkey serum	AbD Serotec, Puchheim, Germany
Epilife & HKGS supplement	Invitrogen, Carlsbad, USA
FBS (fetal bovine serum)	Invitrogen, Carlsbad, USA
Glycerine	Sigma Aldrich, St. Louis, USA
Goat serum	Chemicon, Billerica, USA
IPTG	Promega, Wisconsin, USA
Kanamycin	Roth, Karlsruhe, Germany
LB Broth Base	Thermo Scientific, Waltham, USA
2-YT Broth	Sigma Aldrich, St. Louis, USA
mTeSR1	Stemcell Technologies, Vancouver, USA
Non-essential aminoacids NEAA	Invitrogen, Carlsbad, USA
Neurobasal	Invitrogen, Carlsbad, USA
Optifect	Thermo Scientific, Waltham, USA
Polyfect	Quiagen, Hilden, Germany
PBS (phosphate buffered saline)	Invitrogen, Carlsbad, USA
PBS - - (without Ca, Mg)	Invitrogen, Carlsbad, USA
Stem cell mFreSR	Stemcell Technologies, Vancouver,USA

SOB (super optimal broth)	BD Bioscience, Heidelberg, Germany
Streptomycin sulphate	Gibco, Gaithersburg, USA
Synth-a-Freeze	Invitrogen, Carlsbad, USA
Sorbitol	Sigma Aldrich, St. Louis, USA

Table 8 Supplements

Substance	**Company**
Ascorbic Acid	Sigma-Aldrich, St. Louis, USA
B27	Invitrogen, Carlsbad, USA
cAMP	Sigma Aldrich, St. Louis, USA
Heparin	Sigma Aldrich, St. Louis, USA
Purmorphamine	Calbiochem, Glibbstown, USA
Recombinant human BDNF	Peprotech, Rocky Hill, USA
Recombinant human GDNF	Peprotech, Rocky Hill, USA
Recombinant human IGF-2	Peprotech, Rocky Hill, USA
Retinoic acid (RA)	Sigma-Aldrich, St. Louis, USA
Rock-Inhibitor Y-27632	Ascent Scientific, Avonmouth, UK

Table 9 Coatings

Substance	**Company**
Collagen IV	Sigma-Aldrich, Taufkirchen, Germany
Laminin	Roche, Basel, Switzerland
Matrigel	BD Bioscience, San Jose, USA
Poly-*L*-Ornithine	Sigma-Aldrich, Taufkirchen, Germany
Poly-*L*-Lysin	Sigma-Aldrich, Taufkirchen, Germany

Table 10 Enzymes

Enzyme	Company
BamHI	Fermentas, St.Leon-Rot, Germany
Dispase for Keratinocytes	BD Bioscience, San Jose, USA
HESCs-qualified Dispase	Stemcell Technologies, Vancouver, Canada
High-Fidelity DNA Polymerase	New England BioLabs, Massachusetts, USA
Ligase	Promega, Fichtburg, USA
Lysozyme	Sigma-Aldrich, Taufkirchen, Germany
TrypLE Express	Invitrogen, Carlsbad, USA
Trypsin Versen	Invitrogen, Carlsbad, USA
XhoI	Fermentas, St.Leon-Rot, Germany

Table 11 Chemicals, buffers and mixtures

Substance	Company/Components
Acrylamid stock solution	Applichem, Darmstadt, Germany
APS	Applichem, Darmstadt, Germany
Blocking milk	1xTBS; 5 % milk powder; 0.1 % Tween
10x Blot buffer	180 g Glycerin; 37.88 g Tris; ad 1 l H2O
Bradford reagent	Sigma Aldrich, St. Louis, USA
Bromophenol blue	Sigma Aldrich, St. Louis, USA
Complete mini protease inhibitors	Roche, Basel, Switzerland
EDTA	Sigma Aldrich, St. Louis, USA
Ethanol	Sigma Aldrich, St. Louis, USA
Glutathione Sepharose	GE Healthcare, Freiburg, Germany

Glycine	Applichem, Darmstadt, Germany
Isopropanol	Sigma Aldrich, St. Louis, USA
Methanol	Sigma Aldrich, St. Louis, USA
Milk powder	Applichem, Darmstadt, Germany
PFA	Merck, Darmstadt, Germany
ProLong Gold Antifade Mountant	Thermo Scientific, Waltham, USA
RedSafe	INtRON biotechnology, Korea
SDS	Applichem, Darmstadt, Germany
Sodium chloride	Applichem, Darmstadt, Germany
TAE	Thermo Scientific, Waltham, USA
10x TBS (1l):	24.2 g Tris; 80 g NaCl; pH 7.6
1x TBST(1l)	100 ml 10x TBS; 10 ml 10 % Tween; ad 1 l H2O
TEMED	Applichem, Darmstadt, Germany
Tris	Applichem, Darmstadt, Germany
Triton X 100	Roche, Basel, Switzerland
Tween	Applichem, Darmstadt, Germany

2.2 Molecular biologic methods

2.2.1 Plasmid purification from bacteria

Following instructions in the Jetstar Plasmid Purification Kit Handbook (Genomed), for each construct a 50 ml volume of the over-night culture was centrifuged for 10 min at 4500 rpm at RT and the supernatant was discarded. The pellet was resuspended in 4 ml resuspension buffer E1 including RNase. The alkali lysis was performed with 4 ml lysisbuffer E2 for 5 min at RT. Lysis was interrupted by adding 4 ml of the acid neutralisation buffer E3. The precipitate was pelleted by centrifugation for 30 min at 4500 rpm. The supernatant was pipetted through 4 layers of gauze bandage into the columns of the kit, which had been pre-activated with 10 ml equilibration buffer E4 before. The loaded columns were washed twice

with washing buffer E5. The eluted DNA was precipitated with 5 ml of elution buffer E5. After the addition of 3.5 ml isopropanol, the eluate was centrifuged for 1 h at 4500 rpm at 4 ° C. The supernatant was discarded and 3 ml of 100 % ethanol were added to the pellet. After another centrifugation for 30 min at 4500 rpm at 4 ° C, the new supernatant was discarded and the pellet was air-dried for about 10 min. Finally, the pellet was resuspended in 50 µl aqua demin.

2.2.2 DNA purification from cultured cells

For the DNA purification of hIPSCs, the colonies of one well were washed with PBS - - and were then detached from the cell plate with trypsin-versen (500 µl) treatment for 10 min at 37 ° C. The colonies were dissolved into a single cell solution and centrifuged for 3 min at 300 x g. The cell pellet was resuspended in 200 µl PBS - - and pipetted into a microcentrifuge tube preloaded with 20 µl protease K solution. For cell lysis, 200 µl of buffer AL were added and the suspension was vortexed for 15 sec. After incubation for 10 min at 56 ° C, 200 µl of 100 % ethanol were added, followed by 15 sec pulse-vortexing. After mixing and brief centrifugation, the mixture was applied to the column in a 2 ml receiver tube. After centrifugation for 1 min at 8000 rpm the column was placed into a new collection tube and washed with 500 µl of buffer AW 1. Another centrifugation step for 1 min at 8000 rpm was performed, followed by placement in a new collection tube. Then, 500 µl of buffer AW 2 were added and centrifugation lapplied for 3 min at 14,000 rpm, followed by another minute of centrifugation. For the elution, 200 µl of aqua demin were added and incubated for 5 min at RT. Centrifugation lasted 1 min at 8000 rpm, and the obtained DNA was stored at -20 ° C.

2.2.3 Quantification of DNA concentration

DNA concentration was quantified through measuring the absorption at 260 nm using a spectrophotometer. The purity of the DNA was estimated by the quotient of the absorption quotient at 260 and 280 nm.

2.2.4 Antibody design

The effectiveness of an antibody against a specific antigen depends on many different factors of the epitope. These factors can now be taken easily in consideration with the NHLBI-AbDesigner, an online tool for the design of peptide-directed antibodies. The tool, for example, includes an antigenic index to predict the immunogenicity of a given amino acid sequence. The uniqueness of protein regions and their conservation between different species are taken into consideration, as well as secondary structures and protein hydropathy that could hinder effective antibody binding (Pisitkun et al. 2012). In accordance with these predictions, and given that the antibody against the epitope between C9ORF72 amino acids 112 and 150 shows cross reactivity with GFAP (Satoh et al. 2012), we decided to use two specific regions of the C9ORF72 protein to generate antibodies. The first region contains the amino acids 1 to 100, representing the short isoform of C9ORF72, and the second region extends from amino acid 280 to 380, representing the long isoform.

2.2.5 Enzymatic restriction of DNA

For cloning and restriction analysis, plasmid DNA and PCR products were digested with the restriction enzymes BamHI and XhoI according to the manufacturer´s manual. The restriction reaction took 10 min at 37 ° C, and 30 µl volumes were used:

Enzymatic restriction:	2 µl restriction enzyme 1
	2 µl restriction enzyme 2
	3 µl 10x fast digest green buffer
	2 µl DNA
	Ad 30 µl aqua demin

2.2.6 DNA-agarose-gel electrophoresis

To analyse DNA fragments after enzymatic restriction or PCR, the negatively charged DNA fragments were separated electrophoretically in the agarose gel according to their size. Therefore, we produced a 1 % gel for larger DNA fragments, as follows: 1.5 g agarose were added to 150 ml TAE buffer and heated in a microwave to a final temperature of 100 ° C. After cooling down to 60 ° C, 5 µl/100 ml RedSafe ethidiumbromide were added, and the solution was poured into a gel collector, in which a comb had been placed into the gel to create chambers. After polymerisation of the gel for approximately 15 min, it was placed into an electrophoresis chamber that was filled with TAE buffer. The gel was loaded with the DNA probes that were mixed with 6 x loading dye solution, and a 1kBP-DNA ladder was also loaded in the gel. The DNA probes were separated in the electrical field with a voltage of 90 V – 120 V. The DNA bands were analysed and photographed under UV light and the DNA was extracted from the gel.

50x TAE buffer:	100 ml 1 M EDTA pH 8.0
	42.0 g Tris
	57.0 ml glacial acetic acid
	Ad 1 L aqua demin, pH 8.3
6x loading buffer:	87 % glycine
	40 mM EDTA
	~ 0.1 % bromophenol blue

2.2.7 Extraction of DNA from the agarose gel

After the gel electrophoresis, DNA bands were excised with a scalpel under UV light. Then, the QIAquick Gel Extraction Kit (Quiagen) was used according to the manufacturer's protocol to extract the DNA. Therefore, the agarose was solubilized with a 1:3-fold excess of solution L3 for 15 min at 50 ° C on the shaker and loaded into a column. After centrifugation for 1 min at 12000 rpm, the eluate was discarded and the column was washed with 500 µl of ethanol-reconstituted

L2. After centrifugation for 1 min at 12000 rpm, the eluate was discarded and another centrifugation step was undertaken as before. After incubation for 1 min with 50 µl preheated aqua demin, the DNA was eluted by centrifugation for 2 min at 12,000 rpm.

2.2.8 Ligation of DNA

To ligate the digested DNA fragments with compatible restricted vectors, the Promega ligase was used according to the manufacturer´s manual. The mixture containing an excess of insert was incubated over night at 4 ° C.

Ligation preparation 10 µl:	Vector PGEX 4T1	2 µl
	Insert C9ORF72	3 µl
	Ligase	0.3 µl
	Buffer	1 µl
	H_2O	3.7 µl

2.2.9 Polymerase chain reaction (PCR)

The PCR was used for a selective amplification of specific DNA fragments. 23 – 25 bp-long primers containing 40 – 60 % guanine and cytosine bases, a specific restriction enzyme site, and containing only a few intramolecular secondary structures, were produced to order by MWG Operon Ebersberg, Germany. For the PCR, a thermostable DNA polymerase with proof reading function was used. The annealing step of the PCR was done at 1 ° C above the lowest melting point (Tm) of the different primers because the melting points did not have a huge discrepancy.

Table 12 PCR primer

Primer	Sequence 5` > 3`
C9ORF72 Forward 1 **BamHI**	GAC**GGATCC**ATGTCGACTCTTTGC
C9ORF72 Backward 1 **XhoI**	GCCG**CTCGAG**ATCAAAGATTAATGA
C9ORF72 Forward 2 **BamHI**	GAC**GGATCC**ACAAGGCCTGCTAAAG
C9ORF72 Backward 2 **XhoI**	GACT**CTCGAG**AAGGCTTTCACTAGA

PCR preparation 50 µl:	5x Phusion HF Puffer	10 µl
	10 mM dNTP	1 µl
	10 µM forward Primer	2.5 µl
	10 µM backward Primer	2.5 µl
	100 mM Template DNA	0.5 µl
	Phusion Polymerase	0.5 µl
	H_2O	33 ml

The following PCR program was processed by a thermo cycler:

Table 13 PCR program

Step	Temperature	Time	Repetition
Initial Denaturation	98 ° C	30 s	1 x
Denaturation Annealing Extension	98 ° C Tm Primer 72 ° C	10 s 20 s 15 s	30 x
Final Extension Cooling	72 ° C 4 ° C	10 min unlimited	1 x 1 x

2.2.10 DNA Sequencing

To verify the sequence of the cloned insert, the vector was sent to GATC Biotech, Konstanz, Germany, and sequenced using a standard primer (PGEX-FP).

2.2.11 Purification of total RNA

After the old medium had been removed from the IPSCs and washed with PBS - -, 500 µl of Trypsin-Versen were added for 5 min at 37 °C. The colonies were dissociated into a single cell suspension, collected, and centrifuged for 10 min at 300 x g. Next, the cells were washed twice in PBS - - and the RNA purification was assessed using the RNeasy Mini Kit (Quiagen). Thereafter, the washed cell pellet was resuspended in 600 µl RLT buffer and the probe was frozen. After thawing of the probes to RT, the lysate was pipetted into a QIAshredder spin column placed in a 2 ml collection tube. After centrifugation at full speed for 2 min, the QIAshredder spin column was removed and 600 µl of 70 % EtOH were added to the eluate and well-mixed. Then, 700 µl of the mixed eluate were pipetted on a RNeasy spin column placed in a 2 ml collection tube and centrifuged at 10000 rpm for 15 s. The eluate was discarded and 700 µl of buffer RW1 were pipetted to the spin column and centrifuged at 10,000 rpm for 15 s to wash the column membrane. The eluate was discarded and 500 µl RPE buffer were added and centrifuged at 10,000 rpm for 15 s. After another addition of 500 µl RPE Buffer and centrifugation at 10,000 rpm for 2 min, the spin column was placed in a new collection tube and centrifuged at full speed for 1 min. Finally, the spin column was placed in a 1.5 ml collection tube, and 30 µl of RNase-free water were added to the membrane and incubated for 1 min at RT. Then, the column was centrifuged at 10,000 rpm for 1 min twice, which yielded a 60 µl volume of dissolved RNA. The samples were stored at – 80 ° C until usage.

2.2.12 Quantitative one step real time reverse transcription PCR (qRT-PCR)

To analyse gene expression levels of IPSCs cells in various differentiation stages, we performed a qRT-PCR (Stockmann et al. 2013). In the one step qRT-PCR procedure, the reverse transcription of mRNA into cDNA and the amplification of the resulting cDNA were performed using the QuantiFast SYBR Green RT-PCR Kit (Quiagen). Technical duplicates and biological triplicates were used to verify gene expression analysis by comparison with the expression of the internal control, which was the housekeeping gene HMBS.
During the amplification, the fluorescence of the colorant SYBR Green 1 was measured in real time. This fluorescence correlates with the amount of PCR-products because the fluorescence rises in relation to the intercalation of the colorant to the newly synthesized double-strand PCR-products. The Cycle Threshold (CT) that indicates the number of cycles where the measured signal first rises significantly above the background was used for the quantification. The virtual concentration of the analysed mRNAs was calculated as follows:

$$\text{Virtual concentration} = 10^{(\text{Mean CT-value} / -\text{incline of calibration curve})}$$

Thereby, the relative concentration emerged from the quotient of the virtual concentration of the analysed mRNAs and the virtual concentration of the reference gene.

qRT-PCR preparation 20 µl:

sterile RNAse free water	6.8 µl
QuantiTect Primer Primer (0,5 µmol)	2 µl
Rotor Gene SYBR Green RT-PCR Master Mix 2 x	10 µl
Rotor Gene RT Enzyme Mix	0.2 µl
RNA Lysate	1 µl

The following primers were used:

Table 14 List of used primers

Quanti Tect Primer	Function
CHAT	MN marker
C9ORF72 Long isoform	ALS causing gene, unknown function
C9ORF72 Short isoform	ALS causing gene, unknown function
FUS	ALS causing RNA binding gene
HMBS	Housekeeping gene
HOMER	Postsynaptic marker
KLF4	Pluripotent Stem cell marker
Nanog	Pluripotent Stem cell marker
NEFH	MN marker
OCT4	Pluripotent Stem cell marker
ProSAP3/ Shank1	Postsynaptic marker
ProSAP1/ Shank2	Postsynaptic marker
Shank3	Postsynaptic marker
SOX2	Pluripotent Stem cell marker
TDP-43	ALS causing RNA binding gene

The qRT-PCR was done in a Realtime-PCR-Cycler using the following program:

Table 15 used qRT-PCR program

Step	Temperature	Time	Repetition
Reverse Transcription Initial Denaturation	50 ° C 95 ° C	10 min 5 min	1 x 1 x
Denaturation Annealing & Extension	98 ° C 60 ° C	10 s 30 s	40 x 40 x
Melting curve	60 ° C – 95 ° C (1 ° C/ step)	90 s first step 5 s following steps	1 x
Cooling	40 ° C	2 min	1 x

2.2.13 Fluorescence in situ hybridisation FISH

First, the old medium was removed and the cells were washed with PBS + +. Then, we carried out fixation with 4 % PFA for 5 – 10 min followed by three washing steps with PBS + + for 5 min each. The cells were permeabilized with 0.2 % Triton-X 100 for 5 min and then washed twice with PBS.

The Cy3-labelled probe against the hexanucleotide repeat was dissolved in 50 % formamide in 2 x SSC plus 10 % dextran sulphate (probe concentration 0.02 ng/µl). To hinder unspecific binding, 1µg/µl of salmon sperm DNA was added. The probe was denatured for 5 min in the water bath at 60 ° C, then kept for 3 min on ice. Next, the probe was added to the cells and incubated for 3-4 hours at 42 ° C in a humid, dark chamber. After completion of this incubation, the cells were washed with preheated solutions (42 °C): three times 5 min with 50 % form amide in 2 x SSC, three times 5 min with 2 x SSC and once for 5 min with 4 x SSC plus 0.03 % Tween 20 at RT. Then, the cells were washed once with PBS and aqua demin. Finally, cover slips were mounted with ProLong antifade containing DAPI.

2.3 Microbiological methods

2.3.1 Cultivation of *E. coli* bacteria

DH5 α or XL-1 *E. coli* bacteria were either cultured in Lennox L Broth Base (LB) hydraulic fluid in the shaker at 200 rpm and 37 ° C or *E. coli* bacteria were cultured on LB Agar plates at 37 ° C in the incubator. The LB hydraulic fluid was produced by dissolving 20 g LB dry chemical in 1 l of sterile water, which was autoclaved for 20 min at 121 ° C. For the production of the LB-Agarose plates, 32 g of LB-Agarose were dissolved in 1 l of sterile water, which was autoclaved for 20 min at 121 ° C. Then, the fluid was allowed to cool down on the magnetic stirrer. In order to obtain a selective growth of transformed bacteria, depending on the particular resistance gene, 50 µg/ml of kanamycin or 100 µg/ml of ampicillin was added to the media at a temperature lower than 40 ° C. The fluid medium was cast into 10 cm Petri dishes to harden and dry at RT. Dishes were stored in the fridge at 4 ° C until use. To retain the transformed bacteria for a longer period of time, 300 µl of bacteria were mixed with 300 µl of glycerine (87 %) and stored at -80 ° C in the freezer.

LB bacterial growth medium:	20 g Lennox broth base ad 1000 ml aqua demin
LB agar medium:	32 g LB-agarose ad 1000 ml aqua demin
Supplemented with:	50 µg/ml of kanamycin or 100 µg/ml of ampicillin

Ampicillin/ Kanamycin (100 mg/ml):

5 g Ampicillin/ Kanamycin ad 50 ml aqua demin

2.3.2 Preparation of electro competent *E. coli* bacteria

To enable *E. coli* bacteria to absorb free DNA from the medium, an overnight culture of the bacteria was put in 50 ml 2YT medium. Bacteria were grown in the shaker at 37 ° C. Then the overnight culture was diluted in 300 ml 2YT medium to an optical density OD600 of 0.3. After this dilution the bacteria were again incubated on the shaker at 37 ° C to an OD600 of 0.9 to 1.0. Once the culture had

been incubated on ice for 30 minutes, the bacteria were centrifuged at 3000 rpm for 10 min at 4 ° C. The supernatant was discarded and the pellet was washed in 20 ml ice cold sterile water. After two repetitions of centrifugation and washing in 5 ml ice cold water, the final pellet was mixed with an equal volume of 10 % glycerine, and the 50 µl containing aliquots were stored at -80 ° C.

2.3.3 Transformation of electrocompetent *E. coli* bacteria

For the transformation of *E. coli* bacteria, the bacteria were first electroporated to increase the permeability of cells, which enhances their uptake of free DNA.
The permanent cultures of electrocompetent *E. coli* bacteria were thawed on ice and blended with 0.1 µg of plasmid DNA before they were put into electroporation cuvettes and electroporated at 1.8 kV. The bacteria were then collected in 800 µl SOB-Medium and incubated on the shaker for 1 h at 37 ° C. After centrifugation at 3500 x g, the bacterial pellet was resuspended in about 100 µl of the supernatant and distributed onto the agarose plates. The plates were incubated overnight at 37 ° C.

2.3.4 Preparation of overnight liquid culture

For a liquid overnight bacterial culture, 1 positive selected bacterial colony was picked up with a pipette tip and transferred into 4 ml of LB supplemented with an antibiotic. The bacteria were grown on a shaker at 37 ° C overnight.

2.3.5 IPTG induction of GST-fusion proteins

Gluthatione-S-transferase (GST)-gene fusion proteins are used for inducible protein expression and purification from bacterial cell lysates. The protein is expressed in the pGEX 4T1 vector, with the GST moiety located at the N terminus followed by the target protein. The GST-fusion tag can act as a chaperone to

facilitate protein folding and purification of proteins fused to GST (Harper et al. 2011). The pGEX 4T1 vector is equipped with a tac promotor and an internal lac I gene. The expression of the vector is under the control of the IPTG-inducible tac promotor. In the absence of IPTG, the lac I gene product represses expression by binding the operon region of the tac promoter. To facilitate selection of positive transfected cells, the pGEX 4T1 vector contains an ampicillin resistance gene which enables only the transfected cells to grow on medium supplemented with ampicillin.

For the miniinduction of GST-fusion proteins, around 150 µl of bacterial suspension were placed into 4 ml LB-Amp media and incubated for 1 hour on the shaker at 37 ° C. Then, the cells were induced to perform protein synthesis with 4 µl 1M isopropyl-b-D-thiogalactopyranoside (IPTG) and incubated for 2.5 h on the shaker at 37 ° C. After centrifugation for 5 min at 6000 rpm in 2 ml tubes, the supernatant was discarded and the pellet was suspended in 300 µl PBS. 30 µl portions were mixed with 3x SDS-buffer, boiled for 3 min and centrifuged at 14,000 rpm. After performing SDS-PAGE, the proteins were washed in aqua demin for 10 min and analysed by Coomassie Brilliant Blue staining for 1 h. Then, the gel was rewashed again in aqua demin for 1 h.

For the maxiinduction of GST-fusion proteins, 300 µl of LB-Amp medium were mixed with 5 ml of the overnight bacterial culture. After 2.5 h of incubation in the shaker at 37 ° C, bacteria were induced with 1 mM IPTG and incubated for another 3 h. Then, the cells were distributed to 50 ml Falcon tubes and centrifuged at 5,000 rpm for 8 min at 4 ° C, whereupon the pellet was frozen at -20 ° C. Later, the thawed pellets were resuspended in 5 ml PBS and 6 pellets were pooled into one Falcon tube containing PBS to a volume of 15 ml. The cells were incubated for 15 min at RT in lysozyme (10 mg/ml stock, 1:50) and the suspension went through five cycles of freezing in liquid nitrogen and thawing in a warm water bath. After sonification for 10 s under cooling conditions thrice, the solution was distributed into 2 ml tubes and centrifuged at 14,000 rpm for 20 min at 4 ° C. The supernatant was transferred into new 2 ml tubes and DNA was precipitated with streptomycin sulphate solution (2 % stock solution, 1:20) at 4 ° C overnight. After

centrifugation at 14,000 rpm for 20 min at 4 ° C, the supernatant was placed in 15 ml tubes, with addition of a protease inhibition tablet to prevent protein degradation. The GST-fusion proteins then were purified with glutathione magnetic beads.

IPTG:	2.38 g IPTG ad 10 ml aqua demin

2.3.6 GST-fusion protein purification from a bacterial cell lysate

GST is a protein which is commonly fused to the end of recombinant proteins so as to simplify their purification and detection. The fusion protein is captured on a sepharose matrix column containing immobilized glutathione and then eluted under mild, non-denaturing conditions through the addition of excess reduced glutathione.
In this procedure, the columns were first prepared with 1 ml glutathione-sepharose and washed twice with PBS. The supernatant of the IPTG maxi induction was distributed onto the columns and incubated overnight; the supernatant was redistributed onto the columns a total of three times. Then the eluate was collected in a 15 ml Falcon tube on ice. The column was washed twice with PBS and extinction of the supernatant was monitored in a photometer (280 nm). Then 500 µl of glutathione buffer (10-30 mM in Tris-HCl, pH 8) were distributed onto the column and eluate was collected in a 1.5 ml tube. The elution was carried out with 1 ml glutathione buffer. After the second elution, the extinction was analysed again, to test for retention of fusion protein on the column.

Glutathione (30mM):	0.922 g glutathione, ad 100 ml aqua demin
Glutathione- Tris- HCl:	0.61 g Tris, ad 100 l aqua demin
	pH 8.0 adjust with 37 % HCl
	ad 10-30 mM glutathione

2.3.7 Protein quantification via Bradford Assay

A 96 well plate was used for the protein assay. Every well was filled with 20 µl of 150 mM NaCl, 2 µl of the sample and 200 µl of Bradford solution. For the blank, aqua demin was added instead of sample. The amount of protein was measured with the iEMS reader and quantified relative to a specific calibration curve.

2.3.8 Glycerol stocks

For long-term storage of plasmids, a bacterial glycerol stock which was stored at – 80 ° C was prepared. Glycerol stabilises the frozen bacterial cell membrane and supports viability upon thawing. Thus, 200 µl of an overnight culture were added to 1 ml of LB medium supplemented with antibiotics and incubated for 3 h on a shaker at 37 ° C. Thereafter, 500 µl of the culture were transferred into a 2 ml vial with 50 µl glycerol, mixed gently and stored in the freezer until usage.

2.4 Cell culture methods

2.4.1 General handling of cell lines

The cultivated cells were cultured in an incubator with a water vapour saturated and (5 %) CO_2 -enriched atmosphere at 37 ° C. The cells were always handled under sterile conditions inside a laminar flow hood. All used media were warmed to RT or 37 ° C in a water bath.

2.4.2 Cell culture of cell lines

The cell lines were frozen in liquid nitrogen at -196 ° C. In order to be used, they were thawed in a 37 ° C water bath and placed into 10 ml DMEM ++. To remove the cryoprotectant dimethylsulphoxide, the cells were centrifuged for 5 min at 600 x g, and the cell pellet was collected in 10 ml DMEM ++. Cells were maintained in

Dulbecco`s Modified Eagle Medium (DMEM) supplemented with 10 % foetal calf serum in a 25 cm² bottle.

COS7/HEK cell medium:	DMEM
Supplemented with:	10 % FCS

2.4.3 Transfection of cell lines

At the beginning, 100 µl of COS7 cells were distributed (1:16) to 4 cm² chamber slides. 900 µl DMEM were added to a final volume of 1 ml. The mastermix (MM) for transfection with Polyfect was prepared as follows: 60 µl of DMEM and 6 µl Polyfect were mixed for each sample. The entire 66 µl were added to each plasmid DNA (1 µg) sample. In cases when there was a cotransfection, the different plasmid DNA had been pre-mixed. Incubation lasted 5 min at RT. Then, the 66 µl mixtures containing DNA were applied to the COS7 cells, which were further cultivated until the time of fixation.

2.4.4 Cell culture of primary hippocampal neurons

Primary hippocampal neurons were cultured in neurobasal medium (NB) supplemented with B27, Glutamine, Penicillin and Streptomycin (NB+++). Neurons were maintained either in 24 well cell culture platters with 13 mm cover slides, or were cultured in 6 cm² cell culture plates. Therefore, the cell culture plates and platters were first coated with poly-L-lysine for 1 hour at 37 ° C, and then washed three times with sterile water. Hippocampal neurons were isolated from rat embryos by Christian Pröpper, Michael Schön and Stefan Putz, as described previously by Böckers *et al*., 2005.

Hippocampal neuron medium:	Neurobasal medium
Supplemented with:	2 % B27
	1 % glutamine
	1 % streptomycin

2.4.5 Transfection of primary hippocampal neurons

For the transfection of primary hippocampal neurons which had been cultured for 14 days, neurons were washed at 37 ° C with preheated pure neurobasal medium and covered with 500 µl preheated NB++ (Neurobasal + 2 % B27 + 1 % glutamine). The MM was prepared as follows: for each well and plasmid DNA construct, 50 µl pure NB were mixed with 5 µl Optifect for 5 min . 55 µl of the MM were applied to each prepared plasmid DNA construct (1 µg/µl in 50 µl pure NB) and incubated for 30 min at RT. Then, 55 µl portions per well were distributed to the cells. After 4 hours, the medium was changed to NB++ (500 µl) and neurons were cultured in this medium until fixation.

2.4.6 Cell culture of human keratinocytes

To obtain human keratinocytes, hairs were plucked as described before by Aasen *et al*., 2008. Roots of human hair were cut and fixed with matrigel (1:5 in Epilife) in T 75 flasks that had been pre-coated with matrigel (1:10 in Epilife) for 1 h at 37 ° C. The human hair roots were cultured in an atmosphere containing 5 % CO_2 and 95 % O_2. After 2 h, conditioned MEF Medium was added to the plucked hairs and refreshed every day.

Conditioned MEF Medium:	DMEM
	10 % FBS
	1% NEAA
	1 % Anibiotic Antimycotic
	1 % GlutaMax
Supplemented with:	0.4 µl / ml FGF 2
	1 µl / ml Ascorbic Acid
	1 µl / ml ROCK Inhibitor

Keratinocytes were then cultured at 37 ° C in an atmosphere containing 5 % CO_2 and 95 % O_2 in 6-well plates that had been coated with collagen IV (1:100 in PBS, 700 µl) for 1 hour at RT.
In order to passage the keratinocytes at about 80 % confluence, the cells were washed with PBS and lifted via keratinocyte dispase or TrypLE digestion for 10-15 min at 37 °C in the incubator. The keratinocytes were collected in PBS and after centrifugation for 2 min at 300 x g, the cell pellet was resuspended in 1.5 ml Epilife + Rock-inhibitor (1:1000) per well, and distributed to the cell plates.
For cryopreservation, keratinocytes were detached by keratinocyte dispase or TrypLE treatment, collected in PBS and centrifuged for 10 min at 300 x g. The cell pellet was resuspended in 800 µl Synt-a-Freeze Medium with rock inhibitor (1:1000) per aliquot and put into freezer-tubes. First, the tubes were frozen in a cryo-container at -70 ° C, and then the cells were stored at -196 ° C in liquid nitrogen. For thawing, the keratinocytes were warmed up in a 37 ° C warm water bath and pipetted into 5 ml of Epilife with ROCK inhibitor. After centrifugation for 2 min at 300 x g, keratinocytes were seeded out as described above.

Keratinocyte Medium:	Epilife
Supplemented with:	ROCK Inhibitor (1:1000)

2.4.7 Cell culture of REFs

Rat embryonic fibroblasts (REFs) were isolated from rat embryos and cultured in REF medium in T175 flasks coated with 0.1 % gelatine at 37 ° C in an atmosphere of 5 % CO_2 and 5 % O_2. When cell culture reached confluence, cells were passaged by washing with PBS- -, and dissolved by incubation with 3 ml Trypsin-Versen for 10 min at 37 ° C. Trypsination was stopped by the addition of 7 ml PBS - -, and the cells were collected in a 15 ml Falcon tube and centrifuged at 1500 rpm for 2 min. The pellet was resuspended in REF medium and cells were plated into new flasks at a ratio of 1:5. REFs support the growth of undifferentiated hIPSCs by providing substrate for growth and by secretion of multiple factors required to maintain pluripotency.

REF medium:	DMEM
	10 % FBS
	1% NEAA
	1 % Anibiotic antimycotic
	1 % GlutaMax
Supplemented with:	50 µg/ml Ascorbic acid

Irradiation of REFs

Before REFs can be used as feeder cells for hIPSCs, their division must be stopped by irradiation treatment. Therefore, after detachment of the cells as described above, the cells were collected in a 15 ml Falcon tube and counted in a Neubauer counting chamber to obtain 3 x 10^5 cells per well of a 6 well plate. Then, the necessary amount of the cell suspension was irradiated with 30 Gy, and these feeder cells were plated into the gelatine coated wells. The next day, REFs could be used for culture of hIPSCs.

2.4.8 Cell culture of human IPSCs

Human IPSCs were cultured at 37 ° C in an atmosphere containing 5 % CO_2 and 5 % O_2 in 6-well plates coated with Matrigel (500 µl) for 1 hour at RT. 1.5 ml mTeSR Medium was changed daily and differentiated cells were eliminated by scratching with a pipette tip and washing with DMEM F12. For passaging, the hIPSCs were washed with DMEM F12, and 500 µl hIPSCs dispase (1:5 in DMEM F12) were added for 5 – 7 min until the edges of the colonies were detached. After washing twice with DMEM F12, 1 ml mTeSR medium was added to each well and the colonies were carefully detached with a cell scraper. The hIPSCs were collected and distributed to matrigel coated wells.

For cryopreservation, hIPSCs were detached via dispase treatment and centrifuged for 2 min at 300 x g. The cell pellet was resuspended in 800 µl mFreSR medium per freezer tube, and tubes were frozen stepwise from -70 to -196 ° C, as described above. For thawing, the hIPSCs were warmed up in a 37 ° C

water bath and pipetted into 5 ml of mTeSR. After centrifugation for 5 min at 300 x g, cells were seeded on matrigel coated dishes.

Irradiation of hIPSCs

For the investigation of the susceptibility of patient-derived cells to stress induced by sublethal DNA damage, we irradiated patient-derived IPSCs and control IPSCs with gamma radiation and counted the number of apoptotic cells at several time points post-irradiation. For the irradiation, 1 well of hIPSCs was detached as described in 3.4.8 above and collected in 3 ml mTeSR in a 15 ml Falcon tube for irradiation with 30 Gy/min of gamma irradiation for 2.5 s or 5 s when grown on Ibidis. After irradiation, the cells were seeded onto 6 wells of a 24 well plate coated with matrigel and incubated for 24 h to allow DNA repair. Then, the hIPSCs were fixed and stained for IF analysis of apoptotic events.

To analyse the cells after a shorter period of time post-irradiation, the cells were grown until they reached extensive colonies on Ibidis and then irradiated. In this procedure the cells could be fixed immediately after irradiation treatment.

Sorbitol treatment of hIPSCs

We induced hyperosmolar stress and provoked stress granule formation in hIPSCs by treatment of the cells with sorbitol. In this procedure, we passaged the cells and let them grow for 24 – 48 h. After, we changed the mTeSR medium for 1 h to provide optimal cell culture conditions. Then, we incubated the cells for 30 min with mTeSR containing 0.3 M sorbitol, using a medium that had been sterile-filtered before use. Then, the cells were washed with PBS and fixed with PFA as previously described above.

Colchicine treatment of IPSCs for karyotyping

We karyotyped the IPSCs after reprogramming to ascertain if there were any chromosomal abnormalities. We used the spindle inhibitor colchicine to stop mitotic activity of the cells in the metaphase of the cell cycle, when the

chromosomes are maximally condensed, and therefore, suitable for morphologic chromosomal analysis. We added 0.05 µl of colchicin to 1.5 ml of mTeSR and incubated the cells for 2 hours. Then, the IPSCs were washed with DMEM F12, detached as described in 3.4.8 above and contained in 1 ml mTeSR. Karyotyping was done by the group of Prof. Barbi, human genetics, University of Ulm.

2.4.11 Differentiation of hIPSCs

The differentiation process can be divided into four steps, where differentiation status can be assessed by morphology and by the specific transcription factor expression profile.

Culture of embryoid bodies (Day 1-4)

When the initially flat stem cell colonies that grow attached to matrigel coated wells become embryoid bodies, they form three-dimensional spheres floating in the medium of a non-attachment T75 flask. Thus, in this procedure the hIPSC colonies were completely detached from the culture wells as described in 3.4.8, but were collected in hESC medium instead of mTeSR. The colonies were transferred into a special low-attachment T75 flask. HESC medium was added to a volume of 10 ml and ROCK inhibitor was added. For the daily medium change, the flasks were left standing upright for 5 min to allow the EBs to sink to the bottom. Then 7 ml of the old medium was removed and fresh hESC medium was added.

hESC medium:	DMEM/F12
	20 % knockout serum replacement
	1 % NEAA
	1 % Antibiotic antimycotic
	1 % GlutaMax
	100 µM β-mercaptoethanol

Supplemented with (the first time): 10 µM ROCK inhibitor (1:1000)

Differentiation into germ layers ecto-, meso-, endoderm

For the germ layer differentiation, Ibidis were first coated with 500 µl PLO, washed three times with PBS - - and then coated with laminin (1:25, 20 µg/ml) for 1 h at 37 ° C. HIPSCs were seeded onto the wells and cultured in 2 ml hESC medium. The cells were cultured for 3 weeks and medium was renewed every day.

Differentiation into neuro epithelial rosettes (NE) (Day 4-15)

Differentiation medium 1 was put into the T 75 flasks at day 4 instead of hESC medium. Neural growth factors such as BNDF, GNDF, IGF1 present in differentiation medium 1 promote differentiation of EBs into neurons. To seed the neurospheres at day 7 onto 12 well plates, the spheres were transferred to 15 ml Falcon tubes and centrifuged at 50 (100) x g for 3 min. Then, the neurospheres were plated in 1 ml of differentiation medium 1 on laminin-coated (400 µl 1:25 in PBS for 1 h at 37 ° C) wells of a 12 well plate. Plates were cultured in 5 % CO_2 and medium was filled to 2 ml on day 8. Then, medium was changed 3 times per week. On day 10, the differentiation medium 1 was replaced by differentiation medium 2 containing 0.1 µM retinoic acid (RA), which initiates axis formation by posteriorization of a cell pole.

Generation of motoneuron progenitors (pMNs) (day 15-28)

Neural tube-like cells emerged after one week in culture, and those cells that did not show typical rosettes were mechanically removed from the well. After washing the cells with DEMEM F12, 2 ml of differentiation medium 3 were added to the wells. Using a 5 ml pipette, neuroepithelial spheres were transferred into low attachment T75 flasks, where they formed motoneuron (progenitors pMNs). These cells can be cultured for up to 3 months with medium change three times per week, and can be passaged to increase the cell numbers. Purmorphamine was added to differentiation medium 3, which leads to caudalisation and B27 promotes cell survival of neuronal cells.

Generation of post mitotic motoneurons

For the final plating, pMNs were collected in a 15 ml Falcon tube and centrifuged at 100 x g for 3 min. The pellet was resuspended in differentiation medium 4 and pMNs were seeded onto Ibidis for immunocytochemistry. If the cells were intended to be harvested for mRNA analysis, pMNs were cultured in 12 well plates. Before usage, the Ibidis or wells were coated with poly-L-ornithine (PLO) for 2 h at 37 ° C and laminin for 1 h at 37 ° C, or overnight at 4° C. For the culture, 2 ml of differentiation medium were used, and 1.5 ml of the medium containing less RA was renewed each week.

Basic differentiation medium: DMEM/F12
1 % NEAA
1 % Antibiotic antimycotic
2 µg/ml Heparin
2 % Hormone mix (HM)

Differentiation medium 1 (day 4-10):
Basic differentiation medium
supplemented with 10 ng/ml BDNF (1:1000)
10 ng/ml IGF 1 (1:1000)
10 ng/ml GDNF (1:1000)
0.1 µM cAMP (1:10000)
20 µg/ml Ascorbic acid (1:1000)

Differentiation medium 2 (day 10-15):
Differentiation medium 1 supplemented with 0.1 µM RA

Differentiation medium 3 (day 15-28):
Differentiation medium 1 supplemented with 0.1 µM RA (1:10000)
0.1 µM Purmorphamine (1:10000)
2 % B27 without Vit. A (1:50)

Differentiation medium 4 (day 29-56):

Differentiation medium 1 supplemented with	0.05 µM RA (1:20000)
	0.1 µM Purmorphamine (1:10000)
	2 % B27 without Vit. A (1:50)

2.5 Protein biochemistry

2.5.1 Immunocytochemistry: Immunofluorescence staining of cell lines, hIPSCs and hippocampal neurons

Using antibody staining, it is possible to visualise the expression and localisation of a specific endogenous or transfected protein in different cell types. At 24 hours post-transfection, cells were washed for 5 min with PBS++ (with Ca^{2+}, Mg^{2+}), fixed for 10 min with 500 µl 4 % PFA in PBS and then washed twice with PBS for 5 min. The cell membrane was permeabilized with PBS + 0.2 % Triton X 100 for 5 min and washed twice with PBS for 5 min. To hinder unspecific protein binding, cells were incubated for 1 hour at RT with blocking solution (PBS + 5 % foetal calf, goat or donkey serum). Then the cells were incubated with the primary antibodies in blocking solution for 1 hour at room temperature or overnight at 4 ° C in a humidified staining chamber. The cells were washed twice with PBS for 5 min and incubated for 1 h at RT with the secondary antibodies in blocking solution or PBS. (A list of used antibodies is described in Materials and Methods Table 6). Then, the cells were washed once for 5 min with PBS ++ and once with PBS + 0.002 % DAPI (4´,6-diaminidin-2-phenylindole) for blue nuclear staining. Cells were washed again with PBS - - for 5 min and with aqua demin for another minute. Afterwards, the cells were mounted on microscopy slides with VectaMount AQ (Vector Laboratories, USA) and analysed via fluorescence microscopy. Alternatively, the washing step with DAPI was substituted by mounting the cells using ProLong Antifade with DAPI.

Germ layer immunofluorescence staining of IPSCs

Using IF analysis of IPSCs, it can be shown that colonies are able to differentiate into the three different germ layers: ectoderm, mesoderm and endoderm, as shown by the expression of ß-lll-tubulin, ß-actinin and catenin. The differentiated colonies also express pluripotency markers: NANOG, OCT4, KLF2, SSEA4, TRA-1-60, TRA-1-81. Therefore, the staining of the EBs plated on Ibidis or the IPS colonies plated on glass cover slides was done as described previously by Liebau et al.. An deviation from the published procedure was the use of goat serum instead of calf serum for blocking, and omitted permeabilisation for the staining of an extracellular epitope like SSEA4, TRA-1-60, TRA-1-81, for which no permeabilisation is needed. If the primary antibodies were against OCT4, SOX2 and NANOG, the cell membrane was permeabilised with ice-cold methanol (100%). In the case of Ibidis, the stained cells were mounted on the Ibidi surface with two droplets of ProLong Antifade reagent with DAPI.

Fixation solution 4 % PFA / 2 % Sucrose:
8 g paraformaldehyde (PFA) were dissolved in 80 ml deionized water at 57 °C and 4 g sucrose were dissolved in 100 ml PBS - -. The solutions were combined, and a pH of 7.4 was confirmed.

0.2 % Triton-X:
100 µl Triton-X 100 were dissolved overnight at 4 °C in 50 ml PBS + +.

Blocking Solution: 10 % FCS in PBS + + or
10 % Goat/Donkey Serum + 5 % FCS in PBS + +

2.5.2 Coomassie staining

After polyacrylamide gel electrophoresis, the gel was washed for 10 min in aqua demin on the shaker. Then, Coomassie reagent was added for 1 h, and afterwards the gel was washed three times with aqua demin for 10 min.

2.5.3 Sodium dodecyl sulphate polyacrylamide gel electrophoresis (SDS-PAGE)

A sodium dodecyl sulphate polyacrylamide gel electrophoresis (SDS-PAGE) was performed to detect specific proteins. The SDS condition imparts to the proteins a negative charge, so that they migrate to the cathode in the electric field. A sieving 10 % gel was used to separate the proteins according to their molecular weight. The denaturing polyacrylamide gels were cast between two glass plates, and divied into a stacking and a separating gel. For the electrophoresis, the SDS gel between the glass plates was completely immersed with migration buffer and each lane was loaded with 10 µl portions of the samples. The samples had been mixed with loading buffer and denatured at 95 ° C for 5 min. The gel was loaded with un-transfected cell lysate as input and cell lysate of transfected cells to visualise the presence of the recombinant proteins. The empty pockets in the gel were loaded with one-fold loading buffer. For molecular weight reference, one lane of the gel was loaded with a protein ladder. 110 V were used to let the proteins run through the stacking gel and 210 V for the separation gel. The run stopped just before the dye front reached the bottom of the gel.

Table 16 Components of the polyacrylamide gel

	Separating gel (10 %)	**Stacking gel (10 %)**
water	7.9 ml	4.1 ml
1.5 M Tris pH 8.8	5.0 ml	-
1 M Tris pH 6.8	-	0.75 ml
Polyacrylamide (30 %)	6.7 ml	1.0 ml
SDS (10 %)	0.2 ml	0.06 ml
APS (10 %)	0.2 ml	0.06 ml
TEMED	0.02 ml	0.006 ml

4 x SDS protein sample buffer:	6 ml Tris-HCl pH 6.8 (1 M)
	0.93 g DTT
	1.2 g SDS
	0.24 ml EDTA (0.5 M)
	12 ml Glycerine (100 %)
	Tip of a spatula bromophenol blue (0.02 %)
	Ad 30 ml aqua demin
10 x Migration buffer:	30.30 g Tris
	144 g Glycine
	10 g SDS ad 1000 ml aqua demin

2.5.4 Western blot

A western blot was used in order to visualize the protein bands from electrophoresis. Here, the proteins are transferred from the gel onto a PVDF membrane by applying an electrical field. Now, tightly attached on the membrane, the proteins can be detected by specific binding of primary and secondary antibodies. The primary antibodies, which are produced in certain animals, bind to an antigen of a specific protein on the membrane. The secondary antibodies are raised against the primary antibody of the animal species in which the primary antibodies had been produced, and carry with them a marker for visualization of the antigen-primary-secondary complex.

For the blot, the PVDF membrane was activated in methanol, and transfer of the proteins from the gel to the membrane lasted 90 min at 100 V and a temperature of 4 ° C. Two pads were placed on the black side of a support grid, followed by a Whatman paper and the polyacrylamide gel. The activated PVDF membrane was placed above the gel. Then, one filter and two pads were placed above the gel and the support grid was closed using the grid´s white side. The whole package was placed into a tank filled with transfer buffer, with the black side of the WB support grid positioned to face the cathode. After blotting, the membrane was incubated for 1 hour in blocking milk to hinder unspecific binding of antibodies.

The primary antibodies were applied in blocking milk for 1 hour on a shaker. For the pull-down of GFP-tagged C9ORF72, anti GFP antibodies and the different anti C9ORF72 sera were used to detect the C9ORF72 protein, which had been purified from cell lysate using anti GFP beads.
After washing the membrane on the shaker three times for 10 min in TBST, the membrane was incubated with the secondary antibody for 1 hour. Then the membrane was washed with TBST three times for 10 min. At last, the membrane was incubated with enhanced chemiluminescent (ECL) solution for 1 min or with Super Signal West Femto Trial Solution for 5 min. The ECL solution triggers a luminescent reaction because the secondary antibody is coupled to horseradish peroxidase (HRP). The emitted chemiluminescence was detected with a light sensitive film (GE Healthcare) or with the Intelligent Dark Box.

10 x blot buffer	37.9 g Tris 180 g Glycine ad 1 l Aqua demin
1 x blot buffer:	100 ml 10 x Blot buffer 700 ml Aqua demin 200 ml Methanol 1 ml SDS 10 %
10 x Tris buffered saline (TBS):	48.4 g Tris in 1000 ml aqua demin pH 7.5 adjust with 37 % HCl Add 116.9 g NaCl ad 2 l Aqua demin
1 x 0.2 % TBST: Supplemented with:	1 l 1 x TBS 2 ml Tween
Blocking milk:	50 g Milk powder ad 1 l 0.05 % TBST

2.5.5 Immunoprecipitation

To investigate the specificity of our primary antibodies raised against C9ORF72, we enriched the overexpressed proteins via immunoprecipitation (IP). To this end, we seeded COS7 cells on a 10 cm² plate. The next day, COS7 cells were transfected with 1 µg DNA per plate of the constructs for C9ORF72-GFP, or an empty GFP vector. The DNA was incubated for 5 min with 240 µl DMEM and 24 µl of Polifect to facilitate uptake into the cells. 24 hours post-transfection, the cells were lysed in lysis buffer, as specified in the µMACS Epitope Kit handbook, and scraped from the culture dish into a 1.5 ml Eppendorf tube. The lysate was incubated on ice for 30 min with occasional mixing. Sediment of the cell debris was removed by centrifugation for 10 min at 10,000 g at 4°C. The supernatant was transferred to a new tube and IP was performed according to instructions in the µMACS Epitope Kit handbook. We used anti GFP beads to bind the GFP tail of the constructs. Protein A beads were used as a negative control to confirm absence of unspecific binding of the proteins to the columns. First, the beads were placed in the specific columns, and then the cell lysates were applied. After four washing steps with 200 µl lysis buffer and one washing step with 100 µl wash buffer 2, the columns were incubated with 20 µl elution buffer for 5 min. Using 50 µl of the elution buffer, the immune precipitates were eluted from the columns into a 1.5 ml tube. Then, the eluates were frozen at -20 ° C until western blot analysis was performed.

Lysis buffer:	150 mM NaCl
	1 % Triton X 100
	50 mM Tris HCl (pH 8.0)
	1 x Protease inhibitor mix
Elution buffer:	50 mM Tris HCl (pH 6.8)
	50 mM DDT
	1 % SDS
	0.005 % Bromophenole blue
	10 % Glycerine

2.6 Data analysis and statistics

2.6.1 Image production and analysis

Fluorescence images were taken with a fluorescence microscope (Zeiss Axioskop 2 and Zeiss Imager.Z1, Zeiss, Germany) operated with the AxioVision 4.7.1 software, which was also used for the image editing.

2.6.2 Counting synapses

Counting analysis was assessed with the AxioVision Rel. 4.7.1 software. Signals of pre- and postsynaptic markers (synaptophysin or HOMER1) lying close to microtubule-associated protein 2 (MAP2)-positive dendrites were considered to be synapses. Synapse number was counted per µm of dendrite length. Measurements of dendrites/axons lengths were assessed with the ImageJ Software.

2.6.3 Counting protein/RNA aggregates

Aggregate counting analyses were carried out using the cell counter ImageJ plug-in. The number of aggregates were counted by clicking on the features. Number of foci were counted per cell nuclei. In some analyses, the features were grouped into different categories. Counting of cell nuclei was automated once a binary image was shown. If particles were in contact, the threshold was adjusted until they separated, or a thin line was drawn between them to separate the objects (watershed function).

2.6.4 Statistical tests

Statistical analyses were performed using Student's t-test or using one-way analysis of variance (ANOVA test) with post-hoc Bonferroni correction for multiple comparisons. Results are provided as mean values ± standard deviation (SD). Statistical significance was represented by abbreviations or asterisks as follows: $p > 0.05$ = non-significant (ns); $p < 0.05$ = *; $p < 0.01$ = **; $p < 0.001$ = ***.

3. Results

3.1 Antibody production against C9ORF72

Antibodies are one of the most important tools in research to elucidate the localisation, function and interaction partners of proteins of interest. As the specificity of commercial antibodies against C9ORF72 has been called into question due to their cross reactivity (Satoh et al. 2012), we produced two different glutathione-S-transferase (GST)-fusionproteins from two predicted isoforms of the C9ORF72 protein, which function as antigens for the immunisation of several animal species (rabbit, guinea pig, chicken). For selecting the optimal region of the epitopes, we used the online tool called “AntibodyDesigner“ (Pisitkun et al. 2012). This tool predicted particular protein regions with high immunogenic scores. In addition, we avoided the region of amino acids (AS 112-155) which is known to be cross-reactive with glial fibrillary acidic protein (GFAP) (Satoh et al. 2012). Thus, an N-terminal region of C9ORF72 (AS 1 – 100) and a C-terminal region of the protein (AS 260 – 360), both with high immunogenicity, high conservation and low cross-reactivity were generated by PCR amplification. Then these gene sequences were successfully cloned into the multiple cloning site of the pGEX 4T1 plasmid (Fig. 4). Thereafter, DH5α *E. coli* bacteria were transformed by electroporation and made to express the desired gene product by IPTG induction. After isolation of GST fusion proteins from the bacteria, the antibodies against the two C9ORF72 epitopes were produced commercially by the “Pineda abservice”.
After obtaining the sera intended to contain antibodies against C9ORF72, we tested their avidity and specificity for their intended antigens. For this, COS7 cells (which do not express wt C9ORF72) were transfected with C9ORF72-GFP or empty GFP constructs. Then, the COS7 cell lysate with overexpressed C9ORF72-GFP was purified by IP with magenetically labelled beads against GFP to isolate the GFP tagged C9ORF72 protein. The purified C9ORF72-GFP proteins were transferred by WB, in which the different anti C9ORF72 sera were tested to see if they could in fact recognise C9ORF72-GFP (for more details see 2.5.5).
The presera obtained from the animals prior to their immunisation were used as a negative control, not expected to contain any antibodies against C9ORF72.

In our WB we saw a non-specific pattern of bands (Fig. 5 A), indicating that the preserum did not detect C9ORF72-GFP. The incubation of the WB membrane with anti (α) GFP antibodies indicated the height of the expected band of C9ORF72-GFP long isoform at approximately 72 kDa, showing that the cell lysate contained cells expressing C9ORF72-GFP. However, none of the sera obtained after immunisation of the animals proved specific detection of the C9ORF72 protein in western blot analysis. Five different dilutions (1:50, 1:100, 1:500, 1:1000 and 1:2000) were tested, whereby 1:100 showed the clearest bands. In all the western blot analyses, the sera showed the same non-specific patterns of bands after IP of overexpressed C9ORF72-GFP as were evident under control conditions, in which cell lysates were obtained from cells without transfection of C9ORF72-GFP, but rather containing only empty GFP (Fig. 5 A). In Figure 5 A we show only representative western blot analyses of preserum and serum obtained from rabbit immunised against either the N- or the C- terminus of C9ORF72.

Additionally, COS7 cells that overexpressed C9ORF72-GFP were also immunostained to test the different serums. The sera, which were intended to contain α C9ORF72 antibodies against the N- or C-terminus of the protein, partially detected the overexpressed protein, but failed to perfectly co-localise with the C9ORF72-GFP signal from the overexpressed cells. Furthermore, we also saw non-specific binding to different cellular components, as shown in Fig. 5 B. The same staining pattern was observed when preserum was used (data not illustrated). In Figure 5 B, we show representative IF stainings with serum obtained from rabbits immunised against either the N- or the C-terminus of C9ORF72.

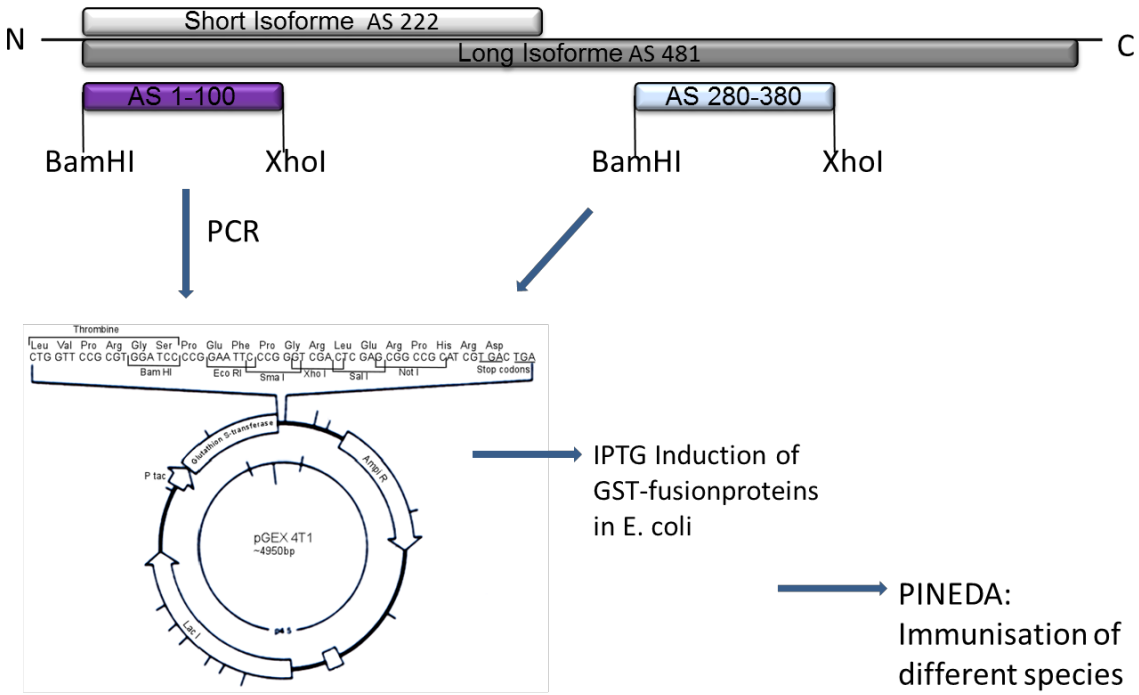

Figure 4 Anti C9ORF72 antibody production
(A) N-terminal amino acids (AS) 1–100 and C-terminal AS 260–360 were amplified using the polymerase chain reaction (PCR) and cloned into the PGEX 4T1 plasmid using the restriction enzymes BamHI and XhoI. Transformed DH5α *E. coli* bacteria expressed the gene product by isopropyl-b-*D*-thiogalactopyranosid (IPTG) induction of glutathione-S-transferase (GST)-fusion proteins and Pineda abservice immunised animals for antibody production.

(A)

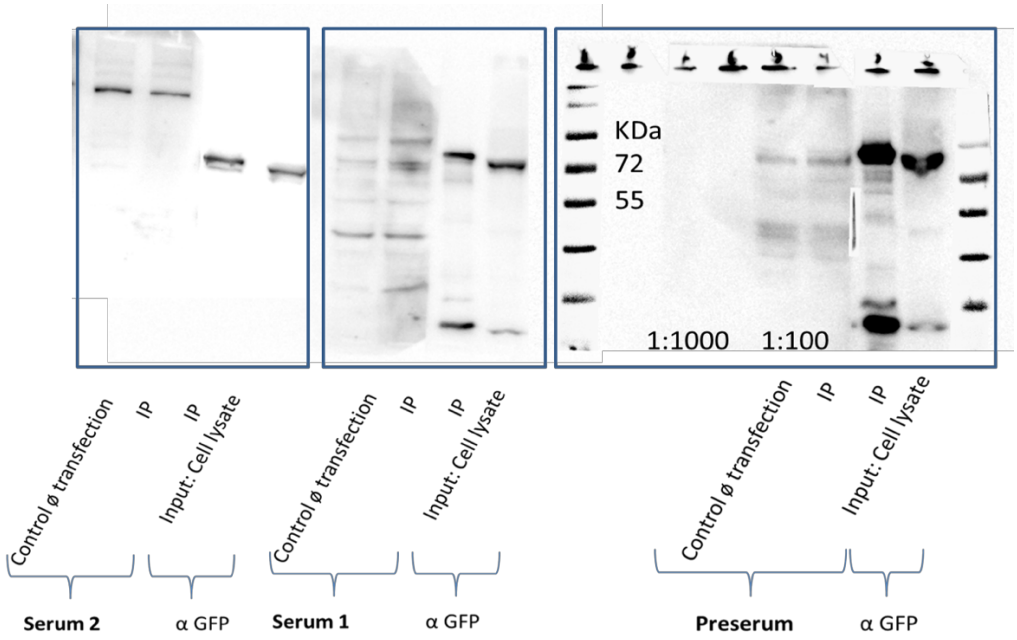

(B)

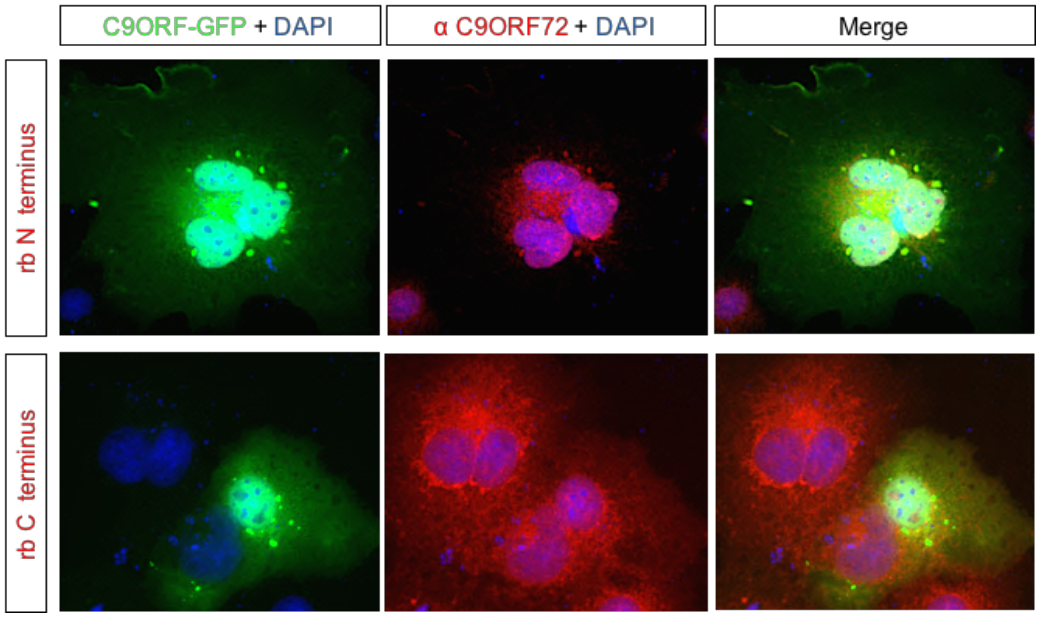

Figure 5 Specification of anti C9ORF72 antibodies
(A) Overexpression of C9ORF72-GFP and western blot specification of antibodies: α GFP antibody indicates the height of the expected band of C9ORF72-GFP long isoform at approximately 72 kDa. Different dilutions of pre-/sera have been used whereby 1:100 produces the clearest bands. Representative image of WB analysis using preserum and serum 1, 2 produced in rabbit (rb). Serum 1 was obtained after immunisation against the N-terminus of C9ORF72 and serum 2 was obtained after the immunisation against the C-terminus of C9ORF72. The presera and the sera show the same non-specific patterns of bands after immunoprecipitation (IP) of overexpressed C9ORF72-GFP as under control conditions without transfection of C9ORF72-GFP. (B) Representative images of immunofluorescence staining of C9ORF72-GFP transfected COS7 cells using the serum produced in rb. The serum containing α C9ORF72 antibodies against the N-terminus of the protein detects the overexpressed protein, but also binds unspecific to cellular components and untransfected cells. The serum containing antibodies against the C-terminus of C9ORF72 partially detects the overexpressed protein, but the serum also binds to untransfected COS7 cells. Nuclei are labelled with DAPI (blue) and different sera are shown in red. C9ORF72-GPF is shown in green.

3.2 Localisation of C9ORF72 in hippocampal neurons and impact of C9ORF72 on synaptic sites

According to a hypothesis that motoneuron degeneration starts at the neuromuscular junctions (NMJs) and proceeds towards the cell body, C9-ALS might be considered as a distal axonopathy or synaptopathy, showing distinct changes of motor synaptic function prior to clinical manifestation of ALS (Moloney et al. 2014). To analyse the localisation of C9ORF72, especially in regard to its synaptic localisation and function, we first tested the antibody from Santa Cruz (SC) in a cell system of COS7 cells to verify the specificity of the antibody. Therefore, we overexpressed C9ORF72-MYC in COS7 cells and co-stained these cells with the SC antibody and a MYC antibody. To verify that the commercially available antibody from SC detects the long and the short isoform, we overexpressed the different isoforms in COS7 cells and stained them with the SC antibody. We observed the same distribution patterns of overexpressed C9ORF72 through the usage of the different antibodies against C9ORF72 or MYC, indicating that the antibody may indeed be specific (Fig. 6 A). Next, we stained hippocampal neurons with the SC antibody, and confirmed localisation at synaptic sites by co-localisation with PSD95 (Fig. 6 B). To verify these results, we transfected hippocampal neurons with C9ORF72 constructs, and found that in these transformed cells the gene product of C9ORF72 was present in all neuronal cell compartments. As C9ORF72 co-localises with other synaptic markers (SYP and BSN), we could confirm its localisation at synaptic sites (Fig. 7 A). However, C9ORF72 does not seem to be enriched within synapses, which would have indicating a major function on synaptic structures compared to other cellular compartments.

We next counted synapse numbers of hippocampal neurons that overexpress C9ORF72-GFP using the synaptic marker synaptophysin, and compared these counts to the synapse numbers of empty GPF-transfected hippocampal neurons. We intended thus to ascertain if C9ORF72 overexpression influences synapse numbers in transfected neurons compared to normal neurons, which would be an indication of altered synaptic function in C9-ALS. In fact, the overexpression of

C9ORF72 in hippocampal neurons significantly reduced the number of mature synapses to 73 % in comparison to the control cells, as illustrated in Figure 7 B.

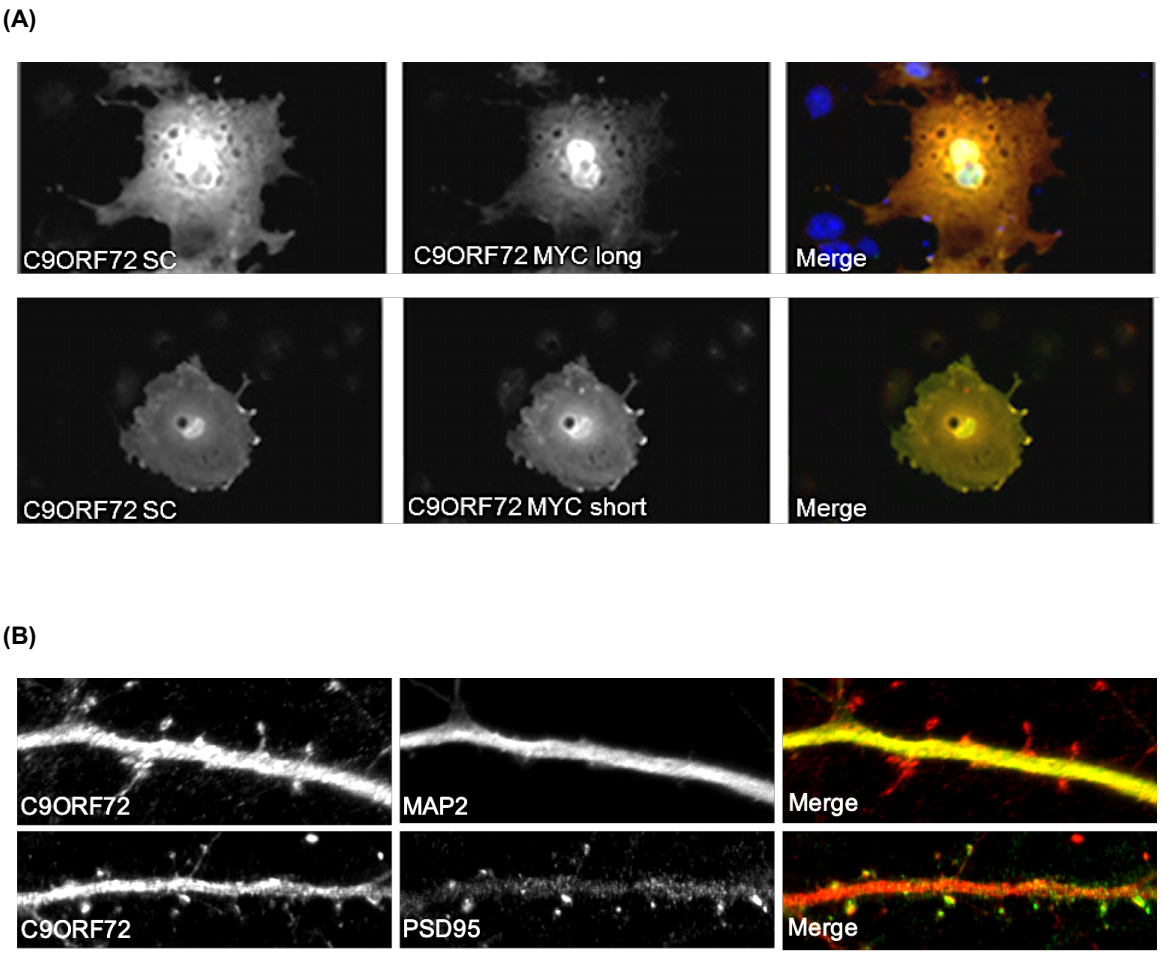

Figure 6 Immunofluorescence staining of C9ORF72 in COS7 cells and hippocampal neurons
(A) Overexpression of the long and short isoform of C9ORF72 in COS7 cells and immunofluorescence staining with the commercial antibody from Santa Cruz (SC). The SC antibody stained the same structures as the antibody against the MYC-tag of C9ORF72 in cells overexpressing MYC-tagged C9ORF72. Nuclei are labelled with DAPI (blue), the SC antibody is shown in red and the antibody against the MYC-tagged C9ORF72 is illustrated in green. (B) Immunofluorescence staining of hippocampal neurons. Endogenous C9ORF72 is stained in red, MAP2 (green) indicates microtubule filaments in neurites and post synaptic density 95 (PSD95) (green) serves as postsynaptic marker. C9ORF72 is localised in neurites and synaptic sites co-localising with PSD95.

(A)

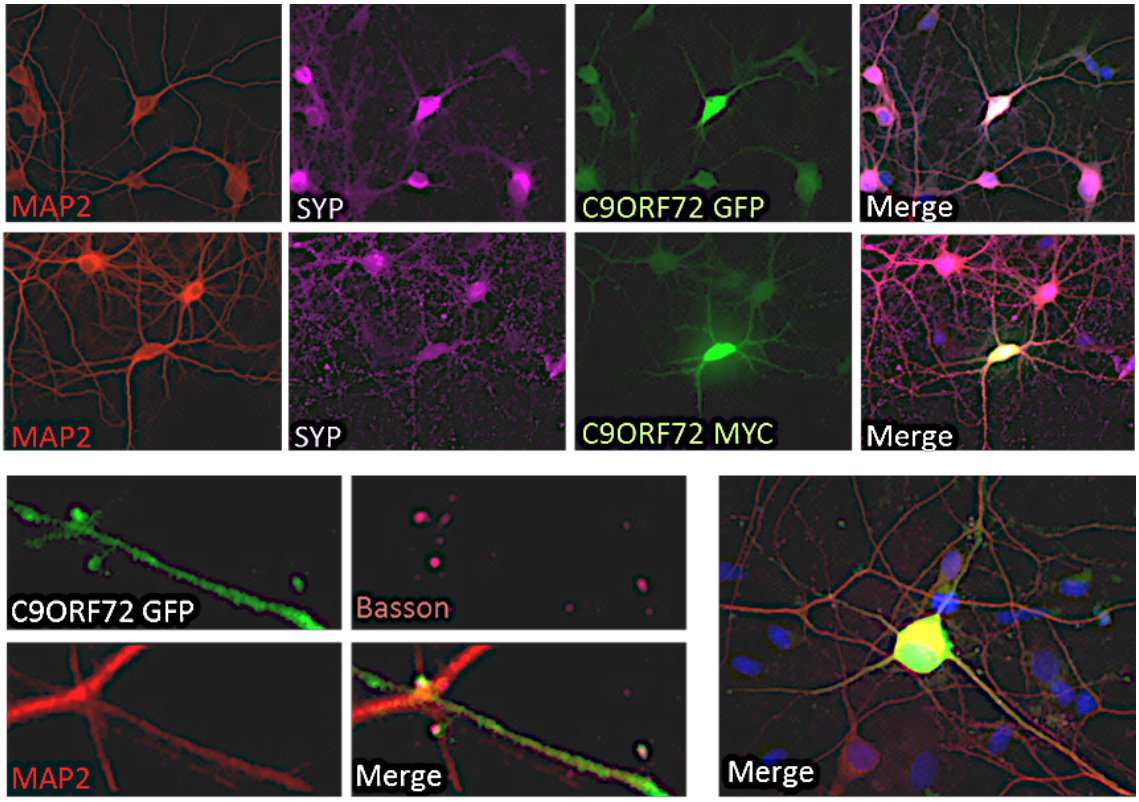

(B)

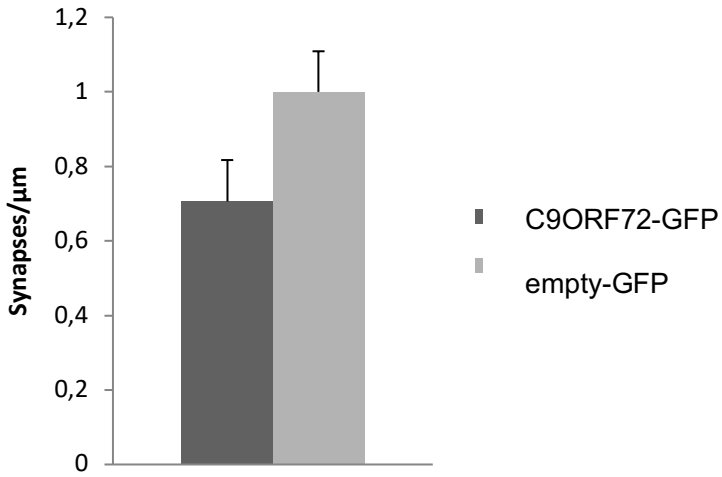

Figure 7 C9ORF72 overexpression in hippocampal neurons
(A) Overexpression of C9ORF72-GFP in hippocampal neurons. Nuclei are stained with DAPI (blue), microtubule with MAP2 (red) and synaptophysin (SYP) or bassoon (magenta) serve as markers for synaptic sites. Green fluorescence protein (GFP)-tagged C9ORF72 can be visualised in all neuronal compartments including cell soma, neurites and synapses. (B) Number of synapses per µm of C9ORF72-GFP transfected hippocampal neurons relative to control cells (transfected with empty GFP construct). Number of synapses was counted by counting SYP+ punctae. T-test analysis revealed significant differences ($p=0.024$) between synapse numbers with adjustment of $p<0.05$ for $n=3$ independent experiments, 15 cells per time point. Error bars show standard deviation (SD).

3.3 RAN translation dipeptide products in hippocampal neurons

Aggregates of misfolded proteins represent a common feature in a number of neurodegenerative diseases (Mackenzie et al. 2010, Manuscript, Todd Peter 2011). Likewise, C9-ALS pathology is similarly characterised by distinct intracellular protein aggregates. For example, TDP-43 inclusions were often found in histopathological analyses of samples from different brain regions of C9-patients. Additionally, inclusions with dipeptide repeat proteins that occur because of unconventional translation were also found within the cerebellum, hippocampus and throughout the neocortex (Mackenzie et al. 2013). To see if we could detect this pathology in our neuronal system, primary hippocampal neurons were transfected with four different recombinant dipeptide constructs: polyGA10, polyGA100, polyGP10 and polyGP100 (constructs obtained from L. Dupuis, University of Strasbourg). We could show that dipeptide aggregates were present in the perinuclear area in the cytoplasm of hippocampal neurons only when we transfected polyGA100 (Fig. 8).

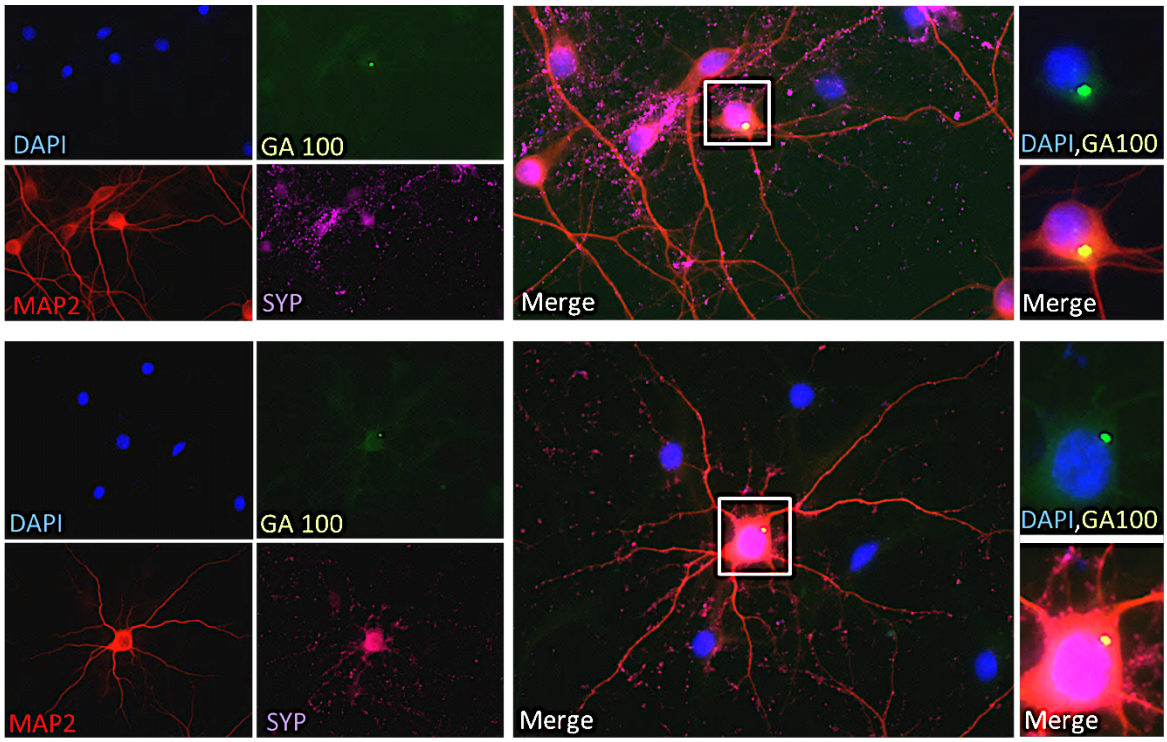

Figure 8 Overexpression of polyGA100 in hippocampal neurons
Immunofluorescence staining showing dipeptide aggregates in hippocampal neurons overexpressing polyGA100. Nuclei are stained with DAPI (blue), MAP2 (red) indicates microtubule filaments in neurites. Aggregates of GFP-tagged poly glycine-alanine (GA100) can be visualised in the cell soma. Aggregation of other dipeptide aggregates could not be observed (data not shown).

3.4 Characterisation of patient-derived human induced pluripotent stem cells

Keratinocytes from two different ALS patients with C9ORF72 hexanucleotide repeat expansion were cultured and successfully reprogrammed by Stefanie Raab and Moritz Klingenstein. Reprogramming was done with a lentiviral polycistronic STEMCCA cassette that contains the four Yamanaca-factors OKT4, SOX2, KLF4 and c-MYC. In order to use these two IPSC lines derived from patient material, we first had to perform a full characterisation of the cell lines. We characterised the two newly reprogrammed hIPSC lines with respect to morphology, the expression of stem cell surface markers and transcription factors, as well as the differentiation capacity into all three germ layers, so as to confirm their stem cell characteristics. Additionally, stem cell specific gene expression was analysed via qRT-PCR. At mRNA level, Nanog, OCT4 and SOX2 were highly up-regulated when compared to our housekeeping reference gene HMBS, and were increased up to 60-fold compared to the patient's keratinocytes mRNA, which were used as somatic cell controls lacking stem cell properties (Fig. 9 A). Furthermore, the two analysed patient-derived IPS cell lines showed typical stem cell morphology, including a flat round shape and high nucleus to cytoplasm volume ratio (Fig. 9 A). Additionally, both IPSC lines were positive for nuclear factors such as KLF4, Nanog, OCT4, and SOX2. The expressed surface markers SSEA, TRA1-60 and TRA1-81 were all indicative of pluripotency, a typical stem cell property (Fig. 9 B and C).

Finally, we wanted to test whether embryoid bodies generated from these cell lines could differentiate into the three germ layers spontaneously, as a further test of their stem cell properties. For that investigation, embryoid bodies were generated and then left for two weeks in culture to differentiate spontaneously. Afterwards, cells were stained with specific markers for endoderm (catenin), mesoderm (α-actinin) and ectoderm (tubulin-β3). The results showed that the two analysed IPSC lines were able to spontaneously differentiate into endoderm, mesoderm and ectoderm (Fig. 10).

(A)

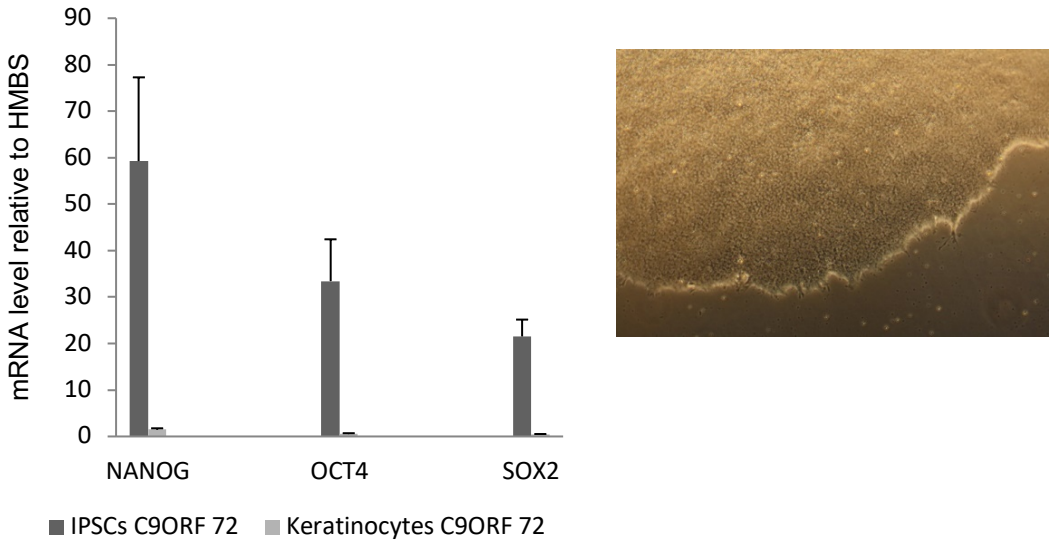
mRNA level relative to HMBS
90
80
70
60
50
40
30
20
10
0
NANOG
OCT4
SOX2
IPSCs C9ORF 72
Keratinocytes C9ORF 72

(B)

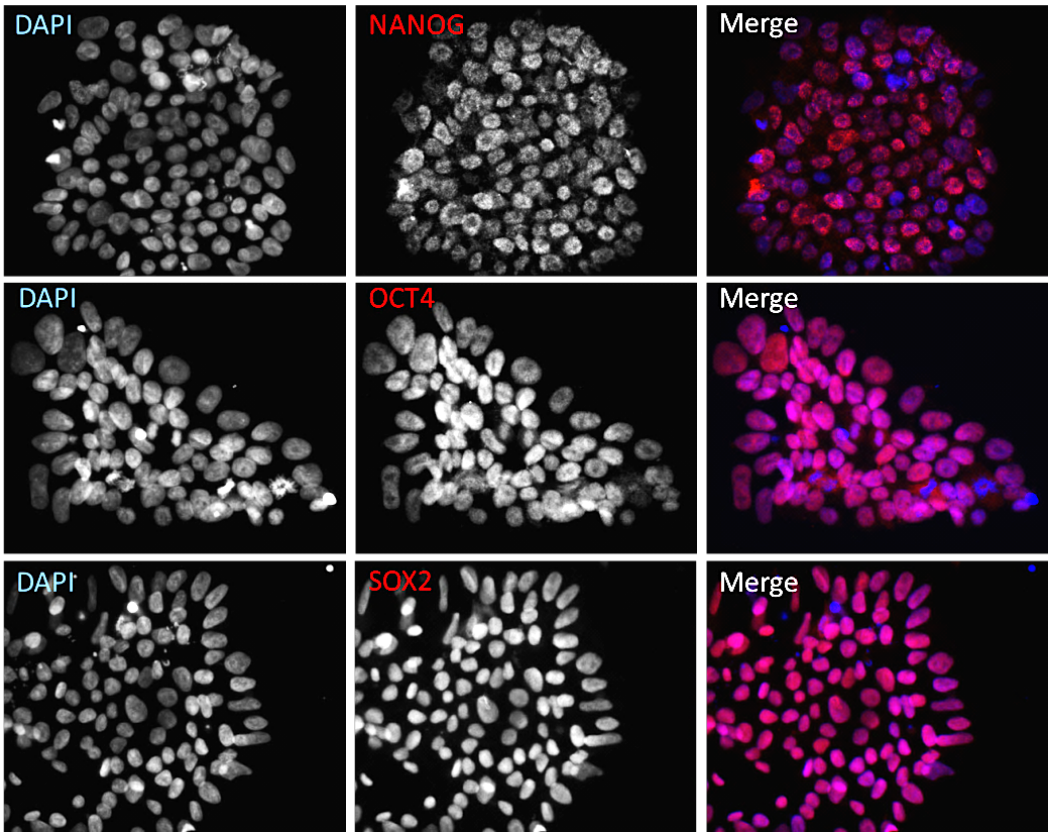
DAPI
NANOG
Merge
DAPI
OCT4
Merge
DAPI
SOX2
Merge

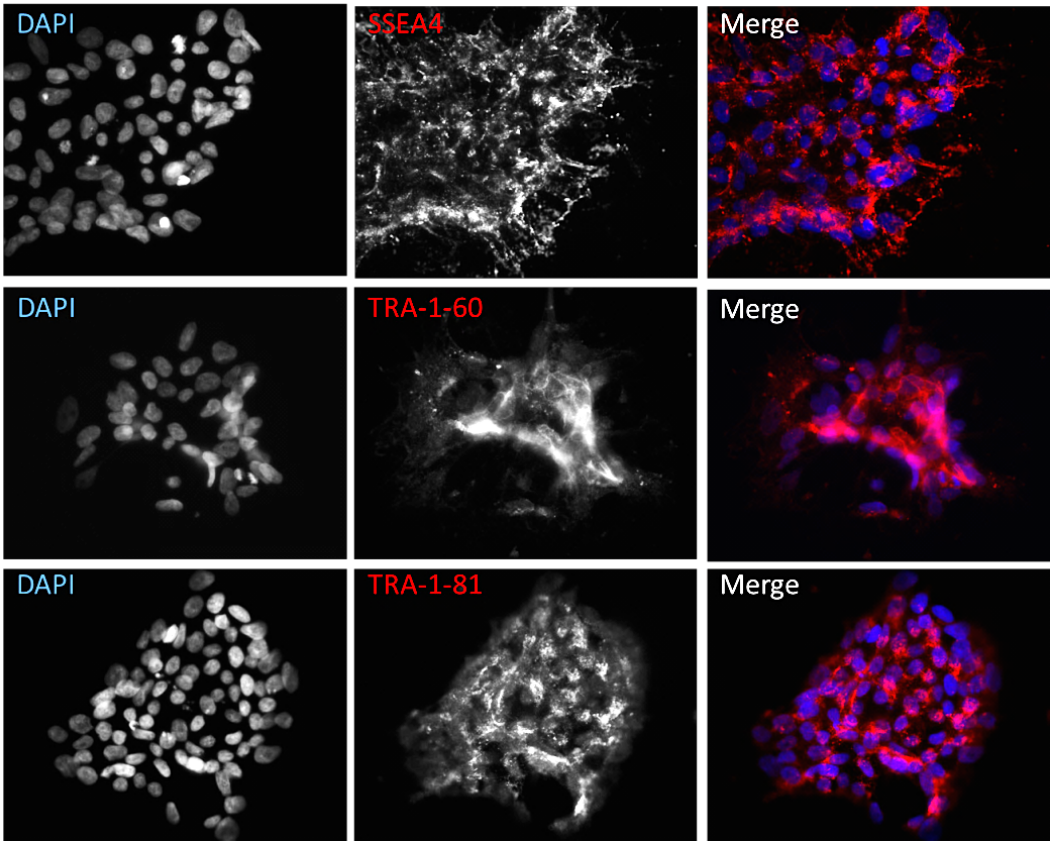
DAPI
SSEA4
Merge
DAPI
TRA-1-60
Merge
DAPI
TRA-1-81
Merge

(C)

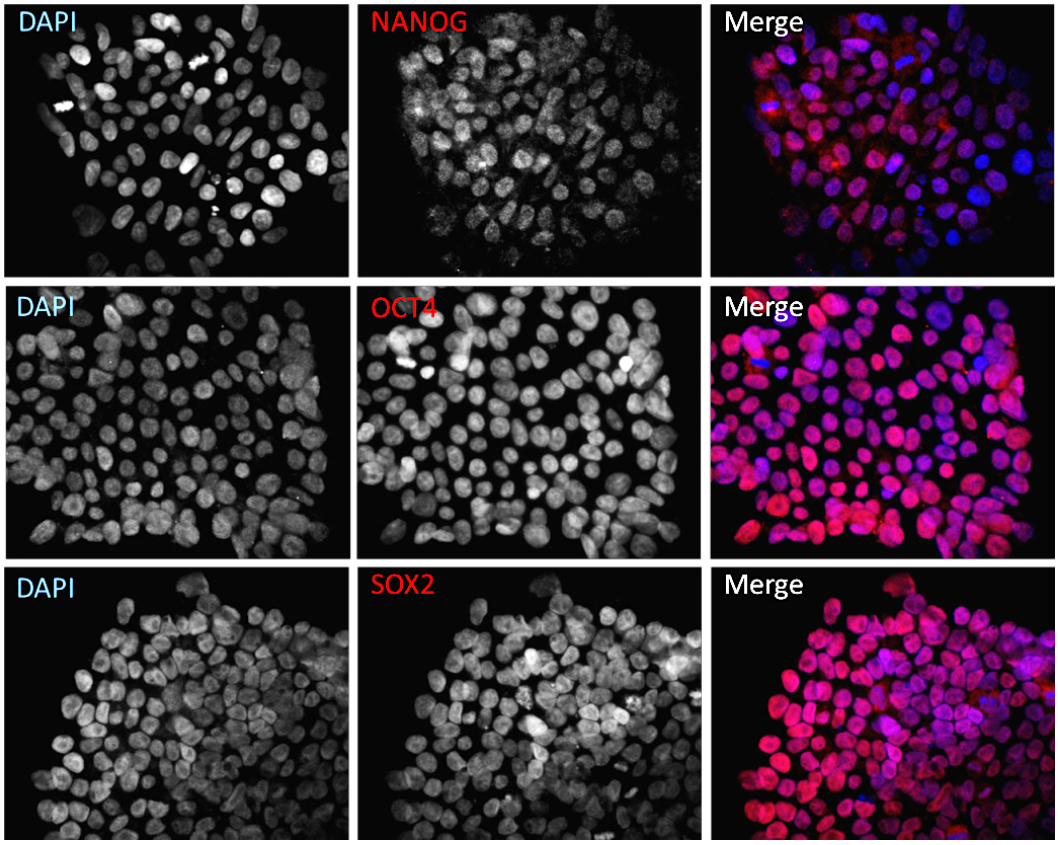
DAPI
NANOG
Merge
DAPI
OCT4
Merge
DAPI
SOX2
Merge

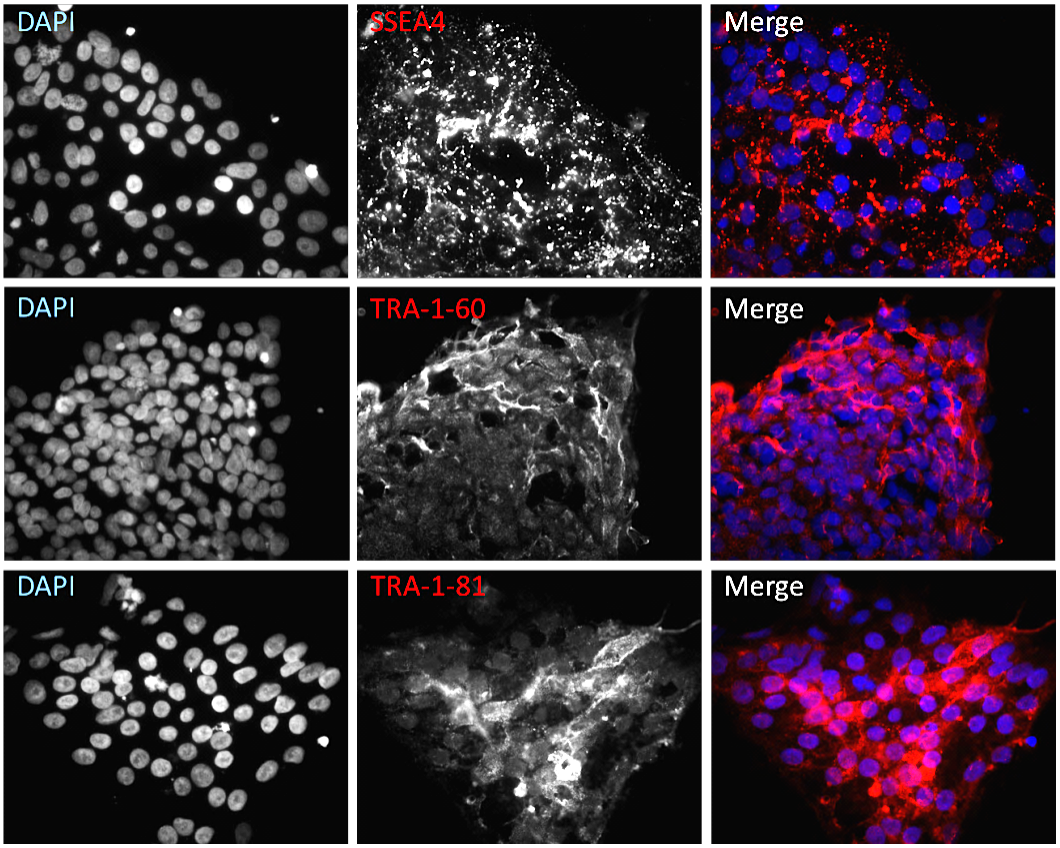

Figure 9 Expression of characteristic genes in pluripotent hIPSCs
(A) MRNA levels of specific pluripotency markers compared to the housekeeping gene HMBS. Gene expression of pluripotency markers Nanog, OCT4 and SOX2 was highly increased in hIPSCs of Patient 1 and 2 compared to patient keratinocytes (data is only shown for Patient 1). Error bars show standard deviation (SD) of technical and biological triplicates. In light microscopy, the cells show a typical stem cell morphology, including round shape, smooth edges and high nucleus to cytoplasm volume ratio. (B,C) Immunofluorescence staining of hIPSCs from Patient 1 and 2. Nuclei are labelled with DAPI (blue), transcription factors NANOG, OCT4, SOX2 as well as the pluripotency surface markers SSEA4, TRA-1-60, TRA-1-81 are illustrated (red).

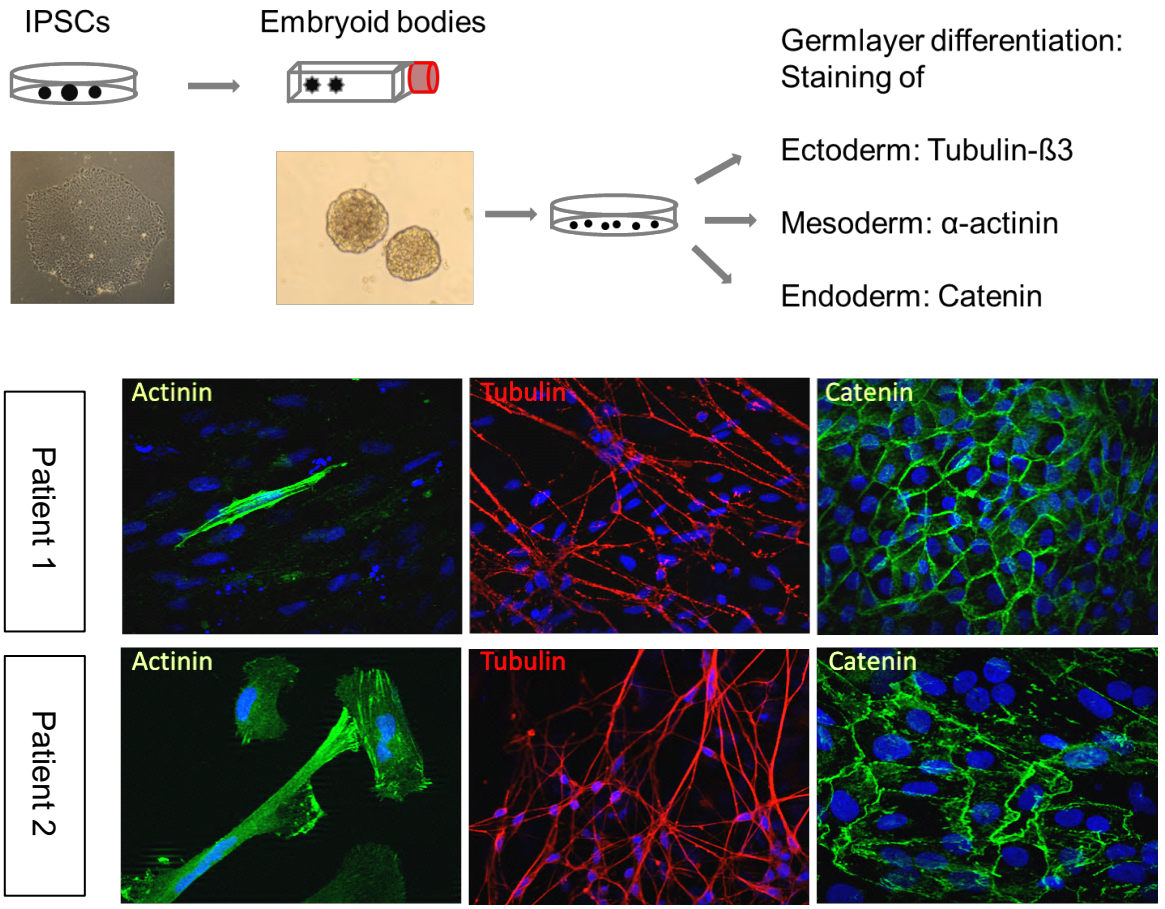

Figure 10 Germ layer differentiation of pluripotent hIPSCs
Embryoid bodies from hIPSC colonies of Patient 1 and 2 were able to spontaneously differentiate into all three germ layers: ectoderm (tubulin-β3, illustrated in red), mesoderm (actinin, green) and endoderm (α-catenin, green). All nuclei were labelled with DAPI (blue).

3.5 Instability of hexanucleotide repeat expansions in patient-derived IPSCs

In order to ensure that the patient-derived cells possess the expected repeat expansion and to check instability of the repeats, we collected DNA from different patient-derived cells (blood cells, keratinocytes, hIPSCs and IPSC-derived MNs) and did southern blot analysis, in cooperation with Kathrin Müller and AG Weishaupt of Ulm University Hospital. In white blood cells, we found a heterozygous repeat expansion of nearby 1800 repeats in Patient 1 and 1200 repeats in Patient 2 (Fig. 11 A and B) (Higelin et al. 2018). In the IPSCs of Patient 2, the repeats still occurred after reprogramming, but in slightly decreased number for the expanded allele and slightly increased number for the normal allele (Fig. 11 B). However, the repeats of Patient 1 could not be detected at the IPSC level after reprogramming and were also absent from differentiated MNs. In addition, to exclude chromosomal abnormalities, we karyotyped the cells in cooperation with Prof. Barbi, Ulm University. We found normal female (46 XX) and male (46 XY) karyotypes (Fig. 11 A and B). Chromosome preparation of trypsinized hIPS cells of passages 10–20 was performed according to standard procedures and karyotyping was carried out after GTG-banding. A total of 38 metaphases were scored.

(A)

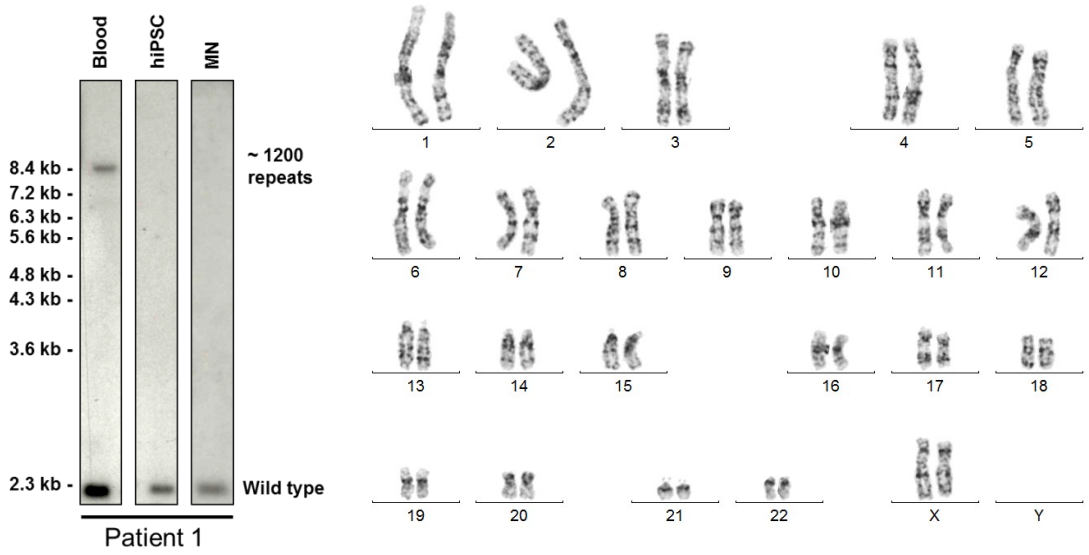

(B)

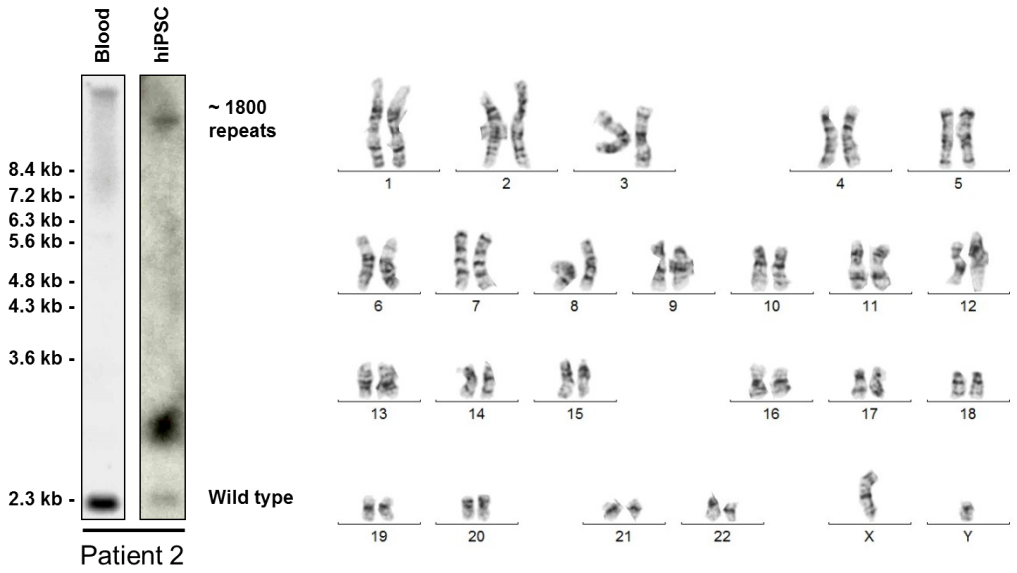

Figure 11 Southern blot analysis and karyotyping of hIPSCs
Cells used for the collection of DNA: Blood cells, hIPSCs and MNs. (A) Using the southern blot technique, we could show that Patient 1 completely lost repeat expansions in hIPSCs and hIPSC-derived motoneurons compared to blood cells. The second normal allele did not vary after reprogramming the cells. Karyotyping of hIPSCs confirmed normal chromosomal setting of patient-derived cells: 46 XX. (B) The repeat expansion of Patient 2 of blood cells exceeded the one in Patient's 2 hIPSCs and, in addition, the size of expansions increased concerning the second normal allele. Karyotyping of hIPSCs confirmed normal chromosomal setting of patient-derived cells: 46 XY. Modified from Higelin et al. 2018, © 2018 The Authors.

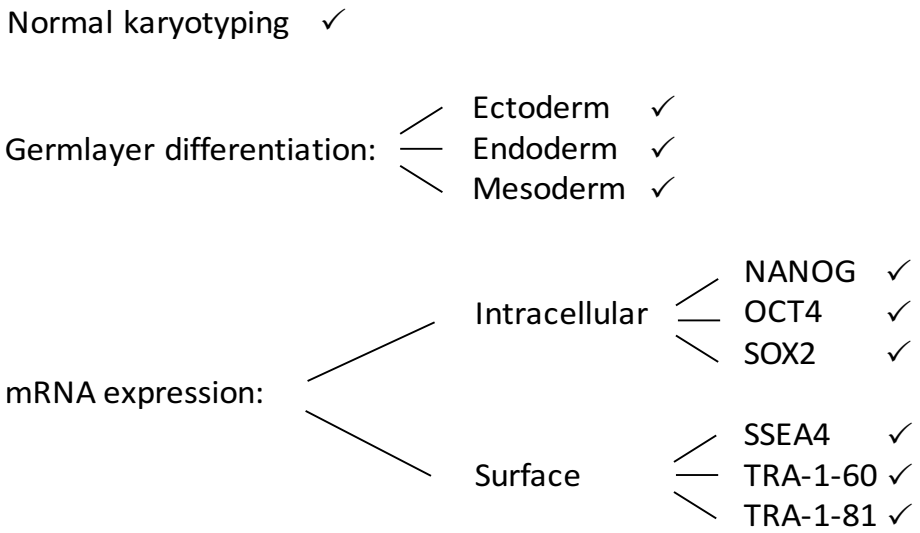

Figure 12 Overview IPSC characterisation
Analysed IPSCs show normal karyotyping, are able to differentiate into all three germ layers and express typical transcription factors NANOG, OCT4, SOX2 as well as the pluripotency surface markers SSEA4, TRA-1-60, TRA-1-81.

3.6 Decreased viability of C9ORF72 hIPSCs after DNA damage

Devlin et al. reported in 2015 that IPSC-derived MNs harbouring C9ORF72 mutation lost their function, although they did not show altered viability compared to control cells (Devlin et al. 2015). To analyse if patient-derived IPSCs show decreased viability after experiencing stress, hIPSCs were irradiated with γ-irradiation to cause DNA damage. Thereafter, the cells were allowed to repair induced DNA damage for different lengths of time to see if mutant C9ORF72 affected the response to this type of stress. As an endpoint, we counted the presence of apoptotic cells before and after irradiation in one control cell line and in the Patient 2 cell line containing the repeats. For that purpose we stained the IPSCs with an antibody-recognising activated caspase-3, which mediates apoptotic cell death. Caspase-3 represents an enzyme of the cysteine-aspartic acid protease family that cleaves and activates key cellular proteins leading to apoptosis. In general, IPSC colonies can be classified morphologically as being normal with typical stem cell morphology, as being differentiated, or as undergoing apoptosis. Apoptotic cells were defined as having a condensed and fragmented nucleus, when stained with DAPI. We investigated the abundance of apoptotic cells 10 min, 1 h, 4 h and 24 h post-irradiation (Fig. 13 A and B). Prior to the irradiation treatment, control and patient-derived IPSCs were not completely devoid of apoptotic cells (3.0±0.6 % of control vs 4.0±0.1 % of C9ORF72 cells). At 10 min post-irradiation, we detected an initial increase of apoptotic cells (4.6±0.3 % of control vs 5.1±0.6 % of patient cells). 1 h post-irradiation the amount of apoptotic cells decreased to 3.1±0.3 % in control and 4.2±0.5 % in patient-derived cells. 4 h post-irradiation, we detected a maximum of 5.6±0.61 % of cells undergoing apoptosis in control cells and 18.9±1.1 % in C9ORF72 cells. Due to delayed repair mechanisms, at 24 h post-irradiation, only 3.6±0.2 % of control IPSCs stained positive for activated caspase-3. However, 6.0±0.6 % of patient-derived IPSCs still showed caspase-3 activity 24 h post-irradiation. To sum up, the unirradiated control cells and the patient cells initially (-irradiation) have lower apoptosis levels than after irradiation. The control cells after irradiation showed the same dynamics of increase and decrease of apoptosis, but in control cells, cell death was always at lower levels than in patient-derived cells (Fig. 13 B).

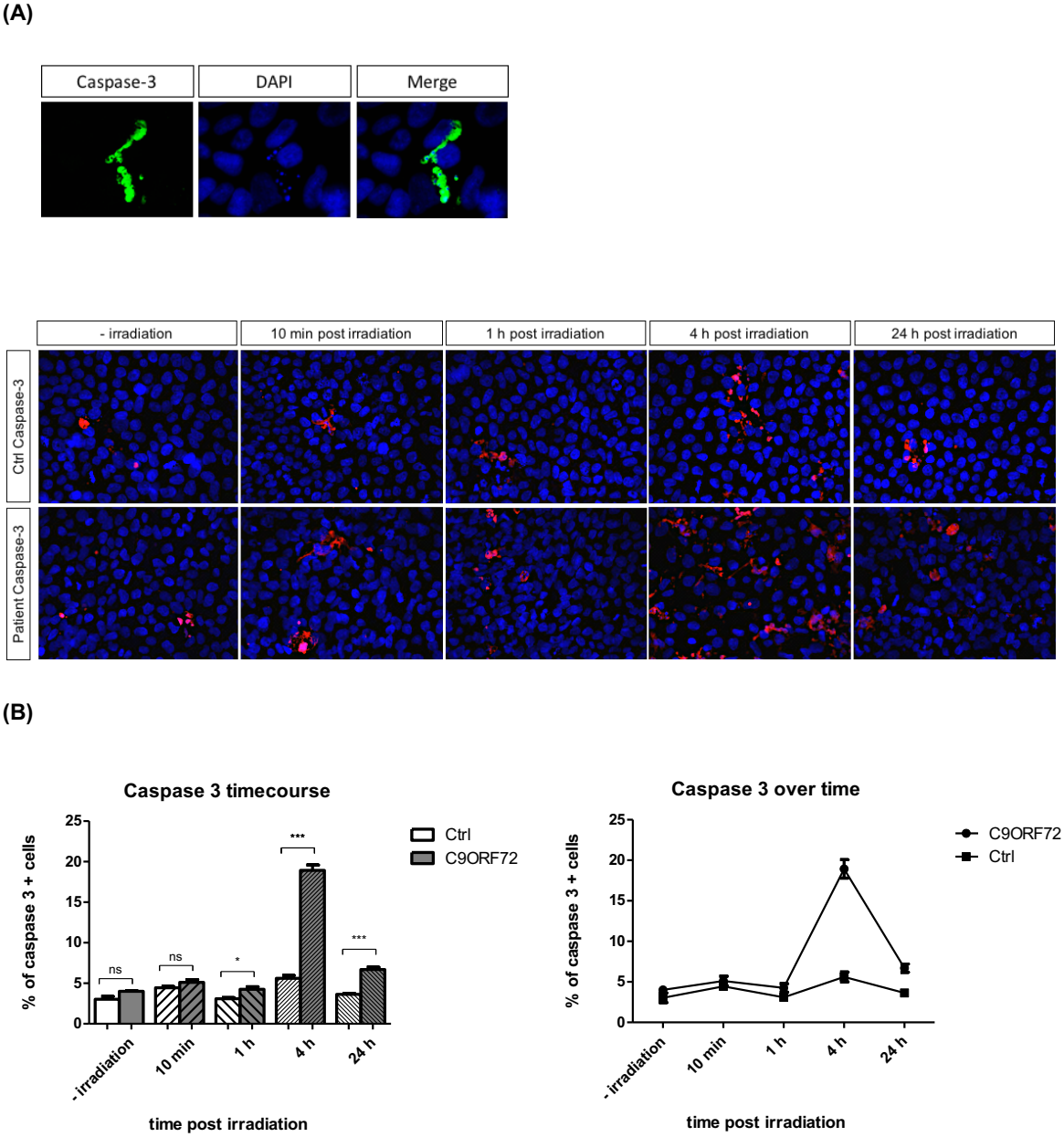

Figure 13 Apoptosis in patient-derived IPSCs without and with DNA damage induction
(A) Representative immunofluorescence images of caspase-3 activation. Apoptotic cells with condensed and fragmented nucleus. Time course analysis of apoptotic cell death before irradiation and after irradiation (10 min, 1 h, 4 h and 24 h) in Patient 2 (with repeats) and control cells. Prior to irradiation, CTRL and C9ORF72 IPSCs were not completely devoid of apoptotic cells. The percentage of caspase-3$^+$ cells was increased at all time points before and after irradiation in C9ORF72 cells compared to CRTL cells. At 24 h post-irradiation the number of caspase-3$^+$ cells in C9ORF72 cells still exceeded the quantity of apoptotic cells prior to irradiation while CTRL cells returned to baseline levels of apoptotic cells. Nuclei are labelled in blue (DAPI), caspase-3 in green or red. (B) Quantification of caspase-3$^+$ cell kinetics before and after γ-irradiation showed significantly increased caspase-3 activity 1 h, 4 h and 24 h post-irradiation (students t-test was performed to compare CTRL versus patient-derived cells; indicated by asterisks, - irradiation CTRL vs. C9ORF72 not significant (ns), 10 min post irradiation CTRL vs C9ORF72 ns, 1 h post irradiation CTRL vs C9ORF72 * $p<0.05$, 4 h and 24 h post irradiation CTRL vs C9ORF72 *** $p<0.001$.) More than 800-1000 cells were counted for each time point. Error bars represent standard deviations calculated from three independent experiments.

3.7 Hyperosmolar stress induced no visible protein aggregation in C9ORF72 hIPSCs

In other ALS mutations (such as FUS and TDP-43) and likewise in C9ORF72 mutation, cytoplasmic aggregation of the mutant RNA binding proteins and RAN translation proteins results in increased stress granule (SG) formation after stress induction, which is critical for cell survival and recovery (Bentmann et al. 2012, Li et al. 2013, Lenzi et al. 2015, Tao et al. 2015). To investigate this process, we treated the IPSCs with sorbitol to cause osmotic stress, and we stained against TIA1 cytotoxic granule associated RNA binding protein (TIA1), a marker for stress granule formation, after hyperosmolar stress induction, and against the RNA binding proteins FUS and TDP-43. Prior to sorbitol treatment, FUS and TDP-43 were mainly located in the nuclei in control and patient-derived cells (Fig. 14 A shows representative images of FUS localisation and Fig. 14 B shows representative images of TDP-43 localisation before and after sorbitol treatment). Low levels of cytoplasmic TIA1, FUS and TDP-43 were detectable in the control cell lines as well as C9ORF72 cells, but to a negligible degree. After sorbitol treatment, however, in some cells the RNA binding proteins TDP-43 and FUS were translocated into the cytoplasm together with TIA1. The staining of the patient-derived cells presented the same pattern of SG formation (TIA1) and RNA binding protein (FUS, TDP-43) localisation before and after sorbitol treatment as did the staining of control cells.

(A)

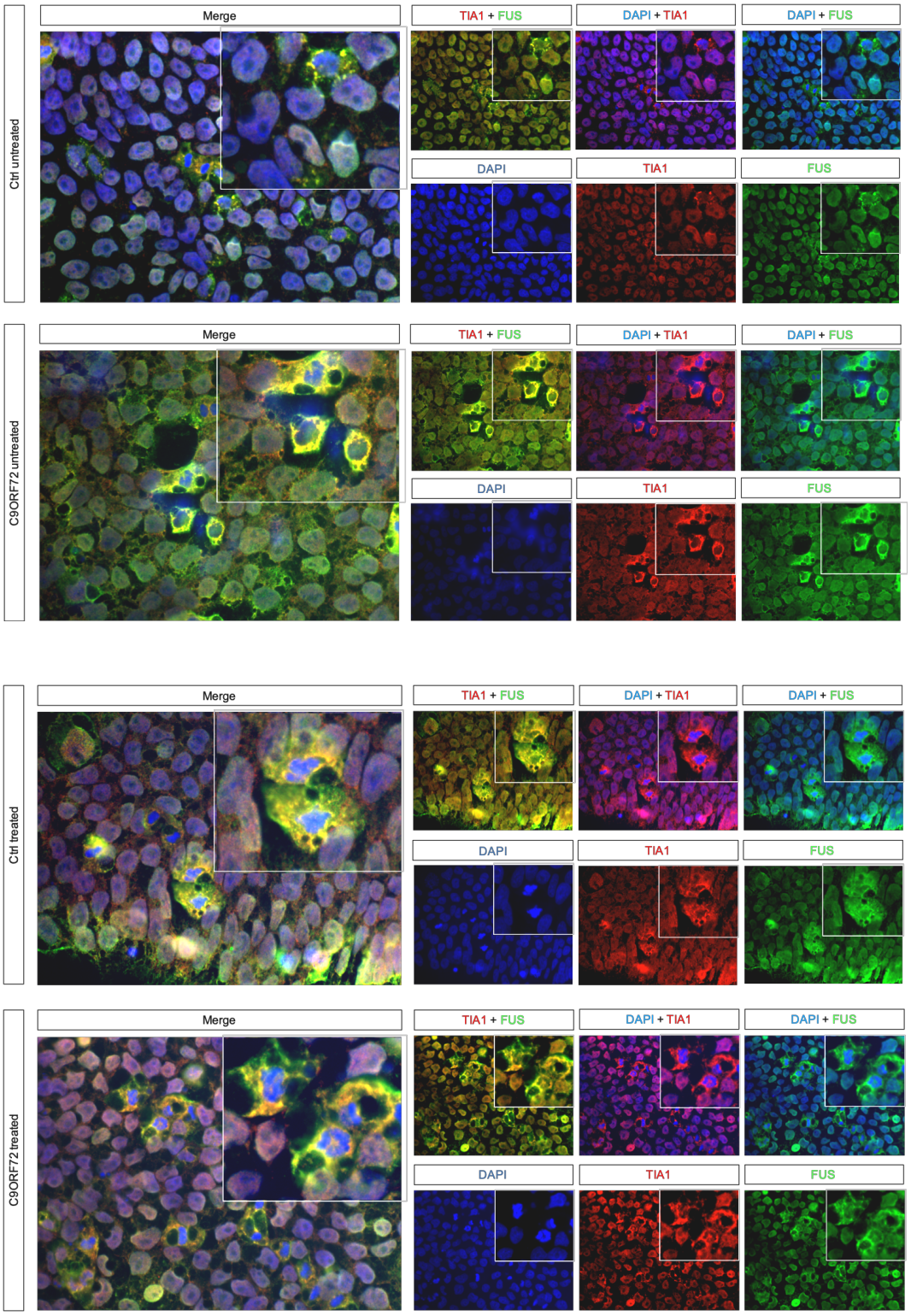
Ctrl untreated
Merge
TIA1 + FUS
DAPI + TIA1
DAPI + FUS
DAPI
TIA1
FUS
C9ORF72 untreated
Merge
TIA1 + FUS
DAPI + TIA1
DAPI + FUS
DAPI
TIA1
FUS
Ctrl treated
Merge
TIA1 + FUS
DAPI + TIA1
DAPI + FUS
DAPI
TIA1
FUS
C9ORF72 treated
Merge
TIA1 + FUS
DAPI + TIA1
DAPI + FUS
DAPI
TIA1
FUS

(B)

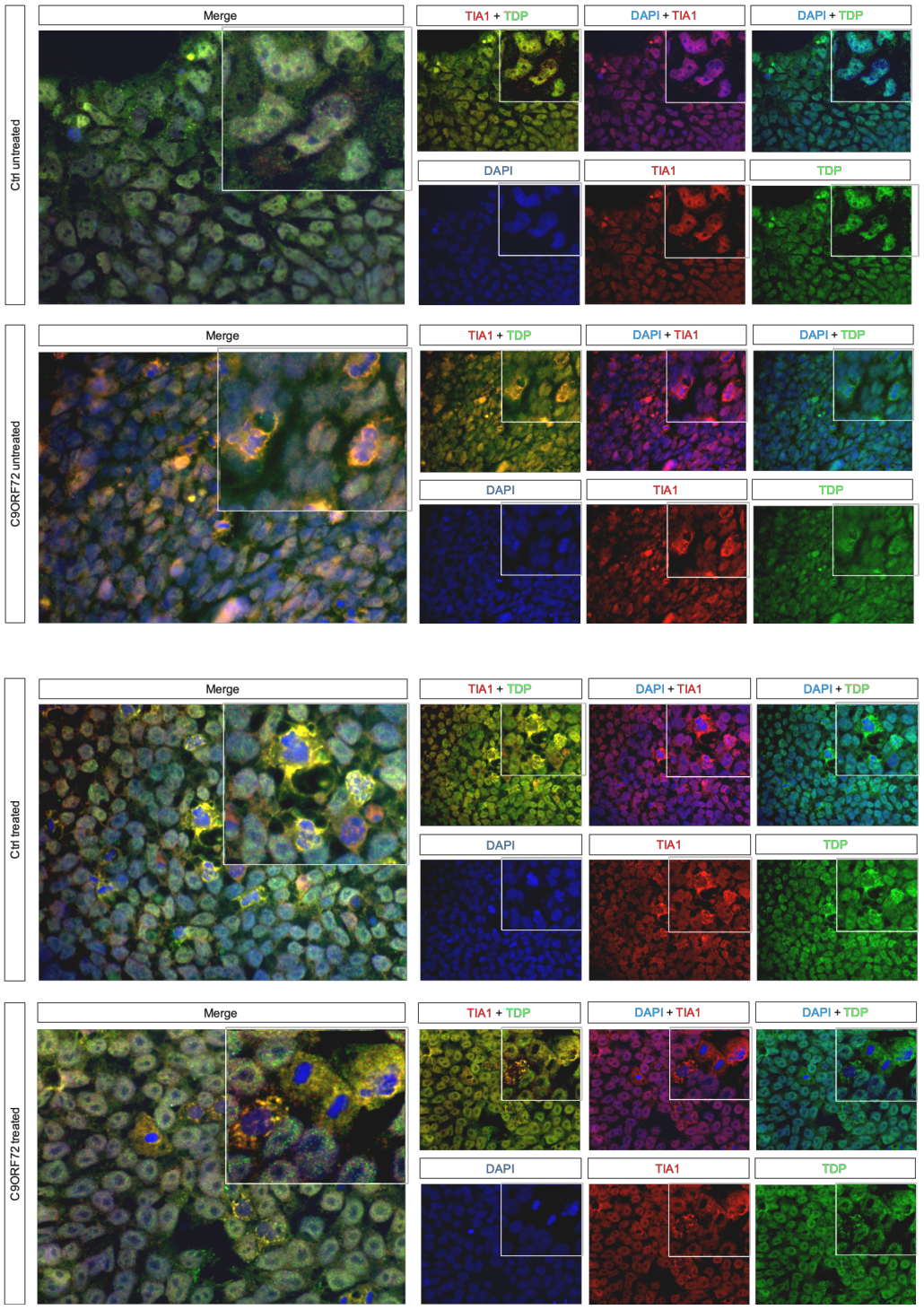

Figure 14 Stress granule formation before and after sorbitol treatment in patient-derived IPSCs
Immunofluorescence staining of (A) FUS, and (B) TDP-43 in control cells and Patient 2 cells (containing repeats) before and after sorbitol treatment. The stress granule marker TIA1 is shown in red and aggregating prone RNA-binding proteins FUS and TDP-43 are shown in green. Nuclei are labelled in blue (DAPI). IPSCs show a diffuse accumulation of TIA1 and the RNA-binding proteins like FUS or TDP-43 in the cytoplasm in patient and control cells after sorbitol treatment. Prior to sorbitol treatment low levels of cytoplasmic FUS and TDP-43 were detectable in the control cell lines as well as C9ORF72 cells, but to a negligible degree.

3.8 RNA-foci and protein aggregates in patient-derived keratinocytes and hIPSCs

As described in the introduction, transcripts of the disease-causing hexanucleotide repeat expansion may form nuclear RNA foci, which sequester RNA binding proteins or undergo RAN translation leading to different protein aggregates. We therefore analysed RNA foci of the hexanucleotide repeat expansion and protein aggregation of DPRs caused by RAN translation in patient-derived keratinocytes and IPSCs. Additionally, we also investigated other disease-specific markers, like aggregating TDP-43, hnRNPK1 or FUS that have been previously detected in postmortem tissue of C9ORF72 patients, or had been shown to be present in other patient-derived cells harbouring C9ORF72 or FUS mutations.

To analyse toxic RNA foci in C9-ALS, patient-derived IPSCs were analysed by using fluorescence *in situ* hybridization (FISH) against the (GGGGCC)n repeats with a Cy3 labelled probe (Fig. 15 A) (Higelin et al. 2018). We detected RNA foci in ~35 % of patient-derived keratinocytes. Cells typically had 1 to 5 foci in the nucleus, but those with >5 foci were not uncommon (Fig. 15 C). This pattern did not change after irradiation of the hIPSCs (data not shown). Although we found evidence for RNA foci, we did not observe repeat-associated non-ATG–dependent C9-RAN protein products in these cells with or without irradiation. To address this, the cell lines were stained with an antibody against poly(GA) (Fig. 15 B). The poly(GA) antibody diffusely stained the perinuclear area, but this pattern was extremely rare compared to non-specific staining of the cells. Furthermore, keratinocytes and stem cells subjected to FISH were subsequently stained against poly(GA) for examination of the relationship between RNA foci and RAN translation. However, GA aggregates were not reliably detected in these cell types, and very few cells showed diffuse staining of poly(GA) and RNA foci, which were localized in the perinuclear area.

Further, we did not detect aggregates for TDP-43, hnRNPK1 or FUS, either in keratinocytes or in hIPSCs, as shown in IF staining, in which TDP-43, FUS and hnRNPK1 are mainly nuclear in distribution (Fig. 16 A). Furthermore, we stained the IPSCs against HDAC1, a histone deacetylase responsible for cell cycle gene expression and DNA repair, which is known to aggregate in cells harbouring a

FUS mutation (Wang et al. 2013). While HDAC1 presented a diffuse nuclear staining in most nuclei, HDAC1 formed nuclear aggregates or foci in some nuclei (Fig. 16 B). We found a slight increase in the number of cells containing nuclear HDAC1 aggregates in patient-derived hIPSC compared to control cells; 3.9 % versus 2.8 % of cells had HDAC1 protein aggregates, but this difference was not significant (Fig. 16 B).

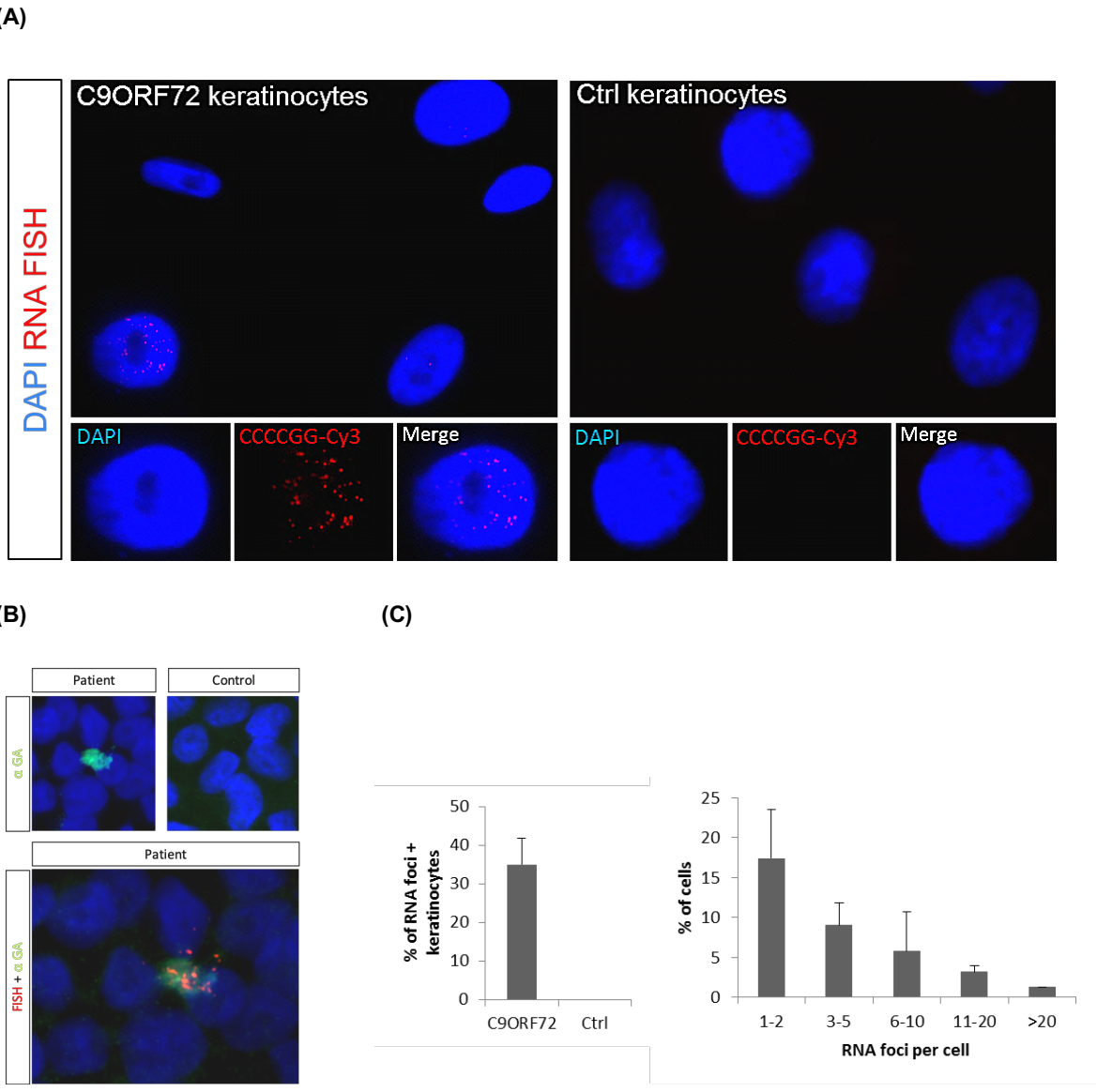

Figure 15 RNA foci in patient-derived keratinocytes
(A) Representative images of fluorescence *in situ* hybridisation (FISH) with a Cy3 (red) labelled antisense probe to the GGGGCC repeat in patient-derived keratinocytes (Patient 2) and control cells. Nuclei are labelled with DAPI (blue). Modified from Higelin et al. 2018, © 2018 The Authors. (B) Immunofluorescence staining of poly(GA) in green and FISH in red. (C) RNA foci were present in ~35 % of cells from C9-ALS patients, but not in keratinocyte cultures from control subjects. Typically, patient-derived cells had 1-5 nuclear RNA foci, but also cells with more than 5 and even 20 foci were detected in decreasing amounts. Error bars show standard deviation (n=3 independent experiments with 50 cells per time point).

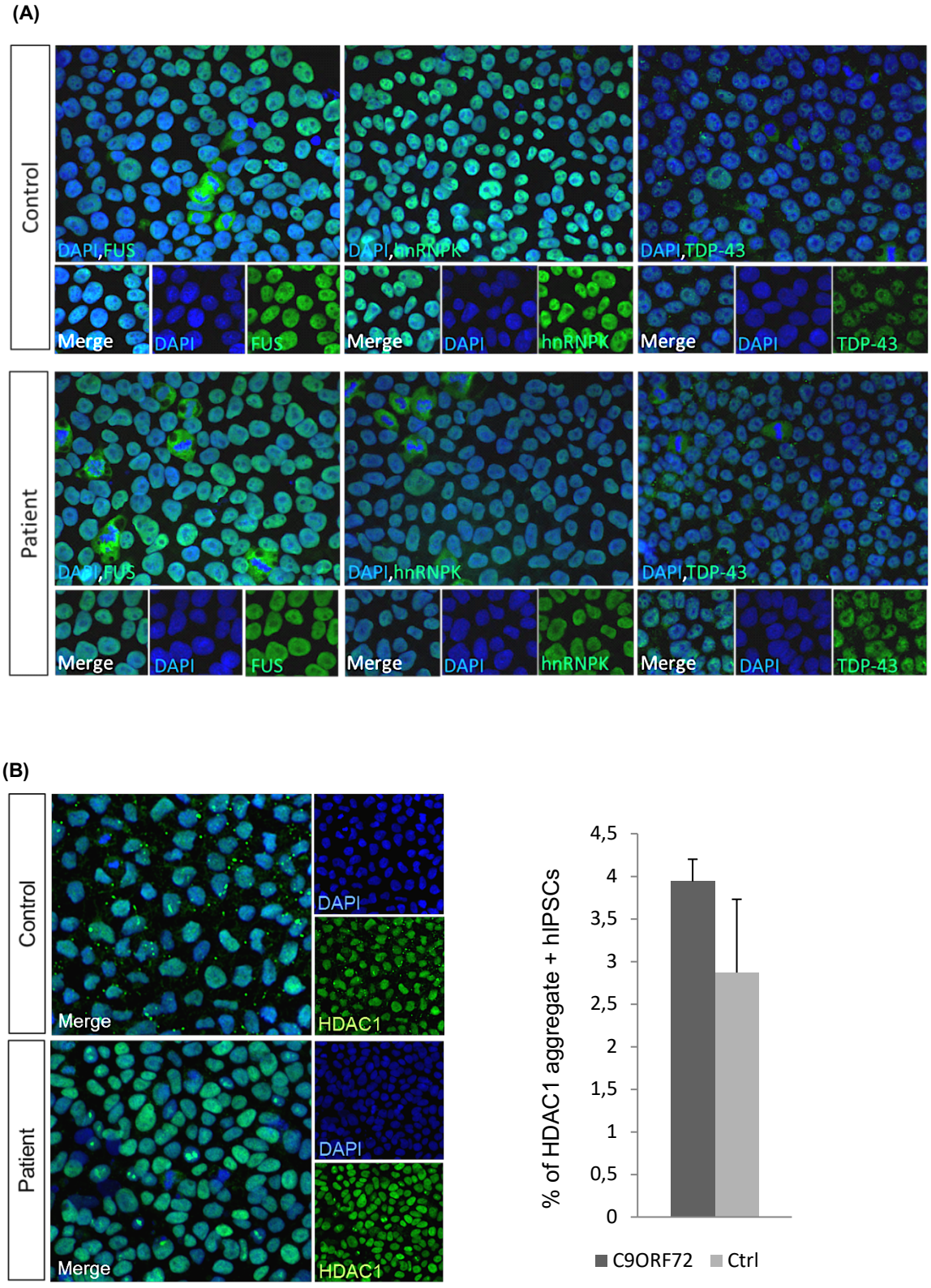

Figure 16 Protein aggregates in patient-derived IPSCs
(A) Immunofluorescence staining of FUS, hnRNPK and TDP-43 in patient-derived (Patient 2) and control IPSCs. Nuclei are labelled in blue (DAPI), different proteins in green. (B) Immunofluorescence staining of HDAC1 (green) in hIPSCs. 3.9 % of patient-derived cells show nuclear protein aggregates compared to 2.8 % of control cells (not significant). Error bars show standard deviation (n=3 independent experiments with 300 cells per time point).

3.9 MRNA level analysis of hIPSCs

First, we analysed mRNA levels of the isoforms of C9ORF72 and the RNA binding proteins TARDBP and FUS of Patient 2 hIPSCs to examine whether there were any alterations in gene expression of RNA binding proteins. Second, in so far as C9-ALS can be considered a distal axonopathy, we analysed gene expression levels of the three isoforms of synaptic Shank molecules in patient-derived cells relative to cells from healthy individuals to check for alterations in synaptic proteins. As it can be seen in Figure 17, there are no notable abnormalities in gene expression of C9ORF72 short isoform or the RNA binding proteins, TDP-43 and FUS. The C9ORF72 long isoform, however, had reduced expression in patient-derived cells. Shank 1 and Shank 2 were also expressed at comparable levels, but Shank 3 had lower expression in patient-derived cells than in normal cells.

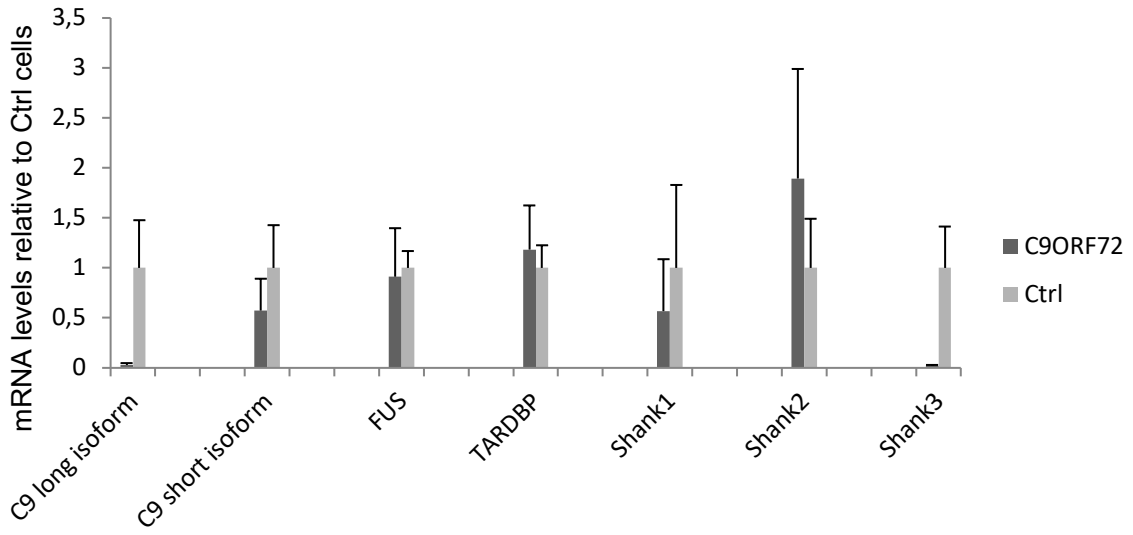

Figure 17 MRNA levels of C9ORF72, RNA-binding and synaptic proteins in hIPSCs
MRNA levels of C9ORF72 short and long isoform, TARDBP, FUS, Shank1,2 and 3 compared to the housekeeping gene HMBS. The long isoform of C9ORF72 and Shank 3 were rarely expressed in patient-derived IPSCs (Patient 2 containing the repeats) in comparison to non-mutated cells. All other analysed genes were slightly less or equally expressed except for Shank 2, which was expressed at a higher level than in control cells. Error bars show standard deviation of technical and biological triplicates.

3.10 Differentiation of hIPSCs into MNs

Differentiation of hIPSCs from Patient 1 into MNs was achieved through the usage of a differentiation protocol established by Hu and Zhang, 2009, with some modifications. This protocol adds RA and purmorphamine (PM) into the media of distinct cell cultures to induce motoneuronal differentiation (Fig. 18) (Hu and Zhang 2009), as is described in detail in 2.4.11. During MN differentiation, the analysis of the transcript levels of the general neuronal marker (TUB-β3) and specific motoneuron markers (NEFH, CHAT) indicate the differentiation of hIPSCs into MNs. We analysed the different steps of differentiation and maturation via IF staining and qRT-PCR. However, the differentiation was mainly evident from morphological changes in the cells, as illustrated in Figure 18. After final plating on coated dishes, the neuroshperes extended neurites which continually grew and build up a dense neuronal network during days 28-48 in culture. After the first 2-4 days of plating, undefined projections grew out of the neurospheres into all directions. In the following days, the projections retracted and one long prominent neurite grew out, followed by several others in the following weeks (Fig. 18).
Differentiation of hIPSCs of Patient 2 into MNs could not be achieved using the same protocol as for Patient 1. The cells proved difficult to handle, and the rate of formation of embryoid bodies or neuroepithelial cells was extremely low, such that neurospheres and mature MNs could not be generated.

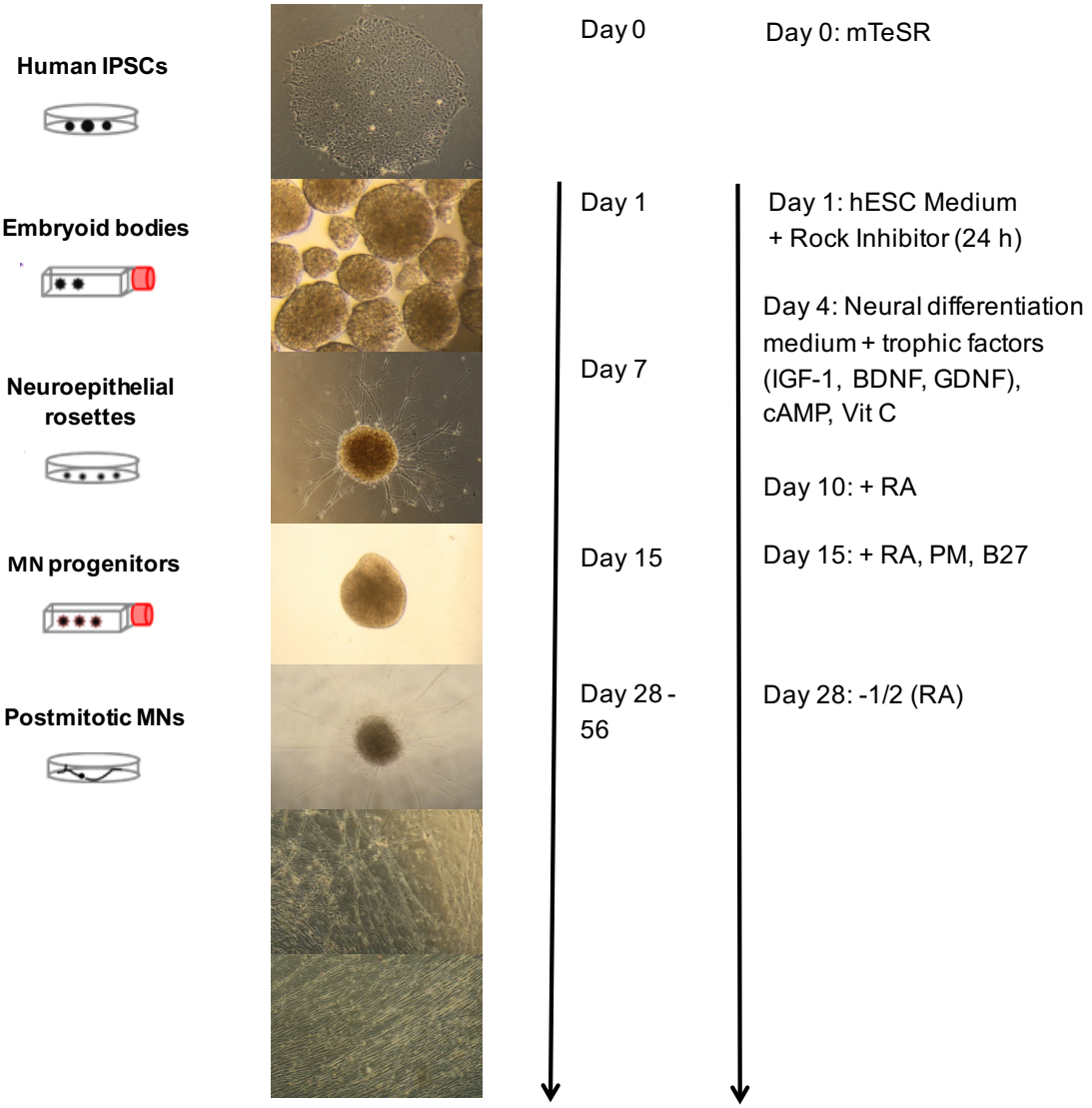

Figure 18 Differentiation of hIPSCs into MNs
Scheme of MN differentiation and bright field images showing morphological changes during differentiation according to the addition of different media supplements. On day 1, with the addition of hESC medium, embryoid bodies (EBs) were generated out of hIPSCs. On day 10 – 15 neurorosettes attached to cell culture plate. Neurorosettes were cultured in neuronal differentiation medium supplemented with different trophic factors. Neurospheres were cultured in suspension from day 15 – 28. Final plating of motoneuron (MN) progenitors took place on day 28 and culture was maintained for up to 56 days.

3.11 Characterisation of MNs

To ensure the differentiation process of hIPSCs into mature MNs of Patient 1 was achieved correctly, we analysed mRNA expression by performing a qRT-PCR analysis of the early neuronal marker tubulin β3, that steadily increased in patient cells and to a much greater extent in control cells. The MN-specific axon marker NEFH (SMI-32) serves for comparison. Choline acetylcholine transferase (CHAT), the enzyme for the neurotransmitter synthesis, serves as marker for mature MNs.
In our study, both isoforms of C9ORF72 were expressed in 21 days old and 42 days old MNs, without any evident difference between patient and normal cells (Fig. 19). Additionally, we examined if there is an altered expression of other ALS-causing genes. TARDBP and FUS were slightly decreased in C9ORF72 MNs compared to control MNs on day 21, but were nearly equal on day 42. We could also detect low expression levels of Shank 1, 2, 3 (S1, S2, S3) and Homer1 as markers for the postsynaptic compartment important for correct synaptogenesis (Grabrucker et al. 2009). Except for Shank 3 and the short isoform of C9ORF72, all analysed genes had lower expression in patient-derived MNs than in control MNs when they were cultivated for 21 days. A higher expression level of Tub β3 compared to NEFH in control cells indicates a larger amount of neuronal cells in comparison to MNs. Patient MNs that were cultured for 42 days also had decreased mRNA levels for all analysed genes, except that FUS was slightly increased.
IF staining of FUS and TDP-43 also did not show protein aggregates or altered distribution of the proteins to that seen in control MNs (Fig. 20 A). Both proteins were found mainly in the nuclei of the analysed MNs. Further, fluorescence *in-situ* hybridisation of patient-derived MNs of Patient 1 did not reveal any RNA foci, but appeared similar to control MNs (Fig. 20 B).

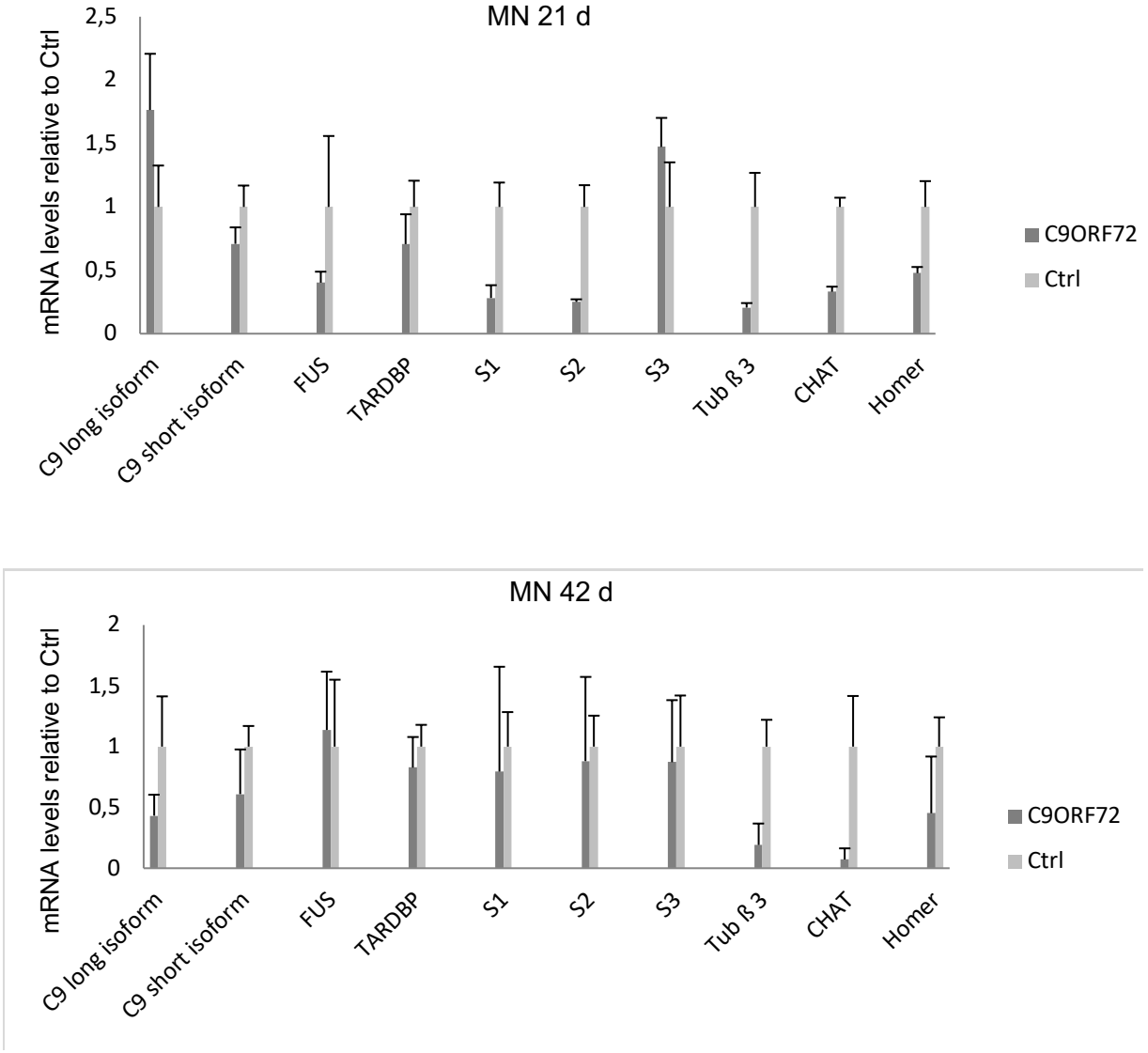

Figure 19 Gene expression analysis of patient-derived MNs
QRT-PCR analysis of 21 days and 42 days old MNs. All mRNA levels are shown relative to the mRNA level of the MN axon marker NEFH. General neuronal marker Tubulin β3 increased during neuronal differentiation in patient-derived MNs and much more in control cells. Choline acetylcholine transferase (CHAT), a marker for mature MNs, is shown in both cell lines. Both isoforms of C9ORF72 were expressed in 21 days old and 42 days old MNs whereby the long isoform was expressed at a higher degree in 21 days old MNs than in 42 days old MNs. TARDBP slightly decreased in patient-derived MNs compared to control MNs on day 21 and day 42. FUS expression increased in 42 days old MNs in comparison to 21 days old MNs. Low expression levels of Shank 1 and 2 in 21 days old MNs were elevated at day 42. The markers for the postsynaptic compartment Shank 3 was initially expressed at a higher level than on day 42, and Homer1 expression was slightly decreased.

(A)

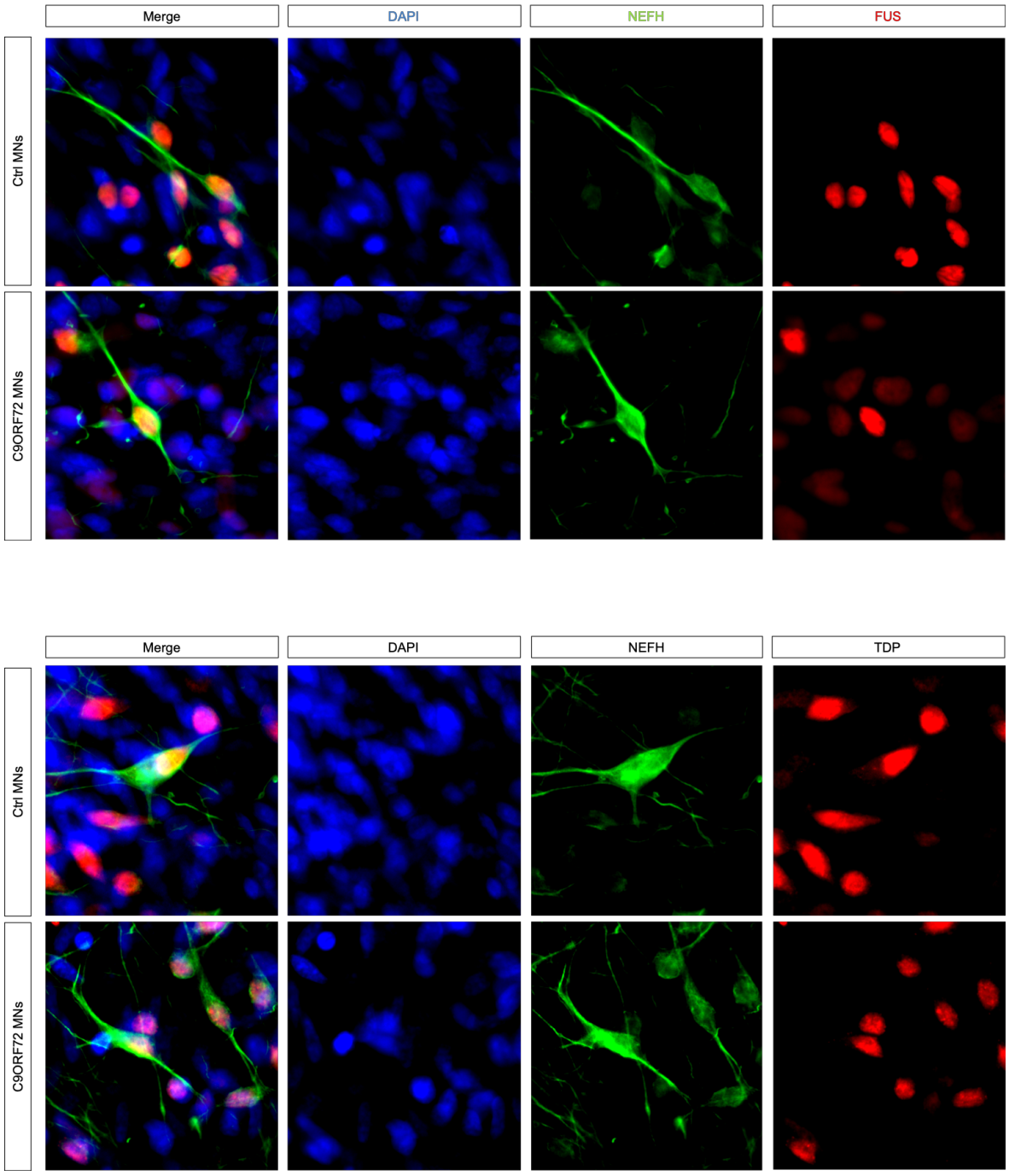
Merge
DAPI
NEFH
FUS
Ctrl MNs
C9ORF72 MNs
Merge
DAPI
NEFH
TDP
Ctrl MNs
C9ORF72 MNs

(B)

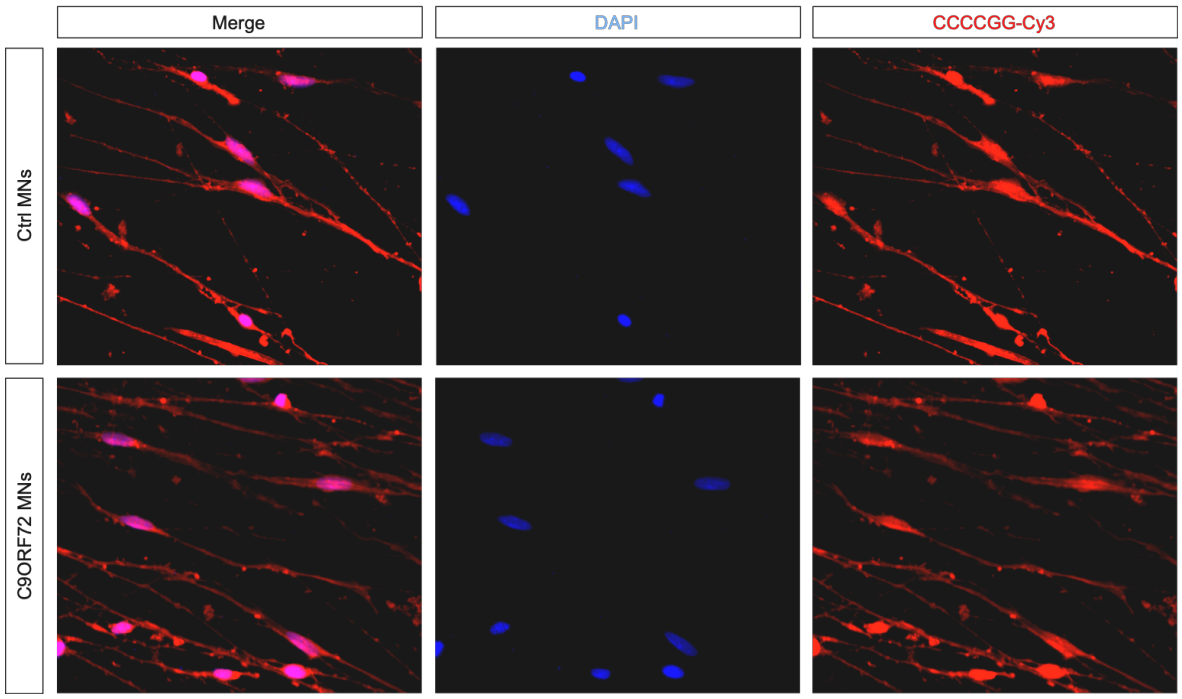

Figure 20 Gene expression analysis of patient-derived MNs
(A) Immunofluorescence staining showing normal distribution patterns of FUS and TDP-43 mainly in the nuclei of MNs derived from control cells and Patient 1 cells. Nuclei are labelled with DAPI (blue), neurites with NEFH (green), and TDP-43 as well as FUS are labelled red. (B) Representative images of fluorescence *in situ* hybridisation (FISH) with a Cy3 (red) labelled antisense probe to the GGGGCC repeat in control MNs and patient-derived motoneurons (MNs) from Patient 1. Nuclei are labelled with DAPI (blue). FISH analysis of 42 days old MNs did not show RNA aggregates.

4. Discussion

4.1 Antibodies against C9ORF72

As the specificity of commercial antibodies against C9ORF72 is questioned, and since some published antibodies are known to be cross-reactive with GFAP (Satoh et al. 2012), we intended to produce our own antibodies against peptides of the two isoforms of C9ORF72. We successfully cloned, induced and isolated the GST-fusion peptides that were used to immunize different animals by a commercial antibodyservice. However, using the obtained sera, we did not detect C9ORF72 specifically in WB and staining analysis, as shown by Figure 5. Poor handling of the fusion-protein could have led to a degradation of our peptides prior to antibody generation, although we always kept the protein solutions on ice and followed best practices. Even if we avoided the amino acid sequence known to be cross reactive with GFAP, AS 112-155, which was shown for the commercial Sigma antibody HPA023873 (against the peptide extending from AS 110-199), non-specific binding patterns could be due to cross reactivity of the chosen epitopes (Satoh et al. 2012). The commercial antibody from Genetex GTX119776 (against AS 1-198), for example, shows, in addition to the C9ORF72 bands, a strong band at around 120 kDa, which seems to be the same band we detected when testing our serum 2. However, Genetex does not discuss or comment upon any cross reactivity in western blot analysis. This band could also be a dimer of the 55 kDa isoform of C9ORF72 that is resistant to the reducing agents used in the western blot technique. In general, it must be mentioned that the difficulties encountered in the creation of a reliable antibody against C9ORF72 poses a huge obstacle for basic approaches to the characterisation of C9ORF72; a specific antibody would allow to study its cellular localisation, and help to identify its function and interaction partners. Therefore, it is a notable achievement that the group of M. Neumann, University of Tübingen, was recently able to produce antibodies that specifically detect the protein, at least in western blot analysis (data not published), and that Robertson et *al.*, 2015 recently reported the successful generation of isoform-specific antibodies and localisation studies of C9ORF72 (Xiao et al. 2015). Interestingly, this group used a short epitope (from AS 321 to 334) which was within the peptide we used for the antibody production against the

long isoform. For the detection of the short isoform, however, they chose the last 12 AS of the isoform, including the unique lysine at the C-terminus. The Santa Cruz antibody sc-138763 also covers the epitope we used, as the peptide spans from AS 165 to 215.

Modelling C9ORF72 associated pathogenesis

4.2 Synaptic localisation of C9ORF72

The dying back hypothesis of MNs in ALS, which results of initial synaptic stainings (Dejesus-hernandez et al. 2012), and the observation that C9ORF72 is found in synaptosome preparations (Atkinson et al. 2015), led us to undertake the quantitative analysis of synapses in primary hippocampal cell culture overexpressing C9ORF72. Since our in-house antibodies were non-specific, we continued our analysis with the partially specific Santa Cruz antibody. This antibody has been reported to detect C9ORF72 in the cytoplasm of neurons, and to reveal enrichement in synapses (Satoh et al. 2012). Recently, it was determined that the short isoform is located in the nucleus and nuclear membrane, where it could potentially influence nucleocytoplasmic trafficking. In contrast, the long isoform is predominantly located in the cytoplasm of neuronal cells (Xiao et al. 2015). However, only the long isoform was detected in synaptosomal fractions, and high expression of C9ORF72 isoforms was detected at the mRNA and protein levels in neurons at early stages of mouse embryo development, indicating a possible participation in neurogenesis and synaptogenesis (Atkinson et al. 2015, Xiao et al. 2015).

In our studies, overexpression of both isoforms and the use of the Santa Cruz antibody (which detects both isoforms), showed that C9ORF72 is expressed throughout the primary hippocampal neuron, including dendrites and synapses. Consequently, we analysed if C9ORF72 overexpression influences the number of synaptic sites; we found a reduction of synapses in the C9ORF72-GFP overexpressing neurons compared to control cells, which overexpressed empty GFP. This result emphasizes the importance of C9ORF72 for synapses. Whether C9ORF72 influences the formation or degeneration of synapses, which

propagates to MN degeneration is a matter for further study, especially when considering a specific function of C9ORF72 in transport processes (e.g. vesicular transport). The functions of C9ORF72 at synaptic sites needs to be better characterized in order to understand the abnormal protein´s putative influence on synaptic degeneration in ALS. Therefore, the study of hIPSCs and hIPSC-derived MNs should be the next step in this endeavor.

4.3 Dipeptide repeat protein aggregates

The haploinsufficiency of the C9ORF72 protein became less prominent in C9-ALS research when it was discovered that RAN translation products of the hexanucleotide repeats accumulate and interfere with neuronal health (Mori et al. 2013). With this in mind, we transfected primary hippocampal neurons with constructs containing polyGA10, polyGA100, polyGP10 and polyGP100 repeats to determine if we could also detect aggregates in our cell model. We only detected aggregates when polyGA100 repeats were transfected, but not in the case of other repeats. The aggregates were located in the perinuclear area, which may be consistent with an association with the Golgi apparatus. Further immunostainings against golgin and other cell compartment-specific proteins could verify the localisation of the dipeptide aggregates, and reveal the presence of co-aggregating proteins. Edbauer et al., 2015 also detected poly(GA) as the major aggregating dipeptide in patient postmortem tissue using specific antibodies, but, besides this, also poly(GP) and poly(GR) aggregates were detected. Petrucelli et al., 2013 observed in an investigation in postmortem tissue that also antisense CCCCGG transcripts undergo RAN translation and form DPR consisting of poly(PR), poly(GP) and poly(PA), likely causing neurotoxic effects (Gendron et al. 2013). We did not detect poly(GA) aggregates in patient-derived cells using the antibody obtained from D. Edbauer in the C9ORF72 patient-derived ALS IPSCs. Donnelly et al., 2013, by contrast, were able to detect DPR in IPSC-derived MNs from ALS patients using the C9RANT antibody that preferentially detects poly(GP). This amplification seems to occur often due to its capacity for forming sense and antisense RAN translation products (Donnelly et al. 2013). These findings of

Donelly et al. (2013) in MNs support the findings in postmortem tissue and, therefore, validate the model system of patient-derived IPSC derived MNs.

4.4 Generation of human induced pluripotent stem cells circumventing most ethical concerns

Another likely factor leading to MN degeneration in C9-ALS is that toxic RNA foci sequester RNA binding proteins, which leads to abnormal RNA metabolism (Haeusler et al. 2016). However, addressing this hypothesis would require the transfection of very lengthly DNA or RNA repeats, which is not presently technically possible. Because of this limitation of primary cell culture models and missing tools, notably reliable antibodies against the wt protein, we proceeded using patient-derived pluripotent stem cells harbouring the pathologic repeat expansions of C9ORF72.

Pluripotent human embryonic stem cells can self-renew and differentiate into all somatic cell types (Amit et al. 2000). Thus, hESCs may be used as models for human diseases to gain further insights into complex pathomechanisms, and may also be used for screening of new drugs or regenerative therapy approaches. Through the induction of defined mutations into hESCs by homologous recombination, hESCs may reflect disease patterns with a complex genetic background, which simple animal models are missing. Additionally, repairing a gene defect through homologous recombination in hESCs represents a promising therapy approach (Zwaka and Thomson 2003). However, as hESCs derive from embryos, hESC research has been hindered by ethical controversy, especially because of religious beliefs about the beginning of human life, as well as concerns about human cloning and modification of human characteristics (Hyun 2010, Lo et al. 2014).

In 2006, when Yamanaka and Takahashi established the method for generating IPSCs by reprogramming somatic cells, it has been possible to circumvent many of these ethical issues. Morphology, proliferation and surface antigens of IPSCs are similar to those of hESCs (Liu et al. 2011) and, furthermore, they can be derived from patients with various diseases, allowing the study of cell biology backgrounds of pathogenesis in a patient-specific setting. Even more importantly,

by differentiating IPSCs into required tissue or cell types, this technology promises to realize the dream of allogenic organ transplantations.

However, as somatic cells are reprogrammed into IPSCs through lentiviral transduction of the transcription factors c-Myc, OCT4, SOX2 and KLF4 (Takahashi and Yamanaka 2006), there arise several safety issues concerning tumourigenicity that must be considered in clinical use. Increased expression of c-Myc and KLF4 by reactivation of the retrovirus would lead to transformation into tumour cells, because c-Myc enables cell proliferation and KLF4 inhibits apoptosis. The immortalised cells with opened and active chromatin structure do not become pluripotent stem cells until OCT4, KLF4 and SOX2 activate the required genes (Yamanaka et al. 2007). Another problem inherent to the generation of IPSCs is the low reprogramming efficiency. In 2008, Aasen et al. reported that reprogramming human keratinocytes from plucked hair is approximately 100-fold more efficient and 2 times faster than the reprogramming of human fibroblasts (Aasen et al. 2008). Based on these findings, we elected to generate IPSCs from reprogrammed human keratinocytes derived from hairs plucked from C9-ALS patients. The generated hIPSCs displayed stem cell characteristics by expressing all pluripotency markers and by their ability to differentiate into all three germ layers, like embryonic stem cells.

4.5 Stem cell model for human motoneuron disease

MNDs are widely limited to adult humans, and symptoms similar to those of human MND are only partially displayed in animals models. Alterations in chaperons, proteasomes and autophagosomes, as well as different lifespans are considered as factors hindering the expression of neurodegenerative diseases in nonhumans (Jucker 2010). However, aspects of MND can be observed in zebra fish (*Danio rerio*) or even fruit flies (*Drosophila melanogaster*) (Ciura et al. 2013, Mizielinska et al. 2013). However, since neither of these models reflect the clinical complexity of human MND, their relevance for gaining understanding of the human disease is controversial. As such, no compelling animal model is currently available to study neurodegeneration in human C9ORF72 ALS. Furthermore, it is neither possible to isolate human motoneurons from the human patients, nor to

induce the disease causing C9ORF72 mutation artificially in model systems (this due to technical impossibility of transfecting many hundreds of nucleotide repeats). Recently, new ALS model systems with human background and patient specificity have been established using hIPSCs, with differentiation into MNs (Sareen et al. 2013a, Devlin et al. 2015). Disease mechanisms present in postmortem brain tissue and animal models can now for the first time be examined in viable human cell systems.

As induced pluripotent stem cells can give rise to all different embryonic cell types, many organotypic cell systems have been established to study physiologic cell behaviour, e.g. development, proliferation, differentiation, or pathologic cell behaviour, e.g. neurodegeneration. The differentiation of patient-specific IPSCs with a predicted phenotype into specific cell types offers substantial new opportunities to model and even treat disease (Ross and Akimov 2014). Thus, through the differentiation of human IPSCs of C9-ALS patients into MNs, it is possible to investigate degenerative processes that cannot be emulated by conventional cell culture experiments or animal models. Therefore, differentiation of patient-derived IPSCs into MNs, the affected cells in ALS, offers a promising model to study neuronal morphology and function in C9-ALS patient-derived cells.

We examined if the patient-derived MNs show physiological cell behaviour and maturation, or if they rather show a perturbed cellular development and morphology. The development and differentiation of our patient-derived MNs did not prove to differ much compared to control lines. We therefore observed morphological differentiation and expression of MN or disease markers. Our Patient 1-derived cells progressively differentiated into MNs in culture. After final plating, the MNs first showed a bipolar morphology and later showed a polarisation into afferent and efferent cell processes, with increasing abundance of neurites and greater neurite length. Additionally, the MNs expressed specific MN markers such as SMI-32 and VAChT. In addition, it would be necessary to study the expression of OLIG2 and HB9 to establish the details of MN differentiation. Our analysed hIPSC-derived MNs from Patient 1 did not show any cospicious pathological features like protein or RNA aggregates. This could be due to the loss of the C9ORF72 repeat expansion in the differentiated patient cell line 1, thus sparing the cells from phenotypic abnormalities. Unfortunately, we did not succeed

in differentiatating the hIPSCs of Patient 2 (with C9ORF72 expansion) into MNs. The latter may be due to the greater severety of the pathologic phenotype when the repeat expansion is present in hIPSCs. It would be necessary to study further cell lines to ascertain if differentiation of hIPSCs into MNs indeed depends on the presence and size of the hexanucleotide repeat expansions of C9ORF72. Other research groups have not yet reported particular difficulties in obtaining MN differentiation of hIPSCs from C9ORF72-ALS patients (Sareen et al. 2013a, Devlin et al. 2015, Toli et al. 2015, Zhang et al. 2015). In general, given the heterogeneity of patient-derived cells, a large number of cell lines will be needed to give reliable data and a proper interpretation of these results. This variability between cases is due to the different genetic backgrounds and environmental influences that affect each patient. To facilitate the interpretation of the results from these studies, it is recommended to compare patient cells with familial healthy control cells, an approach which reduces differences between hIPSCs with regard to epigenetics and environmental influences. Another potential approach is the generation of isogenetic controls by correcting the defect in the mutated cell line, or by introducing a mutation in a non-mutated line. Additionally, when studying pathomechanisms of MND, it is important to examine the influence of inter-cellular interactions, e.g. co-culting MNs and myocytes from the same patient so as to better mimic the physiological system (Demestre et al. 2015).

4.6 Repeat instability upon reprogramming human keratinocytes to hIPSCs and DNA repair mechanisms

As already shown by several groups, the hexanucleotide repeat expansions in patient-derived cells undergo instability after reprogramming of keratinocytes or fibroblasts to hIPSCs, with this instability probably due to DNA repair mechanisms (Almeida et al. 2013). Using Southern blot analysis, we could confirm this result, and furthermore show that the GGGGCC repeats in C9-ALS patient IPSCs derived from keratinocytes can be stable (Higelin et al. 2018) or vary in size after the reprogramming process, or may even disappear altogether. Other groups also mentioned that the repeat length can sometimes be unaffected through cell

reprogramming, but they also saw instances of expansion or contraction of repeat lengths in different patients (Almeida et al. 2013, Donnelly et al. 2013). This variability of repeat lengths may be due to clonal expansion of subclones with different-sized repeats. Alternatively, the shift may indicate somatic variability resulting from local disruption of DNA replication, recombination, or specialised repair mechanisms (Yanovsky-Dagan 2015). In general, mammalian cells have many different DNA repair pathways, which are recruited according to the particular type of DNA damage. Thus, small DNA modifications such as methylation adducts are removed by direct DNA repair (Luo et al. 2012), whereas oxidized bases or alkylated bases are corrected by base excision repair (Memisoglu and Samson 2000). Nucleotide excision repair removes pyrimidine dimers by excising sequences of nearly 30 nucleotides (Gillet and Schärer 2006), while mismatch repair corrects mismatched bases or single-strand loops (Jiricny 2006). Homologous repair corrects DNA double strand breaks (DSBs) using a homologous template to make an error-free replacement, whereas DNA double strand break repair is achieved through non-homologous end-joining (NHEJ); this process is relatively error-prone because no homologous template is required. As single-strand annealing combines two extensive regions of homology that flank either side of a DSB, it leads to deletion, even though it requires a homologous template (Rothkamm et al. 2003, Moynahan and Jasin 2010). Besides these different repair mechanisms, pluripotent cells possess a more heterogeneous and greater DNA repair efficiency than do non-pluripotent cells (Luo et al. 2012). IPSCs express elevated levels of DNA repair proteins, and have an increased capacity for NHEJ repair (Fan et al. 2011). The different mechanisms responsible for repeat instability are based on the formation of specific tertiary structures in the DNA such as hairpins and G-quadruplexes, which are apt through NHEJ to cause addition (expansions) or deletion (contractions) of repetitive units (Yanovsky-Dagan 2015). However, the exact mechanism and the time point of these changes due to instability remains to be determined (López Castel et al. 2010).

4.7 RNA and protein foci in human keratinocytes, IPSCs and MNs

Transcription of the hexanucleotide repeat expansion most likely leads to an RNA gain of function mutation via formation of RNA foci and consequent sequestering of RNA binding proteins, which leads to RNA dysmetabolism. Additionally, short abortive transcripts of the hexanucleotide repeat expansion could act as siRNAs, thereby leading to gene repression (Haeusler et al. 2016). Different research groups have identified RNA aggregates in postmortem brain tissue, in patient-derived fibroblasts, and IPSCs, as well as in approximately 20 % of IPSC-derived MNs (Almeida et al. 2013, Donnelly et al. 2013, Mizielinska et al. 2013, Sareen et al. 2013a). Studies have also shown that the RNA foci co-localize with RNA binding proteins like hnRNPA1 and Pur-a, which suggests a disruption of normal RNA metabolism. RNA foci do not co-localize with hnRNPA3, hnRNPA2/B1, FUS or TDP-43, but hnRNPA1 is a known binding partner for TDP-43 that could mediate between C9ORF72 and TDP-43-caused ALS (Almeida et al. 2013, Donnelly et al. 2013, Sareen et al. 2013a, Cooper-Knock et al. 2014). As different RNA-binding proteins co-localize with the RNA foci, it is unclear whether the toxicity to MNs is due to altered levels of single or multiple proteins. Additionally, co-localisation of RNA aggregates and dipeptide aggregates has been reported in postmortem brain tissue and MNs from ALS patients (Almeida et al. 2013, Gendron et al. 2013, Zu et al. 2013). However, other groups were unable to detect C9-RAN translation products in such material, indicating that RNA foci need not always to correlate with dipeptide aggregates formed by RAN translation (Sareen et al. 2013a). We detected RNA foci in ~35% of patient-derived keratinocytes of Patients 1 and 2. Although we found evidence for RNA foci, we did not consistently observe repeat-associated non-ATG–dependent C9-RAN protein products in these cells. Furthermore, we saw no RNA foci in hIPSCs or MNs for Patient 1. In contrast, the hIPSCs from Patient 2 contained RNA foci (Higelin et al. 2018). As noted above, we could not analyse the presence of RNA foci in MNs, since we failed to differentiate the Patient 2 cells into MNs. Therefore, those hIPSCs and MNs of Patient 1 that showed a loss of repeat expansion after keratinocyte reprogramming might be considered as control cells lacking RNA foci.

However, the Patient 1 keratinocytes, which posses the repeat expansion, did in fact show nuclear RNA foci.

Furthermore, we did not detect dipeptide repeat aggregates or aggregating RNA binding proteins in any of the investigated cell types. In order to trigger RNA or protein aggregation by inducing cell stress, we irradiated the cells to cause DNA damage, or treated the cells with sorbitol, which provokes hyperosmolarity stress. In these stressed cells we did not find alterations regarding dipeptide protein or RNA aggregation. However, other groups have also reported difficulties in the detection of RNA aggregates and RAN translation products using a standard immunofluorescence microscope, as the foci seem to be located in different focal planes, and thus are difficult to visualise (Gendron et al. 2013, Mizielinska et al. 2013, Sareen et al. 2013a). Indeed, the colocalization of GGGGCC foci with hnRNPA1 and Pur-a was observed by confocal imaging in the work described by Mizielinska et al., 2013 (Mizielinska et al. 2013). If the techniques for detecting aggregating RNA and dipeptide proteins could be improved, this could be the next step to explore if these aggregates can serve as biomarkers in cells of young, as-yet asymptomatic C9ORF72 mutation carriers. Furthermore, a possible correlation between repeat length, quantity of aggregates and disease severity could then be investigated.

An inducible transgenic animal model would provide another approach to study the accumulation of RNA and protein aggregates in ALS. This advent of technology would allow researchers to regulate the transcription of the target genes by application of doxycyclin so as to induce disease-specific phenotypes suitable for investigation (Hukema et al. 2014). In addition, rescue systems would be tested by silencing the transcription of target genes, which is impossible in patient-derived cells. As a recent proof of this principle, Yanovsky et al. (2015) targeted RNA foci with antisense oligonucleotides, thus suppressing further foci formation, which gave a partial rescue of the disease phenotype in C9-ALS neuronal cells (Yanovsky-Dagan 2015).

4.8 Gene expression levels in hIPSCs and during MN differentiation

It was recently shown that C9ORF72 mRNA and protein levels alter during mouse developmental processes (Atkinson et al. 2015). Furthermore, C9ORF72 expression is reduced in patient tissue (Dejesus-hernandez et al. 2012) and shows a slight reduction in patient-derived MNs (Sareen et al. 2013a). Our findings in IPSC-derived MNs from Patient 1 (which lost the repeats) confirm a slight reduction of C9ORF72 expression in patient-derived cells, and also the altered expression during MN differentiation compared to that in control cells. The mRNA levels of C9ORF72 in control cells exceed the levels in patient-derived IPSCs and 42 days old MNs, but on day 21 the long isoform was upregulated approximately two fold in patient-derived cells compared to control cells. As the analysed ALS patient-derived MNs lost their repeat expansion during reprogramming, they could be considered as having reverted to control cells without repeat expansion, but they nonetheless still show an altered phenotype compared to control cells. This could be explained by the coexistence of different subclones of cells in culture. Besides the patient-derived cells which lost the repeat expansion, there probably existed some cells which still possessing the expanded allele, and therefore showing altered gene expression. Furthermore, epigenetic modifications, which might have been induced by the repeat expansion could persist after loss of the repeats, and thus influence gene expression in patient-derived cells (Haeusler et al. 2016).

Furthermore, in 2014, 353 differentially expressed genes were identified in patient-derived MNs using exon array datasets (Satoh et al. 2014). By applying molecular network analysis systems, the suspect genes were clustered into different groups according to their broad biological functions, e.g. into “RNA Post-Transcriptional Modification, RNA Damage and Repair, Protein Synthesis”. In particular, most of the RNA-binding protein-encoding genes, such as FUS, were down-regulated in the diseased MNs, whereas the TARDBP gene showed an increased expression level (Satoh et al. 2014). The down-regulation of RNA binding proteins supports the hypothesis that quadruplex structures of C9ORF72-repeat expansions disregulate the homeostasis of RNA metabolism, which plausibly leads to degeneration of stress-vulnerable MNs. However, further studies are needed to determine whether the transcriptional alterations in C9-ALS patient-derived cells

are a direct or indirect consequence of altered functioning of RNA-binding proteins. In our qRT-PCR analysis of hIPSC-derived MNs from Patient 1 (which lost the repeats), FUS expression was reduced in 21 days old MNs, but had control expression levels on day 42 in culture. TARDBP expression levels were almost identical relative to control cells at all investigated time points. We further analysed pre- and postsynaptic proteins to investigate the possibility of altered numbers or morphology of synaptic sites. The expression levels of the master scaffolding molecules of the PSD, Shank 1 and 2 proved to be lower in 21 days old patient-derived MNs than in control MNs, but no such difference was seen in mature MNs on day 42. Conversely, ProSAP2/Shank 3 expression was upregulated in patient cells compared to control cells on day 21, and decreased thereafter. Liebau et al. had reported in 2007 that differentiating neural stem cells showed peak levels of ProSAP2/Shank3 mRNA in the first week of differentiation, which then decreased sharply (Liebau et al. 2007). Additionally, in our hands, the postsynaptic marker Homer and presynaptic marker ChAT showed reduced expression in patient-derived cells compared to control cells, which implies a lesser extent of synapse maturation as these neuronal markers were measured relative to the MN marker NEFH. In general, these results imply that studies especially of ALS-affected MNs in absence of other neuronal cell types, should properly entail purifying the MNs by fluorescence-activated cell sorting (FACS) (Toli et al. 2015), so as to avoid confounds from other cell types.

4.9 Increased susceptibility of hIPSCs to exogen stressors

MND usually manifests in adulthood, suggesting that patient-derived cells may not normally be mature enough to show the entire pathogenic phenotype. Therefore, it follows that there is a need to set up test systems provoking or triggering ALS pathology, including protein or RNA aggregation, mitochondrial dysfunction, perturbated nucleolar or endosomal membrane trafficking and DNA repair (Farg et al. 2014, Devlin et al. 2015, Tao et al. 2015). After induction of pathological alterations by oxidative, excitotoxic, hypermolar or nucleolar stress, patient-derived cells can be investigated for morphological changes (alterations in the

cytoskeleton, axonal length and synapse formation) and functional changes (apoptosis rate, metabolic aspects and electrophysiological features).

With this in mind we tested the apoptotic response of our cells to gamma irradiation-induced DNA damage. The induction of apoptosis following upon inadequate DNA repair has already been well-described. The accumulation of signs of DNA damage, and the cellular responses to DNA damage stressors e.g. apoptosis, was reported to be lower in highly mitotically active hIPSCs than in post-mitotic-MNs. Gamma irradiation is high-energy electromagnetic radiation with a wavelength in the range of 10pm-0.01pm that can be obtained from radioactive sources such as caesium-137 (in our hands actual activity of 33TBq). Irradiation of the IPSCs with a dose of 3.3Gy/min breaks chemical bonds in the DNA double strand. Indeed, DSBs are considered as the most serious DNA damage with regard to DNA repair. Ionizing radiation mostly (80 %) induces isolated DSBs, but may also induce clustered defects consisting of DSBs and oxidized purines, pyrimidines or abasic sites (Asaithamby and Chen 2009). After the induction of DNA damage, the cells show a number of responses, which include cell cycle arrest, DNA repair and apoptosis if DNA damage is too extensive. Momcilovic et al. showed in 2010 that response of IPSCs to DNA damage is altered by the reprogramming process. IPSCs have increased DSB repair efficiency and an increased expression of DNA repair genes. However, the G1/S checkpoint is lost in IPSCs, and their cell cycle arrests at the G2/M checkpoint, which could explain the increased radiosensitivity of IPSCs (Momcilovic et al. 2010, Fan et al. 2011). Momcilovic et al. detected in irradiated IPSCs an increase of γH2AX, a histone component that is phosphorylated by the ataxia telangiectasia (ATM) kinase upon recognition of DSBs. Levels of the specific DSB marker γH2AX increased within 20 min after irradiation and returned to baseline levels within six hours (Momcilovic et al. 2010, Fan et al. 2011). Additionally, they found that irradiated cells restarted the cell cycle after 24 hours, at which time the DSBs are presumably repaired, and apoptotic events normalize (Momcilovic et al. 2010).

For our expertiment we used hIPSCs from Patient 2, which retained the repeat expansion after reprogramming. By inducing DNA damage in our hIPS cells we could see increased apoptosis at all examined time points. The IPSCs showed a maximal apoptosis rate at 4 h after irradiation, attaining in C9ORF72 IPSCs a level

three times as that in control cells. The control cells returned to their initial baseline level of apoptosis at 24 h post irradiation, whereas apoptosis rates in the C9ORF72 IPSCs, although declining, remained higher than the control cells.

It would be interesting to learn more about the dose-dependence of the initiation of apoptosis, and also to ascertain if there are alterations of DNA repair proteins such as γH2AX (which marks DSBs) that were induced either directly by irradiation, or indirectly, for example through oxidative stress, deficient repair and metabolism (Valdiglesias et al. 2013), all of which are known to occur in C9-cells. Furthermore, BRCA1 or ATM, which are both proteins involved in DNA damage signalling (Wu et al. 2010), and thus are potential factors in increased of apoptosis upon ineffective repair of DNA DSBs, should be analysed in patient-derived cells. Other than this, it needs to be determined if other types of DNA damage also cause increased apoptosis in patient-derived cells.

To check cell cycle progression and DNA repair in our irradiated cells, we investigated the presence of HDAC1 aggregates. The histone deacetylase HDAC1 regulates gene expression of cell cycle genes by editing acetyl groups from DNA bases, which facilitates chromatin condensation (Qiu et al. 2014). Furthermore, HDAC1 contributes to DNA repair mechanisms and DNA integrity in the aftermath of DNA damage (Wang et al. 2013). In our study, the number of cells containing HDAC1+ foci was slightly higher in patient-derived IPSCs compared to control cells even prior to irradiation, which could possibly indicate an inherently higher DNA repair requirement of IPSCs with C9ORF72 mutation.

Altogether, these results indicate that C9ORF72 cells have heightened susceptibility to gamma irradiation, and possess reduced viability upon induced DNA damage. In contrast, when we induced hyperosmolar stress in our patient-derived hIPSCs (Patient 2, showing preserved repeats), we did not find alterations of protein expression or viability relative to control cells. This hints at a selective susceptibility of C9-ALS derived cells to DNA damage. Cells with mutant FUS, however, show a strong nuclear depletion and cytoplasmic accumulation of mFUS after hyperosmolar stress induction (Lenzi et al. 2015). In contrast, an increased degree of apoptotic events associated with impaired DNA repair in cells with C9ORF72 hexanucleotide repeat expansion may be relevant for ALS, because it is

already known that cells expressing mutant FUS also show increased DNA damage and apoptosis levels (Wang et al. 2013).

The observed increase of apoptosis in C9-ALS cells could be attributed to the sequestration of RNA binding proteins by RNA or protein foci of the expanded allele, leading to dysregulation of DNA repair mechanisms. In addition, the inherent genomic instability of IPSCs with C9ORF72 hexanucleotide repeat expansions may lead to pathological effects after gamma irradiation.

Present results show that irradiated IPSCs, which reflect C9ORF72-ALS patient-specific pathologies, can be used as a read-out system to gain further insights into MN degeneration. We also stressed the C9ORF72 IPSCs (from Patient 2) with hyperosmolar sorbitol treatment to test if this presents an alternate system accelerating an ALS-associated pathology, i.e. by unmasking an underlying vulnerability. Physiologically, the formation of stress granules (SGs) after hyperosmolar stress regulates RNA homeostasis (e.g. translation or decay) through sequestration of untranslated mRNAs. In cases of sub-lethal cell stress, the SG formation is reversible. The fact that patient-derived IPSCs showed the same SG pattern as control IPSCs may well reflect normal functioning of SG formation. But it should also be considered that the SG formation might be insufficient in patient-derived IPSCs because of an increased amount of abnormal RNA aggregates (including FUS and TDP-43), which are necessary factors for SG formation. Furthermore, the possibility of increased SG association should be considered because of the shuttling function of C9ORF72. The nuclear proteins TDP-43 and FUS can be quickly shuttled to the cytoplasm upon stress induction to form SGs, and then return to the nucleus after stress resolution. We suppose that they may show altered behaviour, e.g. cytoplasmic accumulation, possibly because of defective nuclear-cytoplasmic shuttling. The aggregation of FUS or TDP-43 in SGs may lead to a decrease of RNAs encoding antiapoptotic factors, or indeed proliferative factors required to promote recovery after cell injury. In this scenario, accumulation of FUS or TDP-43 in SGs might inhibit translation of mRNAs critical to cell survival and recovery, and consequently increase the rate of cell death and neuron loss (Li et al. 2013).

4.10 Conclusion

ALS is the most common ultimately fatal MND with adult onset, affecting the upper and lower motoneuron. Approximately 30 % of fALS and 25 % of sALS cases are caused by an intronic C9ORF72 hexanucleotide repeat expansion, but the physiological impact of this expansion remains to be established.

To date, the available animal models that reflect MN degeneration in ALS are of limited translatability to examine human pathomechanisms of neurodegeneration (Hayes and Rothstein 2016). Possible disease-causing alterations in patients harbouring C9ORF72 mutations include a loss of function, peptide aggregation of repeat-associated non-ATG-initiated (RAN) translation products, and a dysregulation of RNA metabolism due to formation of toxic RNA foci. The major part of insights into human MND has been obtained from examination of postmortem tissues collected from ALS patients. However, as these tissues mainly reflect the end-stage of MND, it is necessary to establish other model systems to investigate early pathomechanisms, or even presymptomatic disease markers. Toward achieving this goal we analysed primary hippocampal and patient-derived cells with regard to several disease mechanisms that have been previously postulated. Upon overexpressing C9ORF72, we detected its expression in all neuronal compartments (soma, neurites and synaptic sites), which implies a possible influence of C9ORF72 in neuronal function, and more specifically in synaptic function.

As the model system of primary cells was unavailable in this study, we efficiently reprogrammed keratinocytes of C9-ALS patients into hIPSCs, and subsequently differentiated them into MNs. We describe morphological features of C9ORF72-expressing cells and analyse pathological features of patient-derived cells with hexanucleotide repeat expansion. Similar to others, we found, by reprogramming keratinocytes and generating hIPSC cell lines, that the repeat expansion can in fact be repaired, as was the case in one of our two cell lines. In the other hIPSC line, pathological repeats were maintained at the hIPSC level. The IPSC line in which the repeats were lost did not reflect any conspicuous pathologic phenotype. In patient-derived cells still harbouring the disease-causing mutation we observed RNA foci but no protein aggregates of typical aggregating proteins in ALS. We then proceeded to stress the cells so as to provoke pathological processes, and

could then detect an increased susceptibility to low-dose ionizing irradiation, manifesting in elevated levels of apoptotic cell death in patient-derived cells. The G-quadruplex structures of the hexanucleotide repeat expansion of C9ORF72 could sequester different RNA binding and DNA repair proteins, which would likely lead to a dysregulation of DNA repair and cell cycle upon induction of DNA damage. Thus, MN degeneration may follow from an impaired ability to recover from environmental stressors resulting in DNA damage and apoptosis.

5. Summary

Amyotrophic lateral sclerosis (ALS) is the most common motoneuron disease, which is characterized by adult onset of a rapidly progression of the degeneration of the upper and lower motoneurons (MNs). The hexanucleotide repeat expansion of chromosome nine open reading frame 72 (C9ORF72) is the most common mutation in familial and sporadic ALS cases, but the mutation has been sparsely characterised. *In vitro* cell models of primary rodent MNs or secondary cell systems and some animal models as well as postmortem brain tissue have hitherto been the main model systems in C9-ALS research. However, these model systems are widely restricted in their capacity to capture the full range of human ALS pathogenesis, given the present technical difficulty in the artificial induction of huge repeat expansions. Therefore, we established stem cell-based model systems to study the pathogenesis of ALS in a human-derived, patient-specific setting. In the first stage of this project, to study the cellular localization and function, we attempted to create specific antibodies against the two isoforms of C9ORF72 because the specificity of commercial-available antibodies is inadequate, and some antibodies are known to cross react with glial fibrillary acidic protein. Therefore, we generated antigenic peptides of the two isoforms of C9ORF72, which were then used to immunize different animal species. However, for unknown reasons, the obtained sera failed to specifically recognize C9ORF72 in western blots and immunofluorescence stainings. We next started characterisation experiments of the C9ORF72 hexanucleotide repeat expansion in cell culture models and primary hippocampal neurons. Then, we characterised human induced pluripotent stem cells (hIPSCs) derived from keratinocytes with respect to their physiological and pathological features. Here, the aim was to test the cell lines as a tool to understand the cellular alterations of IPSCs harbouring patient-specific C9ORF72 repeat expansions. With this model we investigated the three different hypotheses of disease-causation: Loss of function, toxic RNA foci, and protein aggregation. Through gain of function by overexpression of C9ORF72 in hippocampal neurons we showed that the gene product of C9ORF72 might be localised in all neuronal cell compartments, including synaptic sites, and that its overexpression leads to a reduced number of mature synapses. Of the several

culprit proteins, only poly-glycine-alanine formed dipeptide aggregates in the cytoplasm of transfected hippocampal neurons. We did not find endogenous aggregates in patient-derived IPSCs. To analyse the toxic RNA foci, we established fluorescence *in situ* hybridization using specific probes for the transcribed hexanucleotide repeat RNA. This technique revealed the occasional presence of RNA foci in keratinocytes derived from Patients 1 and 2, and in IPSCs of Patient 2, but not in control cell lines. We found that the repeat expansions underly dynamic processes including reduction and expansion of the amount of hexanucleotide repeats. We finally focused on cell viability of the patient-derived IPSCs compared to control cells. This study showed that IPSCs from patients have an increased apoptosis rate after γ-irradiation, indicating that C9ORF72 may be involved in DNA repair. We suppose that defective DNA repair in the long term result in increased apoptotic events and neurodegeneration of vulnerable neurons. Upon induction of hyperosmolar stress, we did discern impaired viability or protein aggregates in patient-derived IPSCs in comparison to control cells, as opposed to mutant fused in sarcoma (FUS) cells, which have earlier showed cytoplasmic FUS accumulation and increased cellular vulnerability to exogenous stress (Japtok et al. 2015). This discrepancy underlies the specific susceptibility of C9ORF72 patient cells to DNA damage, which could well be a factor in neurodegeneration in ALS patients (Momcilovic et al. 2010). In support of a two hit hypothesis explaining the FUS-induced pathology (Japtok et al. 2015), we predict that the first hit may be the modification of the C9ORF72 gene product, leading to an increased DNA instability, and the second hit is an external factor such as DNA damage or metabolic stress. To conclude, it must be emphasized that, until now, C9ORF72 pathologies cannot be induced artificially into cell culture systems and human MN material can only be used as postmortem tissue. Furthermore, the few available animal models do not authentically reproduce the affected human phenotype of C9ORF72-caused ALS. Through the use of patient-derived keratinocytes, IPSC reprogramming, and differentiation into the affected MNs and muscle cells, however, all disease-causing mechanisms of C9ORF72 hexanucleotide repeat expansions can be analysed in a cell culture system. Thus, the IPSC based model system is especially helpful for this hexanucleotide repeat expansion mutation, and IPSCs make far more research approaches possible.

6. References

1. Aasen, T., A. Raya, M. J. Barrero, E. Garreta, A. Consiglio, F. Gonzalez, R. Vassena, J. Bilić, V. Pekarik, G. Tiscornia, M. Edel, S. Boué, and J. C. I. Belmonte. 2008. Efficient and rapid generation of induced pluripotent stem cells from human keratinocytes. Nature Biotechnology 26:1276–1284.
2. Almeida, S., E. Gascon, H. Tran, H. J. Chou, T. F. Gendron, S. Degroot, A. R. Tapper, C. Sellier, N. Charlet-Berguerand, A. Karydas, W. W. Seeley, A. L. Boxer, L. Petrucelli, B. L. Miller, and F. B. Gao. 2013. Modeling key pathological features of frontotemporal dementia with C9ORF72 repeat expansion in iPSC-derived human neurons. Acta Neuropathologica 126:385–399.
3. Amit, M., M. K. Carpenter, M. S. Inokuma, C. P. Chiu, C. P. Harris, M. A Waknitz, J. Itskovitz-Eldor, and J. A. Thomson. 2000. Clonally derived human embryonic stem cell lines maintain pluripotency and proliferative potential for prolonged periods of culture. Developmental biology 227:271–278.
4. Aoki, N., S. Higashi, I. Kawakami, Z. Kobayashi, M. Hosokawa, O. Katsuse, T. Togo, Y. Hirayasu, and H. Akiyama. 2012. Localization of fused in sarcoma (FUS) protein to the post-synaptic density in the brain. Acta Neuropathologica 124:383–394.
5. Asaithamby, A., and D. J. Chen. 2009. Cellular responses to DNA double-strand breaks after low-dose -irradiation. Nucleic Acids Research 37:3912–3923.
6. Atkinson, R. A. K., C. M. Fernandez-Martos, J. D. Atkin, J. C. Vickers, and A. E. King. 2015. C9ORF72 expression and cellular localization over mouse development. Acta Neuropathologica Communications 3:59.
7. Bentmann, E., M. Neumann, S. Tahirovic, R. Rodde, D. Dormann, and C. Haass. 2012. Requirements for stress granule recruitment of fused in sarcoma (FUS) and TAR DNA-binding protein of 43 kDa (TDP-43). Journal of Biological Chemistry 287:23079–23094.
8. Boeckers, T. M., T. Liedtke, C. Spilker, T. Dresbach, J. Bockmann, M. R. Kreutz, and E. D. Gundelfinger. 2005. C-terminal synaptic targeting elements

for postsynaptic density proteins ProSAP1/Shank2 and ProSAP2/Shank3. Journal of neurochemistry 92:519–524.

9. Boillée, S., C. Vande Velde, and D. W. Cleveland. 2006. ALS: A Disease of Motor Neurons and Their Nonneuronal Neighbors. Neuron 52:39–59.
10. Bruijn, L. I., T. M. Miller, and D. W. Cleveland. 2004. Unraveling the mechanisms involved in motor neuron degeneration in ALS. Annual review of neuroscience 27:723–749.
11. Chen, Y., M. Yang, J. Deng, X. Chen, Y. Ye, L. Zhu, J. Liu, H. Ye, Y. Shen, Y. Li, E. J. Rao, K. Fushimi, X. Zhou, E. H. Bigio, M. Mesulam, Q. Xu, and J. Y. Wu. 2011. Expression of human FUS protein in Drosophila leads to progressive neurodegeneration. Protein and Cell 2:477–486.
12. Ciura, S., S. Lattante, I. Le Ber, M. Latouche, H. Tostivint, A. Brice, and E. Kabashi. 2013. Loss of function of C9orf72 causes motor deficits in a zebrafish model of Amyotrophic Lateral Sclerosis. Annals of Neurology 57:180–187.
13. Cleveland, D. W., and J. D. Rothstein. 2001. From Charcot to Lou Gehrig: deciphering selective motor neuron death in ALS. Nature reviews. Neuroscience 2:806–819.
14. Cluskey, S., and D. B. Ramsden. 2001. Mechanisms of neurodegeneration in amyotrophic lateral sclerosis. Molecular pathology : MP 54:386–392.
15. Connolly, C. 2012. A nasty hex on chromosome 9 causes FTD/ALS. Clinical Genetics 81:126–127.
16. Cooper-Knock, J., M. J. Walsh, A. Higginbottom, J. Robin Highley, M. J. Dickman, D. Edbauer, P. G. Ince, S. B. Wharton, S. A. Wilson, J. Kirby, G. M. Hautbergue, and P. J. Shaw. 2014. Sequestration of multiple RNA recognition motif-containing proteins by C9orf72 repeat expansions. Brain : a journal of neurology 137:2040–2051.
17. Dejesus-hernandez, M., I. R. Mackenzie, B. F. Boeve, A. L. Boxer, M. Baker, N. J. Rutherford, A. M. Nicholson, N. A. Finch, F. Gilmer, J. Adamson, N. Kouri, A. Wojtas, P. Sengdy, G. R. Hsiung, A. Karydas, W. W. Seeley, K. A. Josephs, D. H. Geschwind, Z. K. Wszolek, H. Feldman, R. Petersen, B. L.

Miller, D. Dickson, and K. Boylan. 2012. Expanded GGGGCC hexanucleotide repeat in non-coding region of C9ORF72 causes chromosome 9p-linked frontotemporal dementia and amyotrophic lateral sclerosis. NIH Public Access 72:245–256.

18. Delatycki, M. B., R. Williamson, and S. M. Forrest. 2000. Friedreich ataxia: an overview. Journal of medical genetics 37:1–8.

19. Demestre, M., M. Orth, K. J. Föhr, K. Achberger, A. C. Ludolph, S. Liebau, and T. M. Boeckers. 2015. Formation and characterisation of neuromuscular junctions between hiPSC derived motoneurons and myotubes. Stem Cell Research 15:328–336.

20. Deng, Q., C. J. Holler, G. Taylor, K. F. Hudson, W. Watkins, M. Gearing, D. Ito, M. E. Murray, D. W. Dickson, N. T. Seyfried, and T. Kukar. 2014. FUS is Phosphorylated by DNA-PK and Accumulates in the Cytoplasm after DNA Damage. The Journal of neuroscience : the official journal of the Society for Neuroscience 34:7802–7813.

21. Devlin, A.-C., K. Burr, S. Borooah, J. D. Foster, E. M. Cleary, I. Geti, L. Vallier, C. E. Shaw, S. Chandran, and G. B. Miles. 2015. Human iPSC-derived motoneurons harbouring TARDBP or C9ORF72 ALS mutations are dysfunctional despite maintaining viability. Nature communications 6:1–12.

22. Ding, V. M. Y., L. Ling, S. Natarajan, M. G. S. Yap, S. M. Cool, and A. B. H. Choo. 2010. FGF-2 modulates Wnt signaling in undifferentiated hESC and iPS cells through activated PI3-K/GSK3β signaling. Journal of Cellular Physiology 225:417–428.

23. Donnelly, C. J., P. W. Zhang, J. T. Pham, A. R. Heusler, N. A. Mistry, S. Vidensky, E. L. Daley, E. M. Poth, B. Hoover, D. M. Fines, N. Maragakis, P. J. Tienari, L. Petrucelli, B. J. Traynor, J. Wang, F. Rigo, C. F. Bennett, S. Blackshaw, R. Sattler, and J. D. Rothstein. 2013. RNA Toxicity from the ALS/FTD C9ORF72 Expansion Is Mitigated by Antisense Intervention. Neuron 80:415–428.

24. Dormann, D., and C. Haass. 2011. TDP-43 and FUS: a nuclear affair. Trends in neurosciences 34:339–348.

25. Dormann, D., R. Rodde, D. Edbauer, E. Bentmann, I. Fischer, A. Hruscha, M.

E. Than, I. R. A. Mackenzie, A. Capell, B. Schmid, M. Neumann, and C. Haass. 2010. ALS-associated fused in sarcoma (FUS) mutations disrupt Transportin-mediated nuclear import. The EMBO journal 29:2841–2857.

26. Dyer, R. B., and C. T. McMurray. 2001. Mutant protein in Huntington disease is resistant to proteolysis in affected brain. Nature genetics 29:270–8.

27. Elden, A. C., H. Kim, M. P. Hart, A. S. Chen-plotkin, S. Johnson, X. Fang, M. Armakola, F. Geser, R. Greene, M. Min, A. Padmanabhan, D. Clay, L. Mccluskey, L. Elman, D. Juhr, J. Gruber, U. Rüb, G. Auburger, J. Q. Trojanowski, V. M. Lee, M. Van Deerlin, N. M. Bonini, and A. D. Gitler. 2011. Ataxin-2 intermediate-length polyglutamine expansions are associated with increased risk for ALS. NIH Public Access 466:1069–1075.

28. Fan, J., C. Robert, Y. Y. Jang, H. Liu, S. Sharkis, S. B. Baylin, and F. V. Rassool. 2011. Human induced pluripotent cells resemble embryonic stem cells demonstrating enhanced levels of DNA repair and efficacy of nonhomologous end-joining. Mutation Research - Fundamental and Molecular Mechanisms of Mutagenesis 713:8–17.

29. Farg, M. A., V. Sundaramoorthy, J. M. Sultana, S. Yang, R. A. K. Atkinson, V. Levina, M. A. Halloran, P. A. Gleeson, I. P. Blair, K. Y. Soo, A. E. King, and J. D. Atkin. 2014. C9ORF72, implicated in amytrophic lateral sclerosis and frontotemporal dementia, regulates endosomal trafficking. Human Molecular Genetics 23:3579–3595.

30. Freischmidt, A., T. Wieland, B. Richter, W. Ruf, V. Schaeffer, K. Müller, N. Marroquin, F. Nordin, A. Hübers, P. Weydt, S. Pinto, R. Press, S. Millecamps, N. Molko, E. Bernard, C. Desnuelle, M.-H. Soriani, J. Dorst, E. Graf, U. Nordström, M. S. Feiler, S. Putz, T. M. Boeckers, T. Meyer, A. S. Winkler, J. Winkelman, M. de Carvalho, D. R. Thal, M. Otto, T. Brännström, A. E. Volk, P. Kursula, K. M. Danzer, P. Lichtner, I. Dikic, T. Meitinger, A. C. Ludolph, T. M. Strom, P. M. Andersen, and J. H. Weishaupt. 2015. Haploinsufficiency of TBK1 causes familial ALS and fronto-temporal dementia. Nature Neuroscience 18:631–636.

31. Fuchs, E., T. Tumbar, and G. Guasch. 2004. Socializing with the neighbors: Stem cells and their niche. Cell 116:769–778.

32. Gendron, T. F., K. F. Bieniek, Y. J. Zhang, K. Jansen-West, P. E. A. Ash, T. Caulfield, L. Daughrity, J. H. Dunmore, M. Castanedes-Casey, J. Chew, D. M. Cosio, M. Van Blitterswijk, W. C. Lee, R. Rademakers, K. B. Boylan, D. W. Dickson, and L. Petrucelli. 2013. Antisense transcripts of the expanded C9ORF72 hexanucleotide repeat form nuclear RNA foci and undergo repeat-associated non-ATG translation in c9FTD/ALS. Acta Neuropathologica 126:829–844.

33. Ghadge, G. D., J. P. Lee, V. P. Bindokas, J. Jordan, L. Ma, R. J. Miller, and R. P. Roos. 1997. Mutant superoxide dismutase-1-linked familial amyotrophic lateral sclerosis: molecular mechanisms of neuronal death and protection. The Journal of neuroscience : the official journal of the Society for Neuroscience 17:8756–8766.

34. Gillet, L. C. J., and O. D. Schärer. 2006. Molecular mechanisms of mammalian global genome nucleotide excision repair. Chemical Reviews 106:253–276.

35. Grabrucker, A., B. Vaida, J. Bockmann, and T. M. Boeckers. 2009. Synaptogenesis of hippocampal neurons in primary cell culture. Cell and Tissue Research 338:333–341.

36. Gurney, M. E., H. Pu, A. Y. Chiu, M. C. Dal Canto, C. Y. Polchow, D. D. Alexander, J. Caliendo, A. Hentati, Y. W. Kwon, and H. X. Deng. 1994. Motor neuron degeneration in mice that express a human Cu,Zn superoxide dismutase mutation. Science 264:1772–1775.

37. Haeusler, A. R., C. J. Donnelly, and J. D. Rothstein. 2016. The expanding biology of the C9orf72 nucleotide repeat expansion in neurodegenerative disease. Nature Publishing Group 17:383–395.

38. Harper, S., D. W. Speicher, and D. Ph. 2011. Protein Chromatography 681:1–15.

39. Hayes, L. R., and J. D. Rothstein. 2016. C9ORF72 -ALS/FTD : Transgenic Mice Make a Come-BAC. Neuron 90:427–431.

40. Higelin, J., Catanese, A., Semelink-Sedlacek, L.L., Oeztuerk, S., Lutz, A.-K., Bausinger, J., Barbi, G., Speit, G., Andersen, P.M., Ludolph, A.C., Demestre, M., and Boeckers, T.M. 2018. NEK1 loss-of-function mutation induces DNA

damage accumulation in ALS patient-derived motoneurons. Stem Cell Research, 30:150-162.

41. Hu, B., and S. Zhang. 2009. Differentiation of spinal motor neurons from pluripotent human stem cells. Nature protocols 4:1295–1304.

42. Hukema, R. K., F. W. Riemslagh, S. Melhem, H. C. van der Linde, L.-A. Severijnen, D. Edbauer, A. Maas, N. Charlet-Berguerand, R. Willemsen, and J. C. van Swieten. 2014. A new inducible transgenic mouse model for C9orf72-associated GGGGCC repeat expansion supports a gain-of-function mechanism in C9orf72-associated ALS and FTD. Acta Neuropathologica Communications 2:166.

43. Hyun, I. 2010. Review series The bioethics of stem cell research and therapy. Journal of Clinical Investigation 120:71–75.

44. Illing, A., M. Stockmann, N. Swamy Telugu, L. Linta, R. Russell, M. Müller, T. Seufferlein, S. Liebau, and A. Kleger. 2013. Definitive Endoderm Formation from Plucked Human Hair-Derived Induced Pluripotent Stem Cells and SK Channel Regulation. Stem cells international 2013:360–373.

45. Ishigaki, S., F. Urano, and D. A. Bosco. 2014. FUS/TLS assembles into stress granules and is a prosurvival factor during hyperosmolar stress. Journal of Cellular Physiology 228:2222–2231.

46. Jaenisch, R., and R. Young. 2008. Stem Cells, the Molecular Circuitry of Pluripotency and Nuclear Reprogramming. Cell 132:567–582.

47. Japtok, J., X. Lojewksi, M. Naumann, M. Klingenstein, P. Reinhardt, J. Sterneckert, S. Putz, M. Demestre, T. M. Boeckers, A. C. Ludolph, S. Liebau, A. Storch, and A. Hermann. 2015. Stepwise acquirement of hallmark neuropathology in FUS-ALS iPSC models depends on mutation type and neuronal aging. Neurobiology of disease 82:420–429.

48. Jessell, T. M. 2000. Neuronal specification in the spinal cord: inductive signals and transcriptional codes. Nature reviews. Genetics 1:20–29.

49. Jiricny, J. 2006. The multifaceted mismatch-repair system. Nature Reviews Molecular Cell Biology 7:335–346.

50. Jucker, M. 2010. The benefits and limitations of animal models for

translational research in neurodegenerative diseases. Nature Medicine 16:1210–1214.

51. Kunihiro, H. N., U. John, R. Sharon, X. X. Howard, H. John, S. E. Arnold, A. Siderowf, M. Grossman, J. B. Leverenz, R. Woltjer, O. L. Lopez, R. Hamilton, D. W. Tsuang, D. Galasko, E. Masliah, V. Je, K. Christopher, T. J. Montine, V. M. Lee, and J. Q. Trojanowski. 2007. Co-morbidity of TDP-43 proteinopathy in Lewy body related diseases. Acta Neuropathologica 114:221–229.

52. Lazo-Gómez, R., U. N. Ramírez-Jarquín, L. B. Tovar-Y-Romo, and R. Tapia. 2013. Histone deacetylases and their role in motor neuron degeneration. Frontiers in cellular neuroscience 7:243.

53. Lemmens, R., A. Van Hoecke, N. Hersmus, V. Geelen, I. D'Hollander, V. Thijs, L. Van Den Bosch, P. Carmeliet, and W. Robberecht. 2007. Overexpression of mutant superoxide dismutase 1 causes a motor axonopathy in the zebrafish. Human Molecular Genetics 16:2359–2365.

54. Lenzi, J., R. De Santis, V. de Turris, M. Morlando, P. Laneve, A. Calvo, V. Caliendo, A. Chio, A. Rosa, and I. Bozzoni. 2015. ALS mutant FUS proteins are recruited into stress granules in induced Pluripotent Stem Cells (iPSCs) derived motoneurons. Disease Models & Mechanisms 8:755–766.

55. Li, Y. R., O. D. King, J. Shorter, and A. D. Gitler. 2013. Stress granules as crucibles of ALS pathogenesis. The Journal of Cell Biology 201:361–372.

56. Liebau, S., B. Vaida, A. Storch, and T. M. Boeckers. 2007. Maturation of Synaptic Contacts in Differentiating Neural Stem Cells. Stem Cells 25:1720–1729.

57. Lin, M. T., and M. F. Beal. 2006. Mitochondrial dysfunction and oxidative stress in neurodegenerative diseases. Nature 443:787–795.

58. Linta, L., M. Stockmann, K. N. Kleinhans, A. Böckers, A. Storch, H. Zaehres, Q. Lin, G. Barbi, T. M. Böckers, A. Kleger, and S. Liebau. 2012. Rat Embryonic Fibroblasts Improve Reprogramming of Human Keratinocytes into Induced Pluripotent Stem Cells. Stem Cells and Development 21:965–976.

59. Liu, S.-P., R.-H. Fu, Y.-C. Huang, S.-Y. Chen, Y.-J. Chien, C. Y. Hsu, C.-H. Tsai, W.-C. Shyu, and S.-Z. Lin. 2011. Induced Pluripotent Stem (iPS) Cell

Research Overview. Cell Transplantation 20:15–19.

60. Liu, Y., A. Pattamatta, T. Zu, T. Reid, O. Bardhi, D. R. Borchelt, A. T. Yachnis, and L. P. W. Ranum. 2016. C9orf72 BAC Mouse Model with Motor Deficits and Neurodegenerative Features of ALS/FTD. Neuron 90:521–534.

61. Lo, B., L. Parham, A. Alvarez-buylla, M. Cedars, S. Fisher, E. Gates, L. Giudice, D. G. Halme, A. Kriegstein, P. Kwok, and R. Wagner. 2014. Cloning Mice and Men: Prohibiting the Use of iPS Cells for Human Reproductive Cloning. Cell Stem Cell 6:16–20.

62. Lomen-Hoerth, C. 2004. Characterization of amyotrophic lateral sclerosis and frontotemporal dementia. Dementia and Geriatric Cognitive Disorders 17:337–341.

63. López Castel, A., J. D. Cleary, and C. E. Pearson. 2010. Repeat instability as the basis for human diseases and as a potential target for therapy. Nature reviews. Molecular cell biology 11:165–170.

64. Luo, L. Z., S. Gopalakrishna-Pillai, S. L. Nay, S.-W. Park, S. E. Bates, X. Zeng, L. E. Iverson, and T. R. O'Connor. 2012. DNA Repair in Human Pluripotent Stem Cells Is Distinct from That in Non-Pluripotent Human Cells. PLoS ONE 7:e30541.

65. Mackenzie, I. R. A., R. Rademakers, and M. Neumann. 2010. TDP-43 and FUS in amyotrophic lateral sclerosis and frontotemporal dementia. The Lancet Neurology 9:995–1007.

66. Mackenzie, I. R. A., P. Frick, and M. Neumann. 2013. The neuropathology associated with repeat expansions in the C9ORF72 gene. Acta neuropathologica 127:347–357.

67. Majounie, E., A. E. Renton, K. Mok, E. G. P. Dopper, A. Waite, S. Rollinson, A. Chiò, G. Restagno, N. Nicolaou, J. Simon-Sanchez, J. C. van Swieten, Y. Abramzon, J. O. Johnson, M. Sendtner, R. Pamphlett, R. W. Orrell, S. Mead, K. C. Sidle, H. Houlden, J. D. Rohrer, K. E. Morrison, H. Pall, K. Talbot, O. Ansorge, D. G. Hernandez, S. Arepalli, M. Sabatelli, G. Mora, M. Corbo, F. Giannini, A. Calvo, E. Englund, G. Borghero, G. L. Floris, A. M. Remes, H. Laaksovirta, L. McCluskey, J. Q. Trojanowski, V. M. Van Deerlin, G. D. Schellenberg, M. A. Nalls, V. E. Drory, C. S. Lu, T. H. Yeh, H. Ishiura, Y.

Takahashi, S. Tsuji, I. Le Ber, A. Brice, C. Drepper, N. Williams, J. Kirby, P. Shaw, J. Hardy, P. J. Tienari, P. Heutink, H. R. Morris, S. Pickering-Brown, and B. J. Traynor. 2012. Frequency of the C9orf72 hexanucleotide repeat expansion in patients with amyotrophic lateral sclerosis and frontotemporal dementia: A cross-sectional study. The Lancet Neurology 11:323–330.

68. Manfredi, G., N. Maragakis, R. G. Miller, and S. L. Pullman. 2015. Mechanisms, models and biomarkers in amyotrophic lateral sclerosis. Amyotrophic Lateral Sclerosis and Frontotemporal Degeneration 14:19–32.

69. Maruyama, H., H. Morino, H. Ito, Y. Izumi, H. Kato, Y. Watanabe, Y. Kinoshita, M. Kamada, H. Nodera, H. Suzuki, O. Komure, S. Matsuura, K. Kobatake, N. Morimoto, K. Abe, N. Suzuki, M. Aoki, A. Kawata, T. Hirai, T. Kato, K. Ogasawara, A. Hirano, T. Takumi, H. Kusaka, K. Hagiwara, R. Kaji, and H. Kawakami. 2010. Mutations of optineurin in amyotrophic lateral sclerosis. Nature 465:223–226.

70. Le Masson, G., S. Przedborski, and L. F. Abbott. 2014. A computational model of motor neuron degeneration. Neuron 83:975–988.

71. Memisoglu, A., and L. Samson. 2000. Base excision repair in yeast and mammals. Mutation Research - Fundamental and Molecular Mechanisms of Mutagenesis 451:39–51.

72. Mitchell, J. C., P. McGoldrick, C. Vance, T. Hortobagyi, J. Sreedharan, B. Rogelj, E. L. Tudor, B. N. Smith, C. Klasen, C. C. J. Miller, J. D. Cooper, L. Greensmith, and C. E. Shaw. 2013. Overexpression of human wild-type FUS causes progressive motor neuron degeneration in an age- and dose-dependent fashion. Acta Neuropathologica 125:273–288.

73. Mizielinska, S., T. Lashley, F. E. Norona, E. L. Clayton, C. E. Ridler, P. Fratta, and A. M. Isaacs. 2013. C9orf72 frontotemporal lobar degeneration is characterised by frequent neuronal sense and antisense RNA foci. Acta Neuropathologica 126:845–857.

74. Mobassarah, N. J., Z. Choudhry, A. A. Rikani, A. M. Choudhry, S. Tariq, F. Zakaria, M. W. Asghar, M. K. Sarfraz, K. Haider, and A. A. Shafiq. 2014. Sonic Hedgehog Signalling Pathway: A Complex Network. Annals of Neurosciences 21:19–22.

75. Moloney, E. B., F. de Winter, and J. Verhaagen. 2014. ALS as a distal axonopathy: molecular mechanisms affecting neuromuscular junction stability in the presymptomatic stages of the disease. Frontiers in Neuroscience 8:1–18.

76. Momcilovic, O., L. Knobloch, J. Fornsaglio, S. Varum, C. Easley, and G. Schatten. 2010. DNA Damage Responses in Human Induced Pluripotent Stem Cells and Embryonic Stem Cells. PLoS ONE 5:e13410.

77. Mori, K., S.-M. Weng, T. Arzberger, S. May, K. Rentzsch, E. Kremmer, B. Schmid, H. A. Kretzschmar, M. Cruts, C. Van Broeckhoven, C. Haass, and D. Edbauer. 2013. The C9orf72 GGGGCC repeat is translated into aggregating dipeptide-repeat proteins in FTLD/ALS. Science 339:1335–1338.

78. Moynahan, M. E., and M. Jasin. 2010. Mitotic homologous recombination maintains genomic stability and suppresses tumorigenesis. Nature reviews. Molecular cell biology 11:196–207.

79. Myers, R. H. 2004. Huntington's disease genetics. NeuroRx : the journal of the American Society for Experimental NeuroTherapeutics 1:255–262.

80. O'Rourke, J. G., L. Bogdanik, A. K. M. G. Muhammad, T. F. Gendron, K. J. Kim, A. Austin, J. Cady, E. Y. Liu, J. Zarrow, S. Grant, R. Ho, S. Bell, S. Carmona, M. Simpkinson, D. Lall, K. Wu, L. Daughrity, D. W. Dickson, M. B. Harms, L. Petrucelli, E. B. Lee, C. M. Lutz, and R. H. Baloh. 2015. C9orf72 BAC Transgenic Mice Display Typical Pathologic Features of ALS/FTD. Neuron 88:892–901.

81. Okada, Y., T. Shimazaki, G. Sobue, and H. Okano. 2004. Retinoic-acid-concentration-dependent acquisition of neural cell identity during in vitro differentiation of mouse embryonic stem cells. Developmental Biology 275:124–142.

82. Patel, M., S. Yang. 2011. Advances in Reprogramming Somatic Cells to Induced Pluripotent Stem Cells. Stem Cell Review 6:367–380.

83. Pera, M. F., and P. P. L. Tam. 2010. Extrinsic regulation of pluripotent stem cells. Nature 465:713–720.

84. Pisitkun, T., J. D. Hoffert, F. Saeed, and M. A. Knepper. 2012. NHLBI-

AbDesigner: an online tool for design of peptide-directed antibodies. American journal of physiology. Cell physiology 302:C154-164.

85. Qiu, H., S. Lee, Y. Shang, W. Y. Wang, K. F. Au, S. Kamiya, S. J. Barmada, S. Finkbeiner, H. Lui, C. E. Carlton, A. A. Tang, M. C. Oldham, H. Wang, J. Shorter, A. J. Filiano, E. D. Roberson, W. G. Tourtellotte, B. Chen, L. H. Tsai, and E. J. Huang. 2014. ALS-associated mutation FUS-R521C causes DNA damage and RNA splicing defects. Journal of Clinical Investigation 124:981–999.

86. Reuveni, H., E. Flashner-abramson, L. Steiner, and K. Makedonski. 2015. HHS Public Access 73:4383–4394.

87. Rosen, D. R., T. Siddique, D. Patterson, D. A. Figlewicz, P. Sapp, A. Hentati, D. Donaldson, J. Goto, J. P. O'Regan, and H. X. Deng. 1993. Mutations in Cu/Zn superoxide dismutase gene are associated with familial amyotrophic lateral sclerosis. Nature 362:59–62.

88. Ross, C. A., and S. S. Akimov. 2014. Human-induced pluripotent stem cells: potential for neurodegenerative diseases. Human Molecular Genetics 23:17–26.

89. Rothkamm, K., I. Krüger, L. H. Thompson, I. Kru, and M. Lo. 2003. Pathways of DNA Double-Strand Break Repair during the Mammalian Cell Cycle. Molecular and cellular biology 23:5706–5715.

90. Roussignol, G., F. Ango, S. Romorini, J. C. Tu, C. Sala, P. F. Worley, J. Bockaert, and L. Fagni. 2005. Shank expression is sufficient to induce functional dendritic spine synapses in aspiny neurons. The Journal of neuroscience : the official journal of the Society for Neuroscience 25:3560–3570.

91. Saccon, R. A., R. K. A. Bunton-Stasyshyn, E. M. C. Fisher, and P. Fratta. 2013. Is SOD1 loss of function involved in amyotrophic lateral sclerosis? Brain 136:2342–2358.

92. Sareen, D., J. G. O'Rourke, P. Meera, A. K. M. G. Muhammad, S. Grant, M. Simpkinson, S. Bell, S. Carmona, L. Ornelas, A. Sahabian, T. Gendron, L. Petrucelli, M. Baughn, J. Ravits, M. B. Harms, F. Rigo, C. F. Bennett, T. S. Otis, C. N. Svendsen, and R. H. Baloh. 2013. Targeting RNA foci in iPSC-

derived motor neurons from ALS patients with a C9ORF72 repeat expansion. Science translational medicine 5:149–208.

93. Satoh, J.-I., H. Tabunoki, T. Ishida, Y. Saito, and K. Arima. 2012. Dystrophic neurites express C9orf72 in Alzheimer's disease brains. Alzheimer's research & therapy 4:33.

94. Satoh, J.-I., Y. Yamamoto, S. Kitano, M. Takitani, N. Asahina, and Y. Kino. 2014. Molecular network analysis suggests a logical hypothesis for the pathological role of c9orf72 in amyotrophic lateral sclerosis/frontotemporal dementia. Journal of central nervous system disease 6:69–78.

95. Schlachetzki, J. C. M., S. W. Saliba, and A. C. P. de Oliveira. 2013. Studying neurodegenerative diseases in culture models. Revista Brasileira de Psiquiatria 35:92–100.

96. Schymick, J. C., K. Talbot, and B. J. Traynor. 2007. Genetics of sporadic amyotrophic lateral sclerosis. Human Molecular Genetics 16:223–242.

97. Sentman, M. L., M. Granström, H. Jakobson, A. Reaume, S. Basu, and S. L. Marklund. 2006. Phenotypes of mice lacking extracellular superoxide dismutase and copper- and zinc-containing superoxide dismutase. Journal of Biological Chemistry 281:6904–6909.

98. Shaw, P. J. 2005. Molecular and cellular pathways of neurodegeneration in motor neurone disease. Journal of neurology, neurosurgery, and psychiatry 76:1046–57.

99. Sheng, M., and C. C. Hoogenraad. 2007. The postsynaptic architecture of excitatory synapses: a more quantitative view. Annual review of biochemistry 76:823–847.

100. Sheng, M., and E. Kim. 2011. The postsynaptic organization of synapses. Cold Spring Harbor perspectives in biology 3:823–847.

101. Stockmann, M., L. Linta, K. J. Föhr, A. Boeckers, A. C. Ludolph, G. F. Kuh, P. T. Udvardi, C. Proepper, A. Storch, A. Kleger, S. Liebau, and T. M. Boeckers. 2013. Developmental and Functional Nature of Human iPSC Derived Motoneurons. Stem Cell Reviews and Reports 9:475–492.

102. Tada, M., E. A. Coon, A. P. Osmand, A. Patricia, W. Martin, M. Wieler, and A.

Shiga. 2013. sclerosis : a clinicopathologic study 124:749–760.

103. Takahashi, K., and S. Yamanaka. 2006. Induction of Pluripotent Stem Cells from Mouse Embryonic and Adult Fibroblast Cultures by Defined Factors. Cell 126:663–676.

104. Tandan, R., and W. G. Bradley. 1985. Amyotrophic lateral sclerosis: Part 1. Clinical features, pathology, and ethical issues in management. Annals of neurology 18:271–280.

105. Tao, Z., H. Wang, Q. Xia, K. Li, K. Li, X. Jiang, G. Xu, G. Wang, and Z. Ying. 2015. Nucleolar stress and impaired stress granule formation contribute to C9orf72 RAN translation-induced cytotoxicity. Human Molecular Genetics 24:2426–2441.

106. Taylor, J. P. 2013. RNA That Gets RAN in Neurodegeneration. Science 339:1282–1283.

107. Thomson, J. A., J. Itskovitz-Eldor, S. S. Shapiro, M. a Waknitz, J. J. Swiergiel, V. S. Marshall, and J. M. Jones. 1998. Embryonic stem cell lines derived from human blastocysts. Science 282:1145–1147.

108. Todd, P., H. Paulson. 2011. RNA Mediated Neurodegeneration in Repeat Expansion Disorders. Annals of Neurology 67:291–300.

109. Toli, D., D. Buttigieg, S. Blanchard, T. Lemonnier, B. Lamotte, S. Bellouze, G. Baillat, D. Bohl, and G. Haase. 2015. Neurobiology of Disease Modeling amyotrophic lateral sclerosis in pure human iPSc-derived motor neurons isolated by a novel FACS double selection technique. Neurobiology of Disease 82:269–280.

110. Valdiglesias, V., S. Giunta, M. Fenech, M. Neri, and S. Bonassi. 2013. γH2AX as a marker of DNA double strand breaks and genomic instability in human population studies. Mutation Research/Reviews in Mutation Research 753:24–40.

111. Van Blitterswijk, M., M. DeJesus-Hernandez, and R. Rademakers. 2014. How do C9ORF72 repeat expansions cause ALS and FTD: can we learn from other non-coding repeat expansion disorders? Current Opinion in Neurobiology 25:689–700.

112. Vance, C., B. Rogelj, T. Hortobágyi, K. J. De Vos, A. L. Nishimura, J. Sreedharan, X. Hu, B. Smith, D. Ruddy, P. Wright, J. Ganesalingam, K. L. Williams, V. Tripathi, S. Al-Saraj, A. Al-Chalabi, P. N. Leigh, I. P. Blair, G. Nicholson, J. de Belleroche, J.-M. Gallo, C. C. Miller, and C. E. Shaw. 2009. Mutations in FUS, an RNA processing protein, cause familial amyotrophic lateral sclerosis type 6. Science 323:1208–1211.

113. Wang, W.-Y., L. Pan, S. C. Su, E. J. Quinn, M. Sasaki, J. C. Jimenez, I. R. A. Mackenzie, E. J. Huang, and L.-H. Tsai. 2013. Interaction of FUS and HDAC1 regulates DNA damage response and repair in neurons. Nature neuroscience 16:1383–1391.

114. Wijesekera, L. C., and P. N. Leigh. 2009. Amyotrophic lateral sclerosis. Orphanet journal of rare diseases 4:3.

115. Wu, D., W. Yu, H. Kishikawa, R. D. Folkerth, A. J. Iafrate, Y. Shen, W. Xin, K. Sims, and G. F. Hu. 2007. Angiogenin loss-of-function mutations in amyotrophic lateral sclerosis. Annals of Neurology 62:609–617.

116. Wu, J., L. Lu, and X. Yu. 2010. Protein & Cell The role of BRCA1 in DNA damage response 1:117–123.

117. Xiao, S., L. MacNair, P. McGoldrick, P. M. McKeever, J. R. McLean, M. Zhang, J. Keith, L. Zinman, E. Rogaeva, and J. Robertson. 2015. Isoform-specific antibodies reveal distinct subcellular localizations of C9orf72 in amyotrophic lateral sclerosis. Annals of Neurology 78:568–583.

118. Yamanaka, S., K. Takahashi, K. Tanabe, M. Ohnuki, M. Narita, T. Ichisaka, and K. Tomoda. 2007. Induction of pluripotent stem cells from adult human fibroblasts by defined factors. Cell 131:861–872.

119. Yanovsky-Dagan, S. 2015. Modeling diseases of noncoding unstable repeat expansions using mutant pluripotent stem cells. World Journal of Stem Cells 7:823.

120. Zhang, K., C. J. Donnelly, A. R. Haeusler, J. C. Grima, J. B. Machamer, P. Steinwald, E. L. Daley, S. J. Miller, K. M. Cunningham, S. Vidensky, S. Gupta, M. A. Thomas, I. Hong, S.-L. Chiu, R. L. Huganir, L. W. Ostrow, M. J. Matunis, J. Wang, R. Sattler, T. E. Lloyd, and J. D. Rothstein. 2015. The C9orf72 repeat expansion disrupts nucleocytoplasmic transport. Nature 525:56-76.

121. Zhang, S. C., M. Wernig, I. D. Duncan, O. Brüstle, and J. A. Thomson. 2001. In vitro differentiation of transplantable neural precursors from human embryonic stem cells. Nature biotechnology 19:1129–1133.

122. Zhou, Y., and F. Zeng. 2013. Integration-free Methods for Generating Induced Pluripotent Stem Cells. Genomics, Proteomics & Bioinformatics 11:284–287.

123. Zu, T., Y. Liu, M. Bañez-Coronel, T. Reid, O. Pletnikova, J. Lewis, T. M. Miller, M. B. Harms, A. E. Falchook, S. H. Subramony, L. W. Ostrow, J. D. Rothstein, J. C. Troncoso, and L. P. W. Ranum. 2013. RAN proteins and RNA foci from antisense transcripts in C9ORF72 ALS and frontotemporal dementia. Proceedings of the National Academy of Sciences of the United States of America 110:4968-4977.

124. Zukor, K., and Z. He. 2011. Regenerative medicine: drawing breath after spinal injury. Nature 475:177–178.

125. Zwaka, T. P., and J. A. Thomson. 2003. Homologous recombination in human embryonic stem cells. Nature Biotechnology 21:319–321.

Acknowledgements

Acknowledgements have been modified for privacy reasons.

All of my persuits have been supported by the loving and professional advice of my brother, Dr. rer. nat. Janosch Sedlacek - I will always be grateful for your unique and precious presence.

Curriculum vitae

Curriculum vitae has been removed for privacy reasons.